5-2015

Investigating the roles of p63 and p73 isoforms to therapeutically treat p53-altered cancers

Avinashnarayan Venkatanarayan

INVESTIGATING THE ROLES OF P63 AND P73 ISOFORMS TO THERAPEUTICALLY TREAT P53-ALTERED CANCERS

By

Avinashnarayan Venkatanarayan, M.S.

APPROVED:

_____
Elsa R. Flores, Ph.D.
Advisory Professor

_____
Mong Hong Lee, Ph.D.

_____
Michael J. Galko, Ph.D.

_____
Kenneth Y. Tsai, M.D., Ph.D.

_____
Sendurai Mani, Ph.D.

_____
Preethi H. Gunaratne, Ph.D.

APPROVED:

_____
Dean, The University of Texas
Graduate School of Biomedical Sciences at Houston

INVESTIGATING THE ROLES OF P63 AND P73 ISOFORMS TO THERAPEUTICALLY TREAT P53-ALTERED CANCERS

A

DISSERTATION

Presented to the Faculty of

The University of Texas

Health Science Center at Houston

and

The University of Texas

MD Anderson Cancer Center

Graduate School of Biomedical Sciences

in Partial Fulfillment

of the Requirements

for the Degree of

DOCTOR OF PHILOSOPHY

By

Avinashnarayan Venkatanarayan, M.S.

Houston, Texas

May, 2015

Dedication

To my grandmothers Janakavalli A & Shanthakumari P who have been a tremendous source of will power, dedication and humility

Acknowledgements

My training and success in the graduate school would have not been possible without the support, mentorship and blessings of many people.

First and foremost, I would like to thank God, the Almighty for giving me the energy and health to complete this endeavor successfully.

I would like to thank my mentor, Dr. Elsa Flores for accepting me as a graduate student in her laboratory; training me and importantly helping me achieve my goals. Dr. Flores has not only been a great mentor, but also a role model from whom I often draw inspiration, sometimes as my friend with whom I tend to chat and sometimes as my scientific mom for the care and affection she has provided me. I learnt to not only appreciate and perform science but more importantly the purpose we serve as scientists and the hope we give to the people by advancing cancer research.

I am also fortunate to have the support and guidance of an excellent committee. Dr. Mong Hong Lee, Dr. Michael Galko, Dr. Sendurai Mani, Dr. Kenneth Tsai and Dr. Preethi Gunaratne have been excellent mentors and always provided me with constructive suggestions and helped me progress in my scientific career. I also wanted to to acknowledge three people, Dr. Elsa Flores, Dr. Michael Galko and Dr. Andreas Bergmann who offered me rotation positions in there labs and made my dream of pursuing a PhD program a reality.

Also, I had the support and guidance of a small but highly talented group of people in the lab. I would like to thank all the present and former members of the Flores Lab. I would like to thank Dr. Min Soon Cho for helping me learn the basics

when I was a rotation student. I had lot of help with the mouse work from Young Jin Gi, Lingzhi Liu and Payal Raulji. Dr. Xiaohua Su is an expert in our lab and she has always been my go to person. Dr. Marco Napoli has been a good friend and excellent person to bounce ideas from him. Marlese Pisegna has been our always-positive lab manager and my bench buddy. She has provided me with moral support and she was always there to share with me my failures and success. And finally, I would like to acknowledge my fellow graduate students Dr. Ramon Flores Gonzalez, Andrew Davis, Ngoc Bui and Sarah Wu. I think we started as lab mates and now we have become friends for life. Our repeated discussions on performing and improving experiments have made our lab a happening place.

I would also like to thank and acknowledge the rotation and summer students who worked closely with me. Particularly, I would like to thank Pruthali Kulkarni and Eliot F. Sananikone for their motivation and enthusiasm while performing experiments in the lab. I would also like to thank my collaborators, Dr. William Norton (Veterinary Medicine) for his help with the mouse surgeries. Dr. James Bankson and members of the Small Animal Imaging Facility (SAIF) for their help with mouse imaging. Dr. Cristian Coarfa for his help with Bioinformatic analysis and Dr. Anil Sood, Dr. Mangala Selenere and Aguayo Cristian for their help with the liposomal siRNA particles.

My success in graduate school is also greatly attributed to help and guidance from Dr. Abinav Jain and Dr. Srikanth Appikonda (Barton Lab), Dr. James Jackson and Dr. Vinod Pant (Lozano Lab) and Dr. Parameshwar Djardiane. We have become good friends over the last few years and I really cherish the time I spent with

all of them. I would also like to thank Elisabeth Lindheim, the Genes and Development program coordinator for her help and support for the last 6 years.

Also, I would like to thank and acknowledge my family for their unconditional love and support during my training as a graduate student. My parents Mr. A. Venkatanarayan and Mrs. V. Ashalatha have always given me the freedom to pursue my interests and never doubted my actions. My brother Dr. Ajay Venkatanarayan, in many ways made sacrifices on my behalf so that I could complete my graduate school, by supporting my parents and being self-less. I also would like to thank my uncle Dr. A. Srinivasan who has always reminded me that hard work leads to success. Finally, I would like to thank my fiancée Ms. Amritha Sathish for her love, support and positive attitude. She has been highly understanding of my busy schedule and helped me stay focused.

Finally, I would like to thank my friends who have been my pillars of strength throughout my graduate school. My friends have become like my family and I am excited to see what the future holds for each of us. I would like to thank Dr. Rajesha Rupaimoole my friend and roommate for the past 8 years. Rajesha and myself have a special understanding and we both have taken similar steps in our life at the same time. Also, I would like to thank Dr. Anantha and Anil Chukkapalli, Dr. Zeynep and Dr. Kadir Akdemir, Uphanya and Dr. Sridhar Eshwaran for their love, friendship and support. Also, a special thanks to Dr. Shankar Venugopalan and my buddies Bharat Chaganty and Dr. Kalyan Nallaparaju for always giving the best and positive advice.

Investigating the roles of *p63* & *p73* isoforms to therapeutically treat *p53*-altered cancers

Avinashnarayan Venkatanarayan, M.S.

Supervisory Professor: Elsa R. Flores, Ph.D.

The *TP53* tumor suppressor is mutated in approximately 50% of human cancers rendering cancer therapies ineffective. p53 reactivation suppresses tumor formation in mice. However, this strategy has proven difficult to implement therapeutically. An alternate approach to overcome p53 loss is to manipulate the p53-family members, *p63* and *p73*, which interact and share structural similarities to p53. *p63* and *p73*, unlike *p53* are less frequently mutated and have two major isoforms with distinct functions which makes them unique targets for therapeutic intervention. The full-length acidic transactivation (TA) isoforms of *p63* and *p73* function similar to *p53*. While the deltaN (ΔN) isoforms of *p63* and *p73*, which lack the acidic transactivation domain, are overexpressed in cancers and function in a dominant negative manner against *p53*, *TAp63* and *TAp73*. As result of the opposing isoform-specific function, the roles of *p63* and *p73* in tumorigenesis requires further characterization. In an attempt to identify novel therapeutic approaches to treat p53-altered cancers by utilizing the p53-family members, I aim to delineate the roles of ΔN isoforms of *p63* and *p73* in tumorigenesis.

I have demonstrated that deletion of ΔNp63 or ΔNp73 in p53-deficient tumors mediates tumor regression through the upregulation of tumor suppressive isoforms, *TAp63* and *TAp73*. Upon loss of ΔNp63 or ΔNp73, TAp63 and TAp73 activate *IAPP*

a metabolic regulator, which induces metabolic reprogramming resulting in tumor regression in p53-deficient mice. I have shown that *IAPP*, which encodes amylin, a 37-amino acid peptide functions as a tumor suppressor in p53-deficient cancers. IAPP functions through the calcitonin and RAMP3 receptors to limit glucose uptake and reduce glycolysis in the cancer cells resulting in ROS accumulation and apoptosis. Additionally, I have also shown that use of Pramlintide, a synthetic analog of IAPP, mediates tumor regression in p53-deficient mice and apoptosis in multiple p53-mutant human cancer cell lines.

Further, to therapeutically treat p53-deficient cancers *in vivo*, liposomal nanoparticle siRNA's targeting ΔNp63 and ΔNp73 were administered into p53-deficient mouse thymic lymphomas, which resulted in tumor regression. Taken together, my work has defined the isoform specific functions of *p63* and *p73* in tumorigenesis. Importantly, I have also demonstrated the use of pramlintide, a diabetic drug to treat p53-altered cancers. Thus, by understanding the interplay among the p53-family members, novel therapeutic methods could be designed to treat p53-altered human cancers.

Table of Contents

Approvals i

Title ii

Dedication iii

Acknowledgements iv

Abstract vii

Table of Contents ix

List of Figures xi

List of Tables xv

List of Appendices xvi

Chapter 1: Introduction 1

Chapter 2: Material and Methods 26

Chapter 3: *ΔNp63* and *ΔNp73* function as oncogenes in a p53-deficient model of thymic lymphoma 43

Chapter 4: IAPP driven metabolic reprogramming induces regression of p53-deficient tumors *in vivo* 71

Chapter 5: IAPP functions through the calcitonin and RAMP3 receptors to suppress tumorigenesis 98

Chapter 6: Therapeutic approaches to treat p53-mutated human cancers 105

Chapter 7: Therapeutically targeting the oncogenic isoforms of *p63* and *p73* to treat p53-deficient tumors 123

Chapter 8: Investigating the roles of p63 and p73 regulated lncRNAs upon DNA damage and in p53-deficient tumors 130

Chapter 9: Discussion, Conclusions & Future directions 141

Bibliography 192

Vita 207

List of Figures

Chapter 1

Figure 1: p53-mutational frequency in human cancers 4

Figure 2: Sequence and structural homology of p53, p63 and p73 ..... .10

Figure 3: Graph representing the mutational status across p53-family members in human cancer 13

Figure 4: Warburg's hypothesis on tumor cell metabolism 17

Chapter 3

Figure 5: Decreased thymic lymphomagenesis and increased survival in mice double deficient for ΔNp63 and p53 or ΔNp73 and p53 46

Figure 6: Increased apoptosis and cell cycle arrest in ΔNp63+/-;p53-/- and ΔNp73-/-;p53-/- thymocytes after genotoxic stress 50

Figure 7: Acute deletion of ΔNp63 or ΔNp73 in p53-deficient thymic lymphomas mediates tumor regression 53

Figure 8: Loss of ΔNp63 or ΔNp73 in p53-deficient thymic lymphomas results in upregulation of TAp63 and TAp73 with induction of apoptosis and cell cycle arrest 56

Figure 9: Ablation of ΔNp63 and ΔNp73 in p53-deficient mice accelerates tumor regression 59

Figure10: Ablation of ΔNp63 and ΔNp73 in p53-deficient thymic lymphomas results in accumulation of ROS, apoptosis and cell-cycle arrest 61

Figure 11: Loss of ΔNp63/ΔNp73 in p53-deficient thymic lymphomas affects the CD4-CD8 double positive cells 62

Figure 12: ΔNp63 and ΔNp73 transcriptionally repress *TAp63* and *TAp73*..... 64

Figure 13: TAp63 and TAp73 are required for activation of apoptosis and cell cycle targets in p53-deficient cells..... 67

Chapter 4

Figure 14: Loss of ΔNp63 and ΔNp73 reveals a novel metabolic gene signature 74

Figure 15: IAPP functions as a downstream target of TAp63 and TAp73 77

Figure 16: IAPP functions as a regulator of glycolysis in mouse embryonic fibroblasts..... 79

Figure 17: IAPP functions as a tumor suppressor *in vivo* 81

Figure 18: IAPP expression induces ROS accumulation and apoptosis in the p53-deficient thymic lymphomas..... 84

Figure 19: ΔNp63/ΔNp73 ablation induces apoptosis and cell cycle arrest in p53-deficient human cancer cells 86

Figure 20: IAPP mediated glycolytic inhibition results in ROS-induced cell death in p53-deficient cancer cells..... 88

Figure 21: IAPP suppresses glycolysis by inhibiting hexokinase..... 90

Figure 22: Systemic delivery of pramlintide mediates tumor regression in p53-deficient mice..... 92

Figure 23: 2-deoxy-D-glucose functions as a potent glycolytic inhibitor 93

Chapter 5

Figure 24: IAPP functions through the activity of the calcitonin and RAMP3 receptors..... 101

Figure 25: Calcitonin and RAMP3 receptors are required for IAPP/ Pramlintide function *in vivo* 102

Chapter 6

Figure 26: Deletion of ΔNp63/ΔNp73 in combination with genotoxic stress induces apoptosis and cell cycle arrest in p53-deficient human breast cancer cells 107

Figure 27: Deletion of ΔNp63/ΔNp73 in combination with genotoxic stress induces apoptosis and cell cycle arrest in p53-deficient human colorectal cancer cells..... 108

Figure 28: Deletion of ΔNp63/ΔNp73 in combination with mutant p53 induces apoptosis and cell cycle arrest in p53-deficient human breast cancer cells 110

Figure 29: Deletion of ΔNp63/ΔNp73 in combination with mutant p53 induces apoptosis and cell cycle arrest in p53-deficient human colorectal cancer cells..... 111

Figure 30: Pramlintide treatment suppresses glycolysis and results in ROS-induced apoptosis in p53-mutant human cancer cells 114

Figure 31: Pramlintide treatment suppresses glycolysis in human SCC cells . 118

Figure 32: Pramlintide treatment induces apoptosis in human SCC cells 119

Chapter 7

Figure 33: Liposomal siΔNp63 administration in p53-deficient thymic lymphomas induces apoptosis and cell cycle arrest 126

Figure 34: Therapeutically targeting ΔNp63 by liposomal siRNA's in p53-

deficient thymic lymphomas mediates tumor regression 127

Chapter 8

Figure 35: Pie chart representing lncRNAs either dependent or independent of genotoxic stress 133

Figure 36: Differentially expressed lncRNAs upon ablation of ΔNp63 and ΔNp73 in p53-deficient thymic lymphomas 136

Chapter 9

Figure 37: TAp63 and TAp73 compensate for p53-loss by IAPP-driven metabolic reprogramming 148

Figure 38: IAPP mediated mechanism of glycolytic inhibition in p53-altered cancers 151

Figure 39: Kaplan Meier survival plots for expression of IAPP-CALCR-RAMP3 in p53-mutated human cancer patients 153

List of Tables

Table 1: Table showing ΔNp63 and ΔNp73 binding sites on the TAp63 and TAp73 promoter regions 65

Table 2: Table showing TAp63 and TAp73 consensus binding sites on the IAPP promoter 76

Table 3: Table representing a panel of patient derived human squamous carcinomas cells with p53 alterations 116

Table 4: Table representing a classification of human SCC cells based on the basal glycolytic profile 117

Table 5: List of differentially expressed lncRNAs that are either dependent or independent of genotoxic stress 134

Table 6: List of differentially expressed lncRNAs with ensemble ID and chromosomal location 138

List of Appendices

Appendix 1: Mouse thymic lymphoma mRNA-heatmap 162

Appendix 2: List of genes differentially expressed in ΔNfl/fl;p53-/- vs ΔNp63Δ/Δ;p53-/ & ΔNp73Δ/Δ;p53-/- thymic lymphoma samples .. 163

Appendix 3: Pramlintide treatment as a preventive approach to treat thymic lymphomagenesis in p53-deficent mice 191

1. Chapter 1: Introduction

Chapter 1: Introduction

1.1. *p53* as a tumor suppressor

The *TP53* gene encodes for p53, which is located on the chromosome locus 17p13.1(1, 2). The *TP53* gene is regarded as the “Guardian of the genome” due to its tumor suppressive functions, however *TP53* is highly mutated in multiple cancers(3, 4). More than 50% of human cancers, harbor a complete inactivation of p53 function or gain of function of p53 due to mutations(5). This effect is well documented in Li-Fraumeni syndrome individuals who harbor p53 loss and are highly susceptible to tumor formation(6) and also the ability of the mouse models to develop spontaneous tumors upon loss of p53(7, 8).

The p53 protein upon initial discovery as a complex with the SV40 T-antigen was hypothesized to function as a proto-oncogene(1). This notion was later proved to be incorrect as the initial experiments were performed using a mutated version of the *TP53* gene. Later, wild-type p53 loss of function was observed in a subset of colon carcinomas suggesting that p53 could have tumor suppressive functions(1). In many cancers, loss of one copy of *TP53* initiates the tumorigenesis process, which is immediately followed by the loss of heterozygosity further accelerating the tumor formation. However, in some cancers, *TP53* loss could be the end result of a much more malignant tumor phenotype that could eventually lead to differentiation of the tumor cells further increasing their invasive and metastatic potential. Thus far, current research has been trying to determine the underlying mechanisms by which *TP53* executes its tumor suppressive function.

Thirty years from its initial discovery, *TP53* is also referred to as the “Master regulator of the genome” for its well-documented cellular functions. *TP53* is a transcriptional factor that is involved in a multiple cellular functions and helps maintains cellular homeostasis. At physiological levels, the protein levels of p53 are low and under the regulation of E3 ubiquitin ligase called MDM2 and MDM4(9, 10), which bind to the amino terminus of p53. Upon different types of cellular stressors like DNA damage, hypoxia and oncogene activation, p53 levels increase in the cells imparting its protective genomic function. p53 forms a homotetramer and functions as a tumor suppressor by inducing cell death by activating *PUMA(2, 11, 12)*, *Noxa(2)* and *BAX(13, 14)* or induces transient cell cycle arrest(15, 16) by activating *p21(17, 18)*, *p16(15, 19, 20)* and *PML*. p53 can also induce cellular senescence, a more permanent form of cell cycle arrest. The normal function of p53 is to activate DNA damage repair pathway upon genomic instability. Apart from these classical functions of p53, more recently p53 has been demonstrated to play important roles in autophagy, cellular metabolism and stem cell maintenance.

Our understanding of the function and roles of p53 in human cancers, were well-recapitulated using mouse models in which p53 is functionally inactivated(21). Trp53-null mice primarily develop thymic lymphomas at 90% incidence while the Trp53-heterzygous mice develop osteosarcomas and thymic lymphomas(22). However, in most cancers, *TP53* is highly mutated that results in p53 gain of function further promoting aggressive tumor formation. The mutation related functions of p53, have generated a whole new area of research in characterizing the mutation related

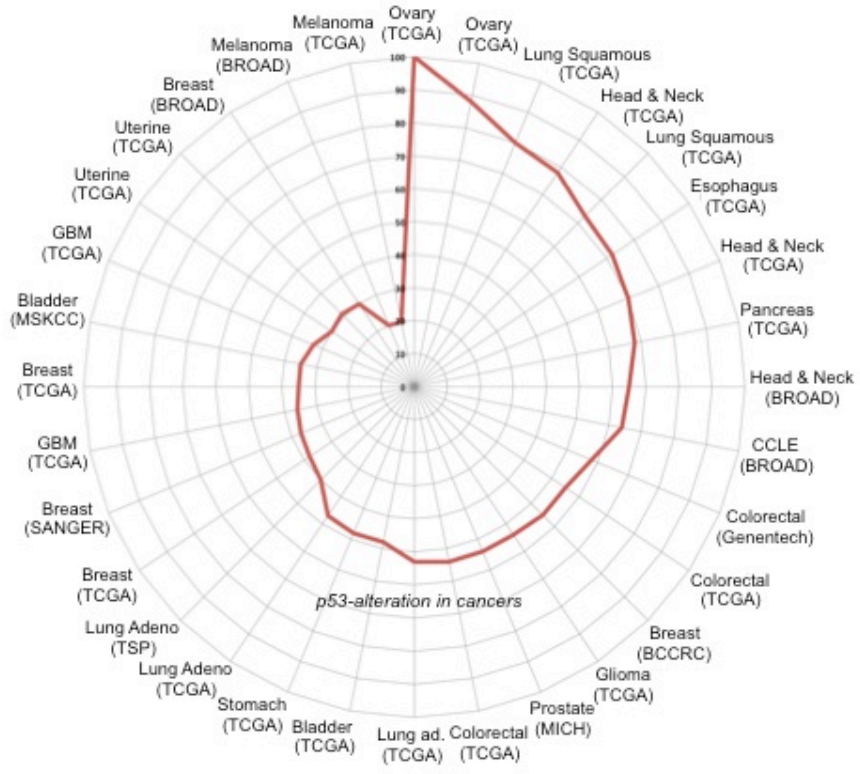

Figure 1: p53-mutational frequency in human cancers. Spider plot representing the mutation frequency in *TP53* across a panel of human cancers. Sequencing data from the Cancer Genome Atlas (TCGA) deposited from multiple human sequencing studies provide an overall mutational frequency for *TP53* in multiple cancer types.

properties of mutant p53 in human cancers using mouse models specific to the common p53-mutations that have been identified(7, 8).

1.2. p53 mutations in human cancer

TP53 gene is highly mutated in multiple human cancers. Recent sequencing efforts from the cancer genome atlas (TCGA) have identified a huge array of cancers in which *TP53* is mutated (Figure 1). Somatic mutations generally occur in multiple genes in human cancer. In the case of TP53, due to its vital tumor suppressive functions it seems to be a commonly mutated target. Unlike most genes which have frame-shift or non-sense mutations, p53 in general has missense mutations that is characterized by single amino acid substitutions(23). These point mutant versions of p53 are stable and serve as dominant negative regulators of wild-type p53. Typically, when mutant p53 expression is higher it affects the tetramer formation of wild-type p53 altering its function. Importantly, in tumors, when one copy of p53 is mutated it is followed immediately by the loss of heterozygosity (LOH) of the wild-type p53. This has led to the classification that p53-mutations result in “gain of function” activities accelerating tumor formation(7, 8). Although in some instances mutant p53 can mediate gain of function activities independent of wild-type p53. Further, from the sequencing efforts on human cancers, p53 mutations are mostly restricted to the DNA binding domain and some of these frequent mutations in p53 are referred as “hotspot” mutations. To the test the effect of these mutations in tumorigenesis, similar to the Trp53-null mice that demonstrated the tumor suppressive function of p53, two knock-in mouse models that harbor hotspot mutations at R175 and R270 were generated(7, 8). These mice had diverse tumor

spectrum with increased metastasis highlighting the aggressiveness of p53-mutation driven tumors in these mice.

Mutant p53, unlike wild-type p53 does not directly bind to DNA to promote its proto-oncogenic functions. However, mutant p53 can interact with targets like NF-Y, Ets1, Pin1, MRE11, PML to promote oncogenic transformation(24, 25) or repress the activity of the other family members p63 and p73 that function as tumor suppressors(26, 27). Because of these widespread effects of mutant p53 function or p53 inactivation in human cancers current therapeutic approaches are targeted towards either reactivating wild-type p53 or to degrade mutant p53. Although, preliminary data in mouse models demonstrating active tumor suppression upon p53-reactivation has shown great promise, thus far therapeutically it is not been feasible. Also, drug inhibitor based approach to degrade mutant p53 is still under developmental stages which necessitates the need to find and develop alternate approaches to treat these human cancers(28-30).

1.3. Therapeutic Strategies to activate the p53-pathway

p53 upon cellular stress, functions to induce cell cycle arrest or cell death in the “radiosensitive” tissues(15). This is one mechanism by which p53-potects the genome from different types of cellular stressors and DNA damage. In the context of the tumor, one mechanism by which chemotherapy functions is to induce damage which elicit a p53 response activating a downstream cellular cascade targeting the tumors cells. However, as previously discussed p53 is completely inactivated with a “loss of function” phenotype or mutated resulting in “gain of function” effects. This

necessitates the need to restore the function of the p53-pathway. Interestingly, *in vitro* restoration of p53 function induced cancer cell death and cell cycle arrest in human cancer cells(31). This was further validated *in vivo* using a conditional p53 *in vivo* mouse model of lymphomagenesis and osteosarcoma(32, 33). Interestingly, when p53 expression was restored the thymic lymphoma cells underwent cell death while the osteosarcoma cells underwent cell cycle arrest and cellular senescence(16, 32). This suggests that p53 executes its tumor suppressive function in a tissue dependent manner. Although these experiments provide a proof of principle mechanism to activate the p53-pathway, thus far restoring p53-function therapeutically as been challenging.

1.3.1. Activating wild-type p53 function in human cancers

At physiological conditions, p53 is under the regulation of its E3 ubiquitin ligase MDM2(9, 34). Research work has demonstrated that in multiple human cancers, MDM2 and its counterpart, MDM4 are significantly overexpressed thereby repressing wild-type p53 function. Hence, one approach that is under development is to abrogate the p53-MDM2 interaction, which will restore wild-type p53 activity(35-37). Multiple small molecule inhibitors(38) are under clinical development, but Nutlin-3a has made significant progress in restoring wild-type p53 activity(39-41). Also, loss of p53 function in some tumors arises due to the mis-folding of the p53 protein. Currently, reconstituting levels of Zinc (Zn) in these cells have corrected the p53 protein conformation in wild-type p53 thereby restoring its function(42). However, this approach cannot be used in mutant p53, as the residues that correspond to the

Zinc are mutated. Hence, alternate approaches need to be adopted to therapeutically treat p53-mutated cancers.

1.3.2. Degrading mutant p53 function in human cancers

Mutant p53 exhibits a “gain of function” effect promoting tumor formation. Hence, current therapeutic strategies are targeted towards abolishing the activity of mutant p53 either directly or indirectly. Mutant p53 stabilization is achieved through its interaction with Hsp70 and Hsp90 through HDAC6(43, 44). Therapeutic use of HDAC inhibitors like SAHA have shown increased efficacy in degrading the mutant p53 in cancer cells, however, use of HDAC inhibitors has been demonstrated to degrade wild-type p53 restricting its use towards cancer treatment. Additional methods to downregulate the mutant p53 function is by targeting the effector pathways like the MAPK or PI-3K pathway that are activated by mutant p53 function. Thus far restoration of the p53-pathway still remains a challenge due the intricate complexities and this necessitates the need to identify and characterize alternate mechanisms to treat these p53-deficient human cancers.

1.4. Utilizing the p53 family members p63 and p73 towards cancer treatment

The p53 superfamily comprises of *TP63* and *TP73* along with *TP53*. For the last 30 years, the role of *TP53* in tumor suppression has been well documented. Inactivation of *TP53* in human tumors has defined the role of *TP53* as a bonafide tumor suppressor. However, the functional roles of the family members *TP63* and *TP73* in tumorigenesis have been shadowed. *TP63* and *TP73* are located in the 3q28 and 1p36 chromosome(45). Although *TP63* and *TP73* are evolutionarily older

to *TP53*, they are still considered as “younger siblings” of the *TP53* gene. Although, p63 and p73 were initially identified as developmental regulators, the roles of these genes in tumorigenesis were indispensible as mice that harbor loss of p63 and p73 were predisposed to tumor formation suggesting the role of these genes in tumor suppression(46).

1.4.1. Structural homology among the p53 family members

The p53 family members, p63 and p73 share significant structural homology with p53 particularly in the DNA binding domain(45). As a result, several functions among the family members tend to overlap with each other. However, there is less similarity between p53 versus p63 and p73 in the oligomerization domain and the transactivation domain (TAD). This might be one of the reasons that p63 and p73 does not form tetramers with p53 while activating other downstream targets. Interestingly, p63 and p73 are unique and encode multiple isoforms at both the N-terminus and C-terminus (Figure 2). In general, *TP63* and *TP73* are broadly classified into two categories, the isoforms that encode an acidic transactivation domain (TA) which produce either TAp63 or TAp73 and the isoforms that lack the acidic domain called ΔN isoforms, which produce either ΔNp63 or ΔNp73 (Figure 2)(45). The function of each of these isoforms is complex and tissue dependent. The full-length TAp63 and TAp73 isoforms in general are thought to function very similar to p53, while the shorter ΔN isoforms of p63 and p73, exhibit dominant negative effects against p53, TAp63 and TAp73(47-49). Similar, to the N-terminal isoforms, more than seven different kinds of C-terminal splice variants have been identified.

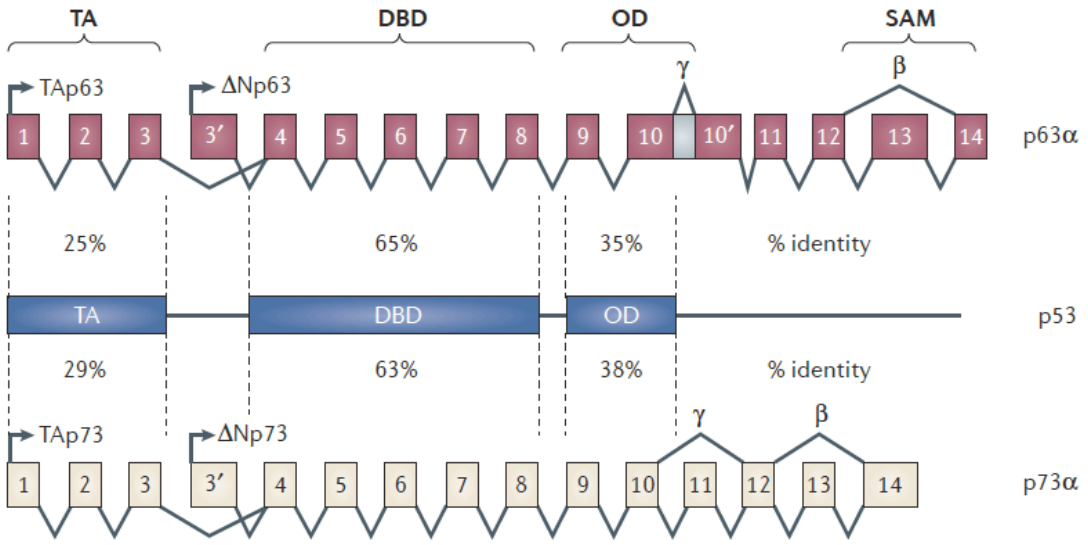

Figure 2: Sequence and structural homology of p53, p63 and p73. p63 and p73 share significant structural homology with p53 particularly in the DNA binding domain. Both, p63 and p73, have unique N-terminal isoforms, the full-length acidic transactivation isoform, TAp63 or TAp73 and the shorter isoform that lacks the transactivation domain called ΔNp63 or ΔNp73 is transactivated from the 3' cryptic promoter. Also, p63 and p73 encompass multiple C-terminal isoforms which requires further characterization.

(Figure is taken with permission from Su, X., Chakravarti, D. and Flores, E.R. p63 steps into the limelight: crucial roles in the suppression of tumorigenesis and metastasis. Nat. Rev Cancer. 2013; 13(2):136-43.) Licence Number: 351121299603.

The function of these C-terminal isoforms is under investigation and requires more characterization.

1.4.2. Mutational status of p63 and p73 in human cancers

More than 50% of human cancers harbor p53 mutations that makes it difficult to target the p53-pathway. These mutations may be a result of the tumor suppressive function exhibited by p53. However, compared to *p53*, the other family members, *p63* and *p73* are less frequently mutated (Figure 2). Recent, sequencing data from multiple human cancers has demonstrated that mutation rates in *p63* and *p73* are less frequent compared to any of the other tumor suppressor genes including p53 (Figure 3). This makes both p63 and p73 novel targets for therapeutic intervention. Importantly, due to the structural similarlity, the functions of the family members could be used to target the p53-pathway. One speculation as to why *p63* and *p73* are not mutated may be due to the important development roles played by the genes.

1.5. Developmental roles of p63 and p73

p63 and p73 knockout mouse models targeting the DNA binding domains had severe developmental abnormalities suggesting the roles of these genes as developmental regulators. p63 knockout mice had a deformed epidermal skin layer with improperly formed limbs and facial structures(50, 51). Most of these mice were embryonic lethal and died due to desiccation and water loss. The phenotype of the p63 knockout mice closely resembled the cleft lip and palate syndrome in humans referred to as the ectrodactyly ectodermal dysplasia (EEC). Upon further

characterization of the developmental roles of the N terminal isoforms using conditional *in vivo* mouse models, it was evident that splice variants have distinct functions. The TAp63 isoforms are required to maintain the skin stem cells in quiescence(50) while the loss of ΔNp63 isoforms prevents skin cell differentiation and targets the cells to be more pluripotent(52, 53). On the contrary, the p73 has been demonstrated to play critical roles in immune response and neural development. p73 knockout mice are embryonically viable but are characterized by a runted phenotype and shortly die a few weeks after birth(54, 55). Upon characterization of the specific roles played by the TAp73 and ΔNp73 isoforms, it has become evident that loss of these isoforms results in defective closure of the neural tube and growth of the sub-ventricular zone (SVZ) required for normal brain development(56-58). This highlights the important developmental functions of p63 and p73.

1.6. Tumor suppressive functions of p63 and p73

The roles of p63 and p73 in the development of skin and the neural development were well documented. However, the functional roles of these genes in other cellular processes were less studied. Given the structural similarity to p53, it was hypothesized that p63 and p73 could have similar function as they function as transcriptional factors as well. However, expression analysis from the human cancer tissues particularly from the colon, intestine and prostate demonstrated increased expression of p63 and p73(59-62). These findings suggested that both p63 and p73 could have oncogenic properties. To further add to the complexity, mouse models targeting p63 and p73 had an accelerated tumorigenesis(46). The tumor spectrum of

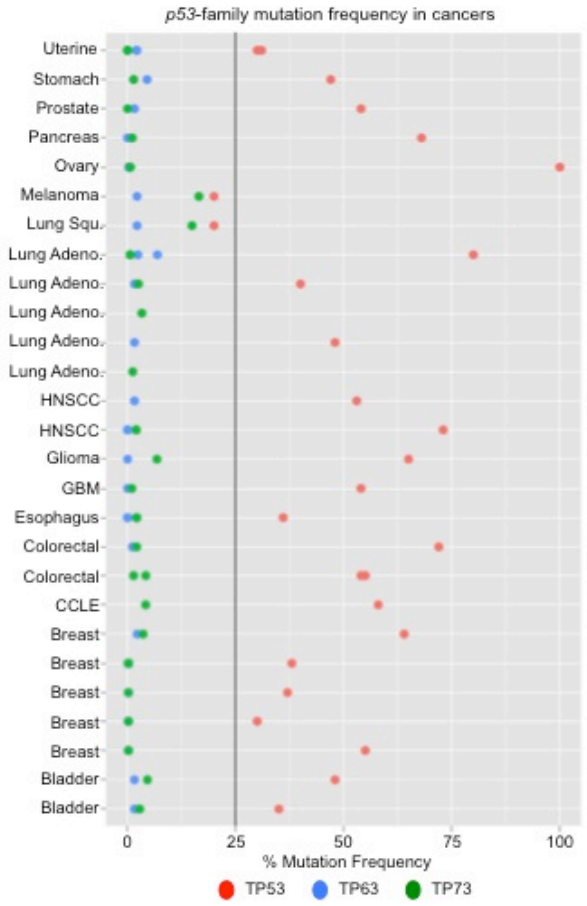

Figure 3: Graph representing the mutational status across p53-family members in human cancers. Unlike TP53, which is highly mutated, TCGA sequencing analysis has revealed that TP63 and TP73 are less frequently mutated.

the p63 and p73 deficient mice had significant carcinomas and was completely divergent from the p53-deficient mice that generally develop lymphomas and sarcomas. This data highlights the indispensable role of p63 and p73 in tumor suppression(46). However, the reason for the increased expression of p63 and p73 in the human tumor samples were not clear.

More recent experiments highlighted the independent roles of the N-terminal isoforms of p63 and p73. The antibodies used for detecting p63 and p73 did not differentiate the individual isoforms but rather p63 and p73 totally. It was demonstrated that TAp63 and TAp73, the full-length isoforms of p63 and p73 had functions similar to p53. *In vitro* experiments that express TAp63-gamma and TAp73-alpha in the human cancer cells induced cell death and cell cycle arrest independent of p53 function(63). Interestingly, in response to genotoxic stress, TAp63 and TAp73 were stabilized and had an increased effect in directing the cancer cells to undergo cell death. Further, to support the tumor suppressive notion of TAp63 and TAp73, mouse models targeting TAp63 and TAp73 were generated. Total loss of TAp63 in these mice had accelerated tumor spectrum with increased incidence of adenocarcinomas and metastasis(64, 65). It was also demonstrated that TAp63 functions to inhibit metastasis through Dicer regulated mechanism(66). Further, the roles of TAp63 in metabolism(67), stem cells(68) and polarity are currently being characterized. Similarly, the TAp73 knockout mice develop lung adenocarcinomas at a higher incidence, which correlates with a previous finding that p73-deficient mice have a 60% lung adenocarcinoma incidence(46). These findings

clearly demonstrate the key roles played by the TA isoforms of p63 and p73 in tumorigenesis and that they function as bonafide tumor suppressors.

1.7. Roles of ΔN isoforms of p63 and p73 in tumorigenesis

In vitro cell culture and *in vivo* experiments have delineated the functions of the different isoforms of p63 and p73 in tumorigenesis and development(63, 69). Particularly, the roles of the TAp63 and TAp73 as tumor suppressors are well documented. However, the roles of the ΔN isoforms of p63 and p73 are less studied and controversial. Studies from human cancer tissues detected p63 and p73 expression utilizing antibodies that do not differentiate the isoforms. Later, semi-quantitative analysis demonstrated that these tumor samples had increased expression of ΔNp63 and ΔNp73 suggesting the oncogenic roles of these isoforms in tumorigenesis(49, 70). Further, *in vitro* experiments expressing ΔNp63 and ΔNp73 inhibited apoptosis and cell cycle arrest in human cancer cells upon genotoxic stress(63, 71, 72). This may be due to the dominant negative effect of ΔN isoforms of p63 and p73 against p53, TAp63 and TAp73. Interestingly, in some instances, both ΔNp63 and ΔNp73 seem to respond upon DNA damage by activating genes involved in DNA repair like *BRCA2*, *Rad51* and *MRE11*(69). This suggests that ΔNp63 and ΔNp73 do have protective genomic physiological functions as well. Thus *in vitro* experimental evidence has clearly demonstrated the complexity within the roles of ΔN isoforms of p63 and p73 in tumorigenesis. This necessitates the generation of conditional knockout mice that are required to decipher the role of these isoforms in tumorigenesis.

Previous total knockout mouse models for ΔNp63 and ΔNp73 have highlighted the roles of these genes in development. The ΔNp63 knockout mouse has defects in epithelial skin development and differentiation(53) while the ΔNp73 knockout mice have defects in neural tube growth and closure(73). However, these models did not depict the roles of these genes in tumorigenesis. Hence, to test the role of these genes, our lab generated conditional knockout mouse models to determine whether ΔNp63(52, 74) and ΔNp73(74) function as oncogenes and tumor suppressors. The ΔNp63 mice were generated with a loss of one allele as ΔNp63 homozygous deficient mice are embryonic lethal. Surprisingly, the ΔNp63 and ΔNp73 deficient mice did not develop any tumors. Hence, to further accelerate tumorigenesis and also determine the role of these isoforms in the context of p53-loss, cohorts of mice harboring loss of ΔNp63 with p53 (ΔNp63+/-;p53-/-) and ΔNp73 with p53 (ΔNp73-/-;p53-/-) were generated.

1.8. Cancer cells and deregulated metabolism

Tumor cell metabolism has emerged as on the most important hallmarks of cancer in the recent years. There has been a tremendous impetus in understanding how a tumor evolves metabolically and adapts to the changes in the nutrients(75). Multiple research groups and studies have tried to delineate the complexities involved in the metabolic regulation. However, a complete characterization of these metabolic circuits is still being a challenge as tumor cells constantly evolve switching to multiple modes of nutrient sensing for survival. Research work is currently focused in understanding how to limit the nutrient consumption of these cancer cells or to deplete the nutrients to starve the cells, which could eventually reduce their

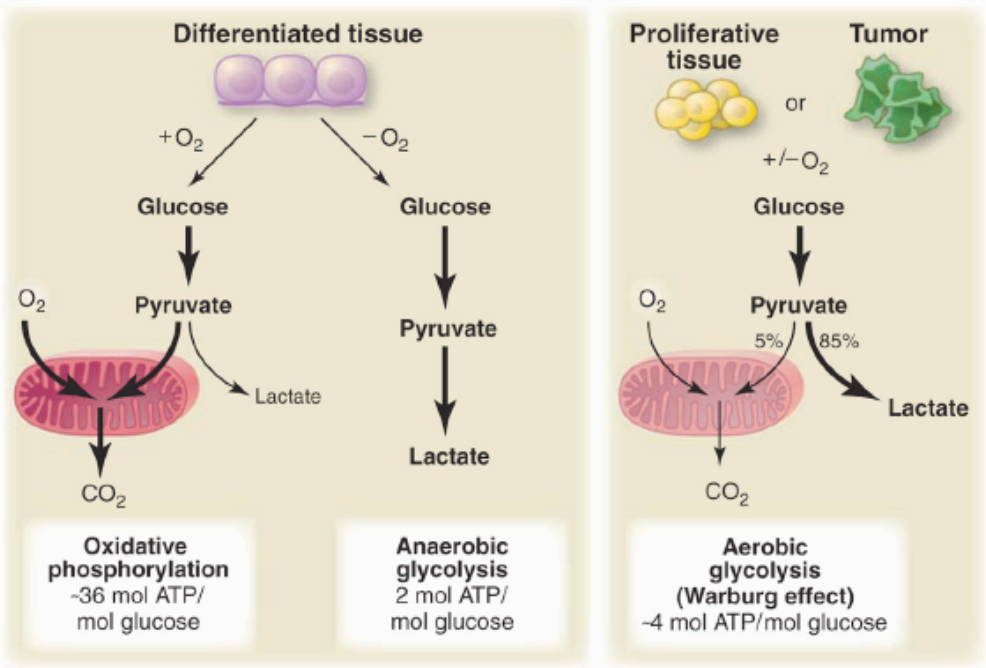

Figure 4: Warburg's hypothesis on tumor cell metabolism. Normal differentiated tissues or cells, utilize glucose as an energy source through the glycolysis pathway and enter into Kreb's cycle to produce more energy through oxidative phosphorylation. On the contrary, cancer cells, consume increased amounts of glucose and switch to produce lactate without entering oxidative phosphorylation. Cancer cells are dependent on this switch to aerobic glycolysis for proliferation.

(Figure is taken with permission from Vander Heiden, M.G., Cantley, L.C. and Thompson, C.B. Understanding the Warburg effect: The metabolic requirements of cell proliferation. Science. 2009; 324(5930):1029-1033.)

proliferation rates and reduce tumor growth and spread. However, this approach as been challenging as the cancer cells do not depend on only one nutrient but constantly switch to other nutrients for their survival and importantly the complexity of the metabolic machinery makes it challenging to target a single pathway. However, a clear understanding of these pathways makes it a viable option to therapeutically target the cancer cells.

1.8.1. Warburg Hypothesis on tumor cell metabolism

In the early 1950, a german scientist Otto von Warburg, postulated that cancer cells proliferate at much higher rates with increased consumption of glucose(76). This results in an increased activity of the glycolysis pathway with the cancer cells secreting an acidic product lactate instead of targeting the cells into mitochondrial respiration. Based on this hypothesis, it was evident that cancer cells have increased glucose consumption and lactate secretion (Figure 4)(75). The acidic lactate medium provided a better environment for the cancer cells to proliferate. Although the amount of ATP from the glycolytic pathway is less in comparison to the Kreb's cycle, the increased rate of proliferation in these cancer cells compensated for ATP loss with increased glucose consumption. Hence, to therapeutically target the glycolytic pathway to inhibit the cancer cells from proliferation and lactate production became a viable option. Current research work as also identified the key players that function as regulators of glucose uptake and those that could inhibit glycolytic pathway. Interestingly many of these regulators are activated by multiple transcription factors including *p53*(77).

However, based on Warburg's hypothesis, it was believed that cancer cells do not depend on mitochondrial respiration(78). However, more recently, some studies have shown that mutations in the mitochondria could have adverse effects in the nutrient sensing functions of the cancer cells. Importantly, cancer cells attain the ability to switch to nutrients like glutamine to continue proliferation. This sudden influx in glutamine consumption accelerates the mitochondrial respiration further promoting tumor cell proliferatio(75). Some of the current research focus is also now targeted towards inhibiting the oxidative phosphorylation pathway in cancers.

1.9. p53 and cancer cell metabolism

p53 functions as a transcriptional factor activating several downstream targets regulating classical cellular function like apoptosis, cell cycle arrest and cellular senescence. More recently, the roles of p53 in new cellular functions like stem cell maintenance, aging and metabolism have been explored. p53 has been demonstrated to regulate and activate genes involved in glycolysis and metabolism(77, 79). Primarily, p53 regulates *GLUT2* and *TIGAR* (TP53-inducible glycolysis and apoptosis regulator)(79, 80). *GLUT2* function to uptake glucose into the cell and p53 inhibits the activity of *GLUT2*. On the contrary, *TIGAR*, which is activated upon DNA damage by p53, encodes a bis-phosphatase enzyme that degrades fructose 2,6-bisphosphate and degrades glucose primarily inhibiting the glycolytic pathway(81). However, in some tissues like the intestine, TIGAR has been demonstrated to promote regeneration of the intestinal stem cells. As a result, expression of *TIGAR* in an intestinal tumor model promotes tumor formation(80). Another known regulator of p53 in metabolism is a gene involved in the

mitochondrial respiration referred to *GLS2*. GLS2 functions to release cytochrome C and regulate intracellular ROS in the cells. Upregulation of GLS2 releases cytochrome C resulting in induction of the apoptosis pathway(82). More recently, a p53 acetylation mutant mouse model demonstrated that p53 inhibits tumorigenesis by activating the metabolic regulators *GLS2*, *TIGAR* and *GLUT2(81)*. This further suggests that utilizing these metabolic regulators could function as a novel approach to target the deregulated metabolism of these cancer cells.

2.10. Islet amyloid polypeptide (IAPP)

IAPP is a transcriptional factor that encodes for amylin(83). Amylin is a 37-amino acid polypeptide that is cosecreted along with insulin from the beta cells of the pancreas. However, expression of IAPP has been detected in other tissues, which include cornea, thymus and the ovary. At physiological levels, IAPP functions to reduce insulin mediated glucose uptake, implicating its role in maintaining glucose homeostasis(84). IAPP has also been demonstrated to induce apoptosis in some cellular contexts(85). Some studies suggest that IAPP mediates apoptosis through activation of p21 independent of p53 function(86), while some studies relate to metabolic stress induced toxicity by IAPP upon glucose clearance in the liver(87). IAPP since is a secreted protein has been shown to function through the activity of the calcitonin and RAMP3 receptors(88). Additionally, a synthetic analog of IAPP called pramlintide involved in glucose regulation is used commercially to treat type I and type II diabetic patients(89).

2.11. Reactive Oxygen Species (ROS)

ROS is a common by-product that is produced from different metabolic processes in the cell. Although, ROS, a class of free radicals primarily originates from the mitochondria, recent evidence suggests that intracellular ROS accumulation occurs upon metabolic stress and inhibition of cellular nutrients like glucose or glutamine or inhibition of the phosphate pentose pathway(78). At physiological state, the levels of ROS in the cells are under tight regulation. Low levels of ROS as in the case of cancer cells, generally promote tumor cell proliferation by activating oncogenes and inducing stress. However, in instances when cells accumulate increased amounts of ROS due to metabolic stress, it results in apoptosis or cellular senescence(90, 91). Recent evidence suggests that targeting a class of phosphatidyl kinases in p53-deficient tumors results in ROS-induced cellular senescence in breast tumors. This highlights the role of ROS as tumor suppressor(91). However, in some cancers, ROS accumulation activates oncogenes like HIF-1alpha driving tumorigenesis representing its oncogenic functions(92). Hence one approach to target cancer cells is to increase ROS levels, which will result in apoptosis or senescence in the tumor cells. Interestingly, the effect of ROS can be controlled or reversed using antioxidants. Antioxidants like hydrogen peroxide and N-acetly cysteine could function to reverse the effect of intra-cellular ROS suppressing the oncogenic functions of ROS(80, 93).

2.12. Therapeutically targeting p53-deficient and mutant cancers

Therapeutically reactivating wild-type 53 or degrading mutant p53 in human cancers has been challenging. But the role of this p53-pathway in activating downstream cellular cascade to induce apoptosis or cell cycle arrest is indispensable. By utilizing the p53-family members, p63 and p73, a new paradigm approach can be taken to reactivate the downstream components of the p53-pathway. Importantly, by delineating the interplay among the family members a more clear strategy could be adopted to utilize p63 and p73 therapeutically(94).

TAp63 and *TAp73* are bonafide tumor suppressors. However, because of the dominant negative effect of ΔN isoforms against p53, TAp63 and TAp73, the expression levels of the TA isoforms of p63 and p73 remain significantly low(49, 60). Ideally, by targeting ΔNp63 and ΔNp73, if the repressive effect is reduced, *TAp63* and *TAp73* can compensate for p53 loss of function by activating downstream targets involved in multiple cellular processes. Hence, approaches to target *ΔNp63* and *ΔNp73* in human cancers could be explored as an option to treat p53-deficient cancers. One approach to target ΔN isoforms of p63 and p73 could be the identification and use of small molecule inhibitors that could be used selectively to downregulate ΔNp63 and ΔNp73. Second approach, could be to identify microRNA's (miRNA's) that specifically bind to ΔNp63 or ΔNp73 and repress its function. miRNA's are approximately 22-35nt oligomers that function to repress gene transcription. By activating these miRNA's specific to ΔNp63/ΔNp73 or by introducing them exogenously we can target ΔNp63 and ΔNp73 to treat these tumors. Additionally, small interfering RNA's (siRNA's) could be used to target

ΔNp63 and ΔNp73 in human cancers. Previously, the use of siRNA's to downregulate gene expression has been well demonstrated in human cancer cells. Recent studies have highlighted the use of *in vivo* delivery methods to deliver these siRNA's. Some methods use cholesterol or other polymer based substances to coat the siRNA oligomers. But with these methods the issue was poor resorption into the tissues and also degradation by the phagosomes. One approach to deliver siRNA's into the tissues that has a high penetrance is to coat the siRNA oligomers with nano-liposomes. Nano-liposomes are neutral particles that do not carry any charge. These particles could be delivered directly into the region of the tumor or by systemic methods and are not phagocytosed. These options could be explored further to target ΔNp63 and ΔNp73 in human cancers.

Alternatively, TAp63 and TAp73, very similar to p53 respond to genotoxic stress and DNA damage. Hence, to illicit a TAp63 and TAp73 response, both ΔN isoforms of p63 and p73 could be targeted along with treating the cells with a DNA damaging agent like cisplatin or doxorubicin. However, in the case of human cancers that harbor mutations in p53, this possibility would not feasible as mutant p53 forms hetero-tetramers with TAp63 or TAp73 and inhibits its transcriptional activity. Hence, to overcome the effects of mutant p53, we could simply target pathways that are independent of the p53 pathway.

2.13. Long non-coding RNAs: Disease and Development

Long non-coding RNAs (lncRNAs) are a class of RNA molecules that are >200 nt in length and do not code for proteins(95). These lncRNAs function very

similar to mRNAs and are involved in multiple cellular process and functions. lncRNAs comprise of the 80% of the non-coding part of the genome along with the other know miRNAs, pseudoRNAs, piwi and piRNAs(96, 97). lncRNAs were discovered in eighties but its functions were less characterized. However, unlike miRNAs or mRNAs, lncRNA are not evolutionary conserved. But with the advent of the sequencing efforts, the gene regulation and functions of the lncRNA in disease and development is being delineated. lncRNAs are classified into multiple types based on the position in the context of mRNA genes. The most common type of lncRNA is called long intergenic non-coding (linc) RNA whose function does not overlap with the neighboring genes(96). lncRNAs have been demonstrated to play diverse roles in gene regulation. They perform these functions by acting as scaffolding proteins, decoys, cofactors and guides(97). However, current understanding of these lncRNAs is limited to *in vitro* experiments and additional *in vivo* models should be developed to completely characterize its function. The functional characterization of these lncRNAs is gaining importance because of its implication in diseases like cancers. *HOTAIR* is one such lncRNA that is significantly overexpressed in prostate cancer(98). By determining the expression pattern of these lncRNAs they can serve as biomarkers for disease prognosis. Additionally, lncRNA can function as regulators or effectors of gene function. These roles of lncRNAs determine whether they function as tumor suppressors or oncogenes.

2.14. lncRNAs and p53 regulation

p53 functions in multiple ways to regulate genomic functions. p53 apart from its classical roles in apoptosis and cell cycle arrest also functions to mediate its

effectors functions by activating lncRNAs. The lncRNAs regulated by p53 are often grouped as “effectors”. This class of lncRNAs, which include *linc-p21*, *PANDA* and *H19* play significant roles in preventing, cell proliferation and prevent tumorigenesis(99-102). Conversely, several lncRNAs function to regulate p53 function which include MALAT1, MEG3 and ROR. Thus, it is evident that regulation of lncRNAs plays a significant role in regulating gene function. By understanding the function of these lncRNAs in regulating mRNA expression we can delineate novel pathways that could help design new therapies or serve as predictors of disease outcome.

2. Chapter 2. Materials & Methods

Chapter 2. Materials & Methods

Contents of this chapter is based on Venkatanarayan, A., Raulji, P., Norton, W., Chakravarti, D., Coarfa, C., Su, Xiaohua., Sandur, S.K., Ramirez, M.S., Lee, Jaehyuk., Kingsley, C.V., Sananikone, E.F., Rajapakshe, K., Naff, K., Parker-Thornburg, J., Bankson, J.A., Tsai, K.Y., Gunaratne, P.H. and Flores, E.R. IAPP driven metabolic reprogramming induces regression of p53-deficient tumors *in vivo*. *Nature.* 2015; 517(7536),626-630. doi:10.1038/nature13910.

2.1. Generation of ΔNp73 Conditional Knockout Mice

The cre-loxP strategy was used to generate the *ΔNp73* conditional knockout allele (*ΔNp73fl*). Genomic *p73* DNA from intron 3 to intron 3’ was amplified from BAC clone DNA (BAC RP23-186N8, Children's Hospital Oakland Research Institute). LoxP sites flanking exon 3’ of *p73* and neomycin (*neo*) gene flanked by frt sites inserted in intron 3’ were cloned into pL253(103). Mouse embryonic stem cells (G4) electroporated with the targeting vector were analyzed by Southern blot analysis for proper targeting of the *ΔNp73* allele. Resulting chimeras were mated with C57BL/6 albino females and genotyped as described below. Mice with germ line transmission of the targeted allele (conditional, flox neo allele, fn) were crossed to the FLPeR mice to delete the neo cassette. Resulting progeny were intercrossed with Zp3-Cre (C57BL/6) transgenic mice(104). *ΔNp73fl/+; Zp3-Cre* females were mated with C57BL/6 males to generate *ΔNp73+/-* mice. The *ΔNp73+/-* mice were intercrossed

to generate *ΔNp73-/-* mice. Compound mutant mice were generated by intercrossing the *ΔNp63+/-* and *ΔNp63fl/fl*(52) and the *ΔNp73-/-* and *ΔNp73fl/fl* mice with the *p53-/-* mice(22). All procedures were approved by the IACUC at U.T. M.D. Anderson Cancer Center.

2.2. Genotyping

Genomic DNA from tail biopsies was genotyped by Southern blot analysis by digesting genomic DNA with AflII and HindIII or by PCR using the following primers and annealing temperatures: 1) for wild-type: wt-F, 5'- ACAGTCCTCTGCTTTCAGC-3' and wt-R (fl-R), 5'- CACACAGCA CTGGCCTTGC -3', annealing temp: 58°C, 2) for ΔNp73flox: fl-F, 5' – CATAGCCATGGGCTCTCCT - 3' and fl-R (wt-R), 5'–TGTCCTGCTGCTGGTTGTAT- 3', annealing temp: 63°C, 3) ΔNp73floxneo: flneo-F, 5'-GGGAGGATTGGGAAGACAAT-3' and flneo-R, 5'-TGTCCTGCTGCTGGTTGTAT-3' annealing temp:60^0C and 4) for ΔNp73KO: ko-F, 5'- CCTAGCCCAAGCATACTGGT-3' and wt-R, 5'-TGTCCTGCTGCTGGTTGTAT-3' annealing temp: 58°C. Primers used to genotype for the Cre gene are as follows: Cre-F, 5'–TGGGCGGCATGGTGCAAGTT-3' and Cre-R, 5'–CGGTGCTAACCAGCGTTTTC-3', annealing temp: 60° C. The primers for ΔNp63WT, ΔNp63KO, ΔNp63flox and p53 were previously described(52, 105).

2.3. Cell Lines

Mouse embryonic fibroblasts (MEFs) for the indicated genotypes were generated as described previously(63). Human lung adenocarcinoma cells (H1299), colorectal adenocarcinoma cells (SW-480) and breast adenocarcinoma cells (MDA-MB-468) were purchased from ATCC and cutaneous SCC cell lines (SRB12, COLO16) were

a gift from Dr. K. Y. Tsai. The MEF's, SW-480 and MDA-MB-468 cells were cultured in DMEM (Cellgro) and H1299 cell lines were cultured in RPMI 1640 (Cellgro). The SRB12 and COLO16(106) cell lines were grown in DMEM/Ham's F12 50/50 (Cellgro). All cell lines used in the study tested negative for mycoplasma.

2.4. Immunhistochemistry

Mice thymic lymphomas or thymii were dissected, fixed in 10% formalin, and embedded in paraffin. Sections were dewaxed in xylene and re-hydrated using decreasing concentrations of ethanol. Antigens were unmasked in citrate buffer unmasking solution (Vector Laboratory) followed by incubation with blocking solution, and 18 hour incubation at 4^0C with the following antibodies: cleaved caspase 3 (1:200)(Cell Signaling), PCNA (1:500)(Cell Signaling), malondialdehyde (1:50)(Abcam). Visualization was performed using the ImmPact DAB peroxidase substrate kit (SK4105, Vector Laboratories) and counter-stained with Hematoxylin (H-3401, Vector Laboratories). The slides were mounted using VectaMount (H-5000, Vector Laboratories). Images were acquired using a Zeiss Axio microscope and analyzed with ProgRes Capture Pro 4.5 software.

2.5. SA-β-gal staining

SA-β-gal staining on mouse thymic lymphoma was performed as described previously(19).

2.6. Quantitative real time PCR

Total RNA was prepared from MEFs or mouse tissues using TRIzol reagent (Invitrogen)(50, 65, 107). cDNA was synthesized from 5mg of total RNA using the

SuperScript® III First-Strand Synthesis Kit (Invitrogen) according to the manufacturer's protocol followed by qRT PCR using the SYBR Fast qPCR master mix (Kapa Biosystems). qRT-PCR was performed using a ABI 7500 Fast Real-time PCR machine. Primers for mouse *TAp63, ΔNp63, PUMA, Noxa, bax, PML, p16* and *p21(50, 65)* and human *TAp63, ΔNp63* and *GAPDH* were used as described previously (66, 68). Human primers for *PUMA, Noxa, bax, PML, p16, p21* were used as described previously(19) and *GLS2* and *TIGAR* as described previously. Mouse primers for *TAp73* are FOR:5'- GCACCTACTTTGACCTCCCC-3', REV: 5'-GCACTGCTGAGCAAATTGAAC-3', *ΔNp73* are FOR: 5'-ATGCTTTACGTCGGTGACCC-3', REV: 5'-GCACTGCTGAGCAAATTGGAAC-3', *IAPP* are FOR: 5'- CTCCAAACTGCCATCTGAGGG-3', REV: 5'-CGTTTGTCCATCTGAGGGTT-3'. Human primers used for *TAp73* are FOR: 5'-CAGACAGCACCTACTTCGACCTT-3', REV: 5'-CCGCCCACCACCTCATTA-3' and for Δ*Np73* are FOR: 5'- TTCAGCCAGTTGACAGAACTAAG-3', REV: 5'-GGCCGTTTGTTGGCATTT-3'.

2.7. Western blot analysis

Fifty micrograms of protein were electrophoresed on a 10% or 15% SDS PAGE and transferred to PVDF membrane as described previously(50, 65, 107). Blots were probed with anti-p63 (1:500) (4A4, Santa Cruz), anti-TAp63 (1:1000) (BioLegend), anti-TAp73 (1:500)(IMG-246, Imgenex), anti-p73 (Mouse) (1:250)(IMG-259A, Imgenex), anti-p73 (1:1000) (human) (EP436Y, Abcam), anti-p53 (WT) (1:1000)(CM5, Vector Labs), anti-IAPP (1:1000)(ab103580, Abcam), anti-His (1:1000)(G18, Santa Cruz), anti-Hexokinase II (1:10000)(C64G5, Cell Signaling),

anti-calcitonin receptor (1:1000)(ab11042, Abcam), RAMP3(1:1000)(H125, Santa Cruz), and cleaved caspase 3 (1:1000)(Asp 175, Cell Signaling), at 4^{o}C for 18 hours followed by incubation for one hour at room temperature with the appropriate secondary antibodies conjugated to horseradish peroxidase (1:5000)(Jackson Lab). b-actin (Sigma 1:5000) was used as a loading control. Detection was performed using the ECL Plus Kit (Amersham) following the manufacturer's protocol and x-ray autoradiography.

2.8. Characterization of thymus using flow cytometry

Thymii from 4 week old mice and thymic lymphomas from 10 week old mice were collected 48 hours after adenovirus infection. Single cells were obtained by homogenizing the thymii through a 0.75 mM filter. Cells were stained with CD3-PE (145-2C11), CD4-PerCP-Cy5.5 (RM4-5), CD8-APC (53-6.7), CD45-FITC (30-F11)(BDPharmingen), AnnexinV-Pacific Blue (A35122, Life Technologies), and 7-AAD (V35124, Invitrogen) and sorted using a BD Aria Cell Sorter or analyzed using the LSR Fortessa Cell Analyzer and FlowJo software.

2.9. Chromatin Immunoprecipitation (ChIP)

MEFs were grown to near confluence at passage 2 on DMEM media with 10% serum as previously described(63). Thymocytes from 6-week-old mice were collected 48 hours after adenovirus infection. Cellular proteins were cross-linked to DNA using 1% formaldehyde and chromatin was prepared as described previously(50, 65, 107). TAp63 and ΔNp63 ChIP analysis was performed using a pan-p63 antibody (4A4, Santa Cruz) as described previously and the TAp73 ChIP

was performed using a TAp73 antibody (ab14430, Abcam) and ΔNp73 ChIP was performed using a p73 antibody (IMG 259A, Imgenex). Putative TAp63 and TAp73 binding sites were scanned 3000bp upstream of the 5'UTR and in intron 1 of the IAPP gene (NCBI Reference Sequence: NC_000072.5). qRT–PCR was performed by using primers specific for the indicated regions of the *IAPP* promoter: Site 1 (-406) -forward 5'-GTACATGAGGCTTGCTAAAGGC-3' and (-329) -reverse 5'-AGACCACAGAAAGCTCCCTC-3', Site 2 (+761)-forward 5'GCACAGAGTTGTTGCT-3' and (+842) – reverse 5'-CACACATGCAATGACAAACATTCT-3', and non-specific site (+74911)- forward 5'-GGTGGCTCCTGTAGTATGTCT-3' and (+75011) - reverse 5'-ACATCTCTAACAGCAAGAGACTCC-3'. Similarly, putative ΔNp63 and ΔNp73 binding sites were scanned 10000 bp upstream of the 5'UTR and in intron 1 of *TAp63* and *TAp73*. qRT-PCR was performed by using the primers specific for the indicated regions on the *TAp63* promoter: Site 1 (-41) –forward 5'-CAGGAGCTCTCAAATCAAGTCAGA-3' and (+37) –reverse 5'-ATCACAGAAGCCAGGACTTGTCAC-3' , and non-specific site (-3030) - forward 5'-GCTATAAATGTTTCCATGTGATGGATTGC-3' and (-2973) - reverse 5'-TGCAGACTTAGCTATGGTCTCTTG-3'. Similarly, qRT-PCR was performed using the primers specific for the indicated regions on the *TAp73* promoter: Site 1 (-1103) –forward 5'- CTAGCACACCAATCCAAGGAAAGA and (-1059) –reverse 5'-GCCTGCAGTCCGGGTTT-3' and non-specific site (-2488) –forward 5'ACTAGACCTCTGTACTTGTGAACATACATTT-3' and (-2382) –reverse 5'-GCACTCTCAFFATCCTGTAACAAAA-3'.

2.10. Dual luciferase reporter assay

Luciferase assays were performed using *p53-/-;p63-/-* and *p53-/-;p73-/-* MEFs as described previously(69). To generate the luciferase reporter gene (pGL3-IAPP), the DNA fragment containing the TAp63/TAp73-binding site identified by ChIP was amplified from C57BL/6 genomic DNA by PCR with the following primers containing 5' XhoI and 3' HindIII cloning restriction enzyme sites: IAPP 5'-ATACTCGAGGCACATCTAAGTTCATGAAGTGG-3'(forward) and 5'-ATAAAGCTTAGTTAACTCCTCAGTGGCCTTG-3' (reverse). Similarly, a mutant version of the luciferase reporter gene (pGL3-IAPP^{Mut}) was generated using QuikChange Lightning (Agilent Technologies) following the manufacturer's instructions. The following primers 5' CATGAAGTGGGCAATTATAAAAGTACATCAGGGTTGCTAAAGGCTTTT-3'(forward) and 5'-AAAAGCCTTTAGCAACCCTGATGTACTTTTATAATTGCCCACTTCATG-3'(reverse) were used to generate the mutant version.

2.11. Reverse Transfection

Cells were transfected with 50 nM siΔNp63 (SASI_Hs02 00328367)(Mission siRNA, Sigma), siΔNp73 (SASI_Hs02_00326884)(Mission siRNA, Sigma), siTAp63 (SASI_Hs01_00246771) (Mission siRNA, Sigma), siTAp73 (SASI_Hs02_00339573) (Mission siRNA, Sigma), siRAMP3 (SASI_Hs01_00199036)(Mission siRNA, Sigma), siCalcitonin receptor (SASI_Hs01_00077738)(Mission siRNA, Sigma), siIAPP (SASI_Hs01_00183962) (Mission siRNA, Sigma) or siNT(SIC_001)(Mission siRNA, Sigma) using Lipofectamine RNAiMAX (Invitrogen). The mixture of siRNA and

Lipofectamine were combined together and added to the well followed by the addition of 200,000 cells/well in a 6-well dish.

2.12. Transfections - Generation of IAPP and Hexokinase II expressing cells

$3x10^5$cells were plated in 10cm dishes. MEFs and human cancer cells were transfected with 8 mg Myc-DDK-IAPP (RC215074)(Origene) or 3.3mg HKII (Plasmid #25529)(Addgene) using X-tremeGENE HP (Roche) and incubated for 48-60hrs. Cells were selected with G418, MEFs (350mg/ml) and human cancer cells (500mg/ml) for a period of 9 days.

2.13. Secreted IAPP Protein concentration

Twelve hours after knockdown of ΔNp63/ΔNp73 in human cancer cells, fresh serum free media was added to the cells. Following a sixty-hour incubation, the media was collected and concentrated using Amicon Ultra-15 Centrifugal Filter Units (UFC901008, EMD Millipore).

2.14. RNA Sequencing and Analysis

Five µg of polyA+ RNA were used to construct RNA-Seq libraries using the standard Illumina protocol. Mouse mRNA sequencing yielded 30-40 million read pairs for each sample. The mouse mRNA-Seq reads were mapped using TopHat(108) onto the mouse genome and build UCSC mm9 (NCBI 37) and the RefSeq mouse genes. Gene expression and gene expression differences were computed using Cufflinks(108). For each species, a combined profile of all samples was computed; mRNA abundance was mean-centered and Z-score transformed for each mRNA individually. Principal component analysis was executed using the implementation within the R statistical analysis system. Hierarchical clustering of

samples was executed by first computing the symmetrical sample distance matrix using the Pearson correlation between mRNA profiles as a metric, supervised sample analysis was performed using the t-test statistics, and heatmaps were generated using the heatmap.2 package in R. For gene signatures and pathway analysis gene list from the RNA-Seq comparing *ΔNfl/fl;p53-/-* versus *ΔNp63Δ/Δ;p53-/-* and *ΔNp73Δ/Δ;p53-/-* were obtained at a p-value <0.01. The genes upregulated in the *ΔNp63Δ/Δ;p53-/-* and *ΔNp73Δ/Δ;p53-/-* and down regulated in the *ΔNfl/fl;p53-/-* were selected. The relative fold change of the genes were calculated and sorted from highest to lowest. Genes with a greater than 1.5 fold-increase were selected and run through the Ingenuity Pathway Analysis (IPA) (Ingenuity Systems) to screen for pathways and processes. Genes from the selected pathways were cross-referenced with the Gene Set Enrichment (GSEA)(Broad Institute) data analysis, DAVID Bioinformatics Resource 6.7 and GSEA implementation at the Molecular Signature Database (MSigD)(109).

2.15. Magnetic Resonance Imaging

MRI imaging was performed at 10 weeks of age when the tumours were established and the volumes range from 2.3 mm^3 to 5 mm^3. To reduce the variation between different groups of mice, a cohort of n=5 with similar tumour volumes was established and tumors regression was monitored by MRI. All mice were scanned once a week for a period of 35 weeks on a 7-Tesla, 30-cm bore BioSpec MRI system (Bruker Biospin Corp., Billerica, MA) .

2.16. Hyperpolarized Magnetic Resonance Spectroscopy

Dynamic MR spectroscopy (MRS) of hyperpolarized (HP) [1-^{13}C] pyruvate was performed *in vivo* in tumour bearing mice. To achieve polarization, a 26-mg sample of pyruvic acid (Sigma-Aldrich, St. Louis, MO) with 15 mM of OX063 radical (GE Healthcare, Waukesha, WI) and 1.5-mM Prohance (Bracco Diagnostics Inc., Monroe Township, NJ) was polarized in a HyperSense DNP system (Oxford Instruments, Abington, Oxfordshire, UK) as previously described(110, 111). The frozen sample was dissolved in a 4-mL buffer containing 40-mM TRIS, 80-mM NaOH, and 50-mM NaCl, resulting in a final isotonic and neutral solution containing 80-mM [1-^{13}C] pyruvate. A dual-tuned 1H/13C linear RF volume coil with 72mm ID was used in conjunction with imaging gradients with 12cm ID. For anatomic imaging, the ^{1}H channel was used in transmit/receive mode. In addition to localizing scans, flow-weighted oblique gradient echo images (TE = 1.4ms; TR = 55ms; 90° excitation; 3cm x 3cm FOV encoded over a 64 x 64 image matrix) were acquired to confirm that the slice prescription for 13C measurements would not be obfuscated by signals originating from within the heart. For carbon spectroscopy, the RF volume coil was used in transmit-only mode in conjunction with a custom-built 15-mm ID ^{13}C surface coil for signal reception. After dissolution, 200 µL of the HP [1-^{13}C] pyruvate solution was administered to the animals via tail-vein catheter. A slice-selective pulse-acquire sequence (TR = 1,500 ms; 15° flip angle; 5 KHz spectral bandwidth; 2048 spectral points; 8-mm oblique slab; 120 repetitions) was used for dynamic spectroscopy beginning approximately 15s prior to injection. Data were processed to generate spectral time-courses of the HP-pyruvate and its lactate product.

Spectra were phase adjusted and the area under the spectral peaks associated with [1-^{13}C] pyruvate and [1-^{13}C] lactate were integrated over time to reflect the overall signal observed from each metabolite over the course of the measurement. Total lactate signal, which could only arise from interaction of HP pyruvate with relevant metabolic enzymes, was normalized to the total signal from pyruvate.

2.17. Glycolysis Stress Assay

Extra-cellular acidification rate (ECAR) was measured using the extracellular flux analyzer (SeaHorse Bioscience XF96) following the manufacturer's instructions. Forty-eight hours after transfection, the cells were plated at a density of $1.5x10^4$ cells per well in the XF 96-well cell culture plates. Twenty-four hours after seeding, the culture medium was replaced with 180 ml of running medium and incubated for 1 hour at 37^0C in a non-CO_2 incubator. Before calibration, 20 ml of 50 mM glucose, 11 mM oligomycin and 650 mM 2-DG were aliquoted into each port in the sensor cartridge. ECAR was measured after the addition of glucose and oligomycin and before the addition of 2-DG. Extra-cellular acidification rate was normalized to mpH/min.

2.18. Glucose Uptake Measurement

Glucose uptake was calculated as a measure of glucose dependent proton secretion from the maximum and basal glucose consumption after addition of 20 ml of 50 mM glucose and measured using the extracellular flux analyzer (SeaHorse Biosciences XF96).

2.19. Glucose-6-phosphate Assay

Glucose-6-phosphate was measured using the Glucose-6-phosphate assay kit (ab83426, Abcam) following the manufacturer's instructions. Forty-eight hours after transfection, $2x10^6$ cells were collected, homogenized and passed through a 10 kD spin-column filter. The eluate was collected and glucose-6-phosphate enzyme and substrate reaction was performed for 30 min and absorbance was measured at 450nm.

2.20. Proliferation Assay

The transfected human cancer cells were plated at a density of $5x10^3$ cells in 6 replicates in a 96-well dish. Twelve hours later, the cells were labeled with 10 mM EdU (5'-ethynyl-2'-deoxyuridine) for a period of 8 hours. The assay was performed using the Click-iT EdU microplate assay (Invitrogen). Images were obtained using a Zeiss Axio fluorescent microscope and analyzed using the AxioVision Image 4.5 software.

2.21. Apoptosis Assay

Cells were plated at a density of $1x10^4$ cells in 6 replicates in a 96-well dish. Twelve hours later, the cells were washed with 1X Annexin binding buffer and a cocktail of 5ml Annexin V-Alexa Fluor 488 for 100mg/ml propidium iodide (PI) and 2mg/ml Hoechst 33342 (Invitrogen) was added. Images were captured using the Zeiss fluorescent microscope and Axiovision Image 4.5 software. Quantification of the percent apoptosis was obtained using a high-throughput immunofluorescence plate reader (Celigo).

2.22. ROS Assay

Cells were plated at a density of $1x10^4$ cells in 6 replicates in 96-well dish. Twelve hours later, the cells were incubated with a cocktail of 5 mM concentration of CellROX Deep Red Reagent (C10422, Invitrogen) and 2 mg/ml Hoechst 33342(Invitrogen) for 45 minutes at 37^{o}C. Images were captured using a Zeiss fluorescent microscope and Axiovision Image 4.5 software. Quantification of the percent ROS was obtained using a high-throughput immunofluorescence plate reader (Celigo)(112).

2.23. *In vitro* Adeno-Cre Infection

ΔNp63fl/fl;p53-/- and *ΔNp73fl/flp53-/-* MEFs were plated at a density of $2.5x10^5$ cells in 10 cm dishes before infection. Twelve hours later, MEFs were infected with Adeno-CMV-mCherry or Adeno-CMV-Cre-mCherry (Gene Transfer Vector Core Facility, University of Iowa). The cells were infected at an MOI of 6000 particles/cell. The efficiency of infection was quantified by assessing mCherry positive cells.

2.24. *In vivo* Adeno-virus Infection and IVIS Lumina Imaging

All mice were anesthetized using isoflurane and 2% oxygen and placed on a custom bed. An incision was performed to expose the sternum. Using a 28.5G U100 Insulin syringe, Adeno-mCherry/Adeno-Cre-mCherry (Gene Transfer Vector Core Facility, University of Iowa), Adeno-IAPP-mCherry(Vector Labs) or Adeno-shIAPP-U6-mCherry (TRCN0000416196, Mission shRNA)(Vector Labs) was surgically administered by intra-thymic injection ($5x10^{12}$ viral particles/gram of body weight) through the 2nd and 3rd sternum. The incision was sealed using wound clips and

mice were allowed to recover. To determine the efficiency of the *in vivo* viral delivery to the thymic lymphoma, IVIS Lumina Imaging (Perkin Elmer) was performed 48 hours later. Images were captured using a Mid-600 series bandwidth filter and analyzed using the Living Image® data analysis software.

2.25. shRNA Knockdown

shRNA plasmids for TAp63 (Clone ID: V3LMM_508694) and TAp73 (Clone ID: V3LMM_438557) were obtained from the MD Anderson shRNA core facility (Open Biosystems). 293T cells were plated at a density of 2.5 x 10^5 cells in 10 cm dishes. Three micrograms of shRNA and packaging vectors were transfected as described previously. Cells were selected using puromycin (3 mg/ml) for 7 days.

2.26. *In vitro* and *in vivo* administration of 2-Deoxy-D-glucose

1x10^4 cells were plated in 6 replicate wells in a 96-well dish. Twelve hours later, the human cancer cells were treated with 50 mM final concentration of 2-Deoxy-D-glucose (2-DG) (D8375-5G, Sigma) for 1 hour. Similarly, 2-DG (500 mg/kg of tumour weight)(D8375-5G-Sigma) was administered directly into the lymphoma of mice as described earlier(110).

2.27. **N-acetyl-L-cysteine treatment**

1x10^4 cells were plated in 6 replicate wells in a 96-well dish. Twelve hours later, cells were treated with N-acetyl-L-cysteine (NAC) (2 mM)(A8199, Sigma) final concentration for a period of 1 hour.

2.28. Amylin and caspase inhibitor treatment

2x10^5 cells were plated in triplicate in a 6-well dish. Twelve hours later, cells were treated with Amylin peptide (5mM) (A5972, Sigma) or with a Caspase 1

inhibitor (20mM)(Z-YVAD-FMK-218746, Calbiochem) for a period of 48 hours.

2.29. *In vitro* and *in vivo* administration of Pramlintide Acetate

$2x10^5$ cells were plated in duplicate in a 6-well dish. Twelve hours later, cells were treated with 10 mg/ml Pramlintide acetate (AMYLIN Pharmaceuticals) or placebo for a period of 48 hours. Pramlintide acetate (AMYLIN Pharmaceuticals) or placebo (sodium acetate/acetic acid) was surgically administered through non-invasive intra-thymic injection using a multiple dose protocol of Pramlintide acetate (30 mg/gram of tumour weight). One injection per week for three weeks was administered directly into the thymic lymphoma of the animal. Another cohort of mice was treated bi-weekly for 3 weeks by intra-venous (I.V.) tail-vein injection of Pramlintide acetate (45 mg/kg body weight) or placebo. The investigator was blinded to the treatment administered to each mouse. Tumour volumes were monitored weekly by MRI. Health and blood glucose levels of the treated animals were monitored weekly.

2.30. *In vitro* and *In vivo* administration of Calcitonin receptor antagonist

$2x10^5$ cells were plated in duplicate in a 6-well dish. Twelve hours later, cells were treated with Calcitonin receptor antagonist (1 nM)(AC187, Tocris Bioscience) for a period of 48 hours with or without simultaneous Pramlintide treatment. Similarly, a chronic dose of Calcitonin receptor antagonist (1 nM/gram of tumour weight) was administered through non-invasive intra-thymic injections with one injection every week for a period of three weeks with or without simultaneous Pramlintide treatment. Tumour volume was monitored and measured weekly by MRI.

2.31. Survival Analysis

Survival analysis was conducted for the IAPP, RAMP3 and CalCR gene in the following datasets: the Memorial Sloan Kettering Cancer Center and the TCGA Cancer cohort. We considered four major cancer types with high p53 mutation rates, which include lung squamous cell carcinoma(113), head & neck squamous cell cancer(114), basal breast cancer(115), and colon cancer(116). The co-expression of the three genes was analyzed in cases only with p53-mutation. In all cases, we considered gene expression changes above or below 2 standard deviations with respect to the normal controls. The log-rank test and Cox P test was used to assess significance between the samples with or without expression changes of the IAPP, RAMP3 and CalCR gene using the cBioPortal for cancer genomics(117).

2.32. Statistics

Sample size for mouse cohorts in each experiment was chosen based on the penetrance of the thymic lymphoma phenotype of the *p53-/-* mouse model (80%). Twenty to thirty mice were used for survival analyses. Data were analysed using a one-way ANOVA test or a Student's t-test (two-sided) was used for comparison between two groups of data. A p-value of 0.05 was considered significant. Data are represented as mean ± s.e.m.

3. Chapter 3: *ΔNp63* and *ΔNp73* function as oncogenes in a p53-deficient model of thymic lymphoma

Chapter 3. *ΔNp63* and *ΔNp73* function as oncogenes in a p53-deficient model of thymic lymphoma

Contents of this chapter is based on Venkatanarayan, A., Raulji, P., Norton, W., Chakravarti, D., Coarfa, C., Su, Xiaohua., Sandur, S.K., Ramirez, M.S., Lee, Jaehyuk., Kingsley, C.V., Sananikone, E.F., Rajapakshe, K., Naff, K., Parker-Thornburg, J., Bankson, J.A., Tsai, K.Y., Gunaratne, P.H. and Flores, E.R. IAPP driven metabolic reprogramming induces regression of p53-deficient tumors *in vivo*. *Nature.* 2015; 517(7536),626-630. doi:10.1038/nature13910.

3.1. Introduction & Rationale

Most human cancers harbor inactivating or gain of function mutations in the *p53* tumor suppressor gene(118). In order to develop a better therapeutic alternative to treat these human cancers with p53 mutation, we explored the role of the p53-family members *p63* and *p73*(119). However, the function of p63 and p73 is complex due to the presence of multiple splicing isoforms, namely the TA and ΔN isoforms(45). Previous research work has demonstrated that both *TAp63* and *TAp73* function as bonafide tumor suppressors(65, 120). However, the role of the ΔN isoforms has been controversial due to its dominant negative functions(60). Both ΔNp63 and ΔNp73 function as dominant negative inhibitors of p53*,* TAp63 *and* TAp73. *In vitro* experiments suggest that *ΔNp63* and *ΔNp73* could function both as tumor suppressors and oncogenes(72, 121). Hence, to determine the role of the ΔN

isoforms of p63 and p73 in tumorigenesis, we generated conditional knockout mouse models for ΔNp63 (ΔNp63fl/fl)(74) and ΔNp73 (ΔNp73fl/fl)(74). These mice were further crossed to a Zp3 transgenic mouse to generate a ΔNp63+/-(52) and a ΔNp73-/- (74)compound mouse.

To further accelerate tumorigenesis and also understand the role of ΔNp63 and ΔNp73 in the context of p53 deficiency, I crossed the ΔNp63+/- mice to the p53-null mice and generated a ΔNp63+/-;p53-/- mice cohort and similarly, the ΔNp73-/- mice were crossed to the p53-null mice to generate a ΔNp73-/-;p53-/- mice. In this chapter, I further characterize the tumor spectrum obtained from these double mutant compound mice. I also investigate the response of these double mutant compound mice in response to genotoxic stress. Finally, I perform an acute deletion of the ΔN isoforms in the p53-deficient thymic lymphomas *in vivo* to determine the mechanistic function of the ΔN isoforms of p63 and p73 and also the interplay among the *p63* and *p73* isoforms in cancer.

3.2. Results

3.2.1. ΔNp63 and p53 or ΔNp73 and p53 double deficient compound mice have reduced thymic lymphomagenesis

A cohort of ΔNp63+/-;p53-/- (n=30) and ΔNp73-/-;p53-/- (n=30) mice were generated along with a cohort of p53-/- mice (n=30). I observed that the mice double deficient for ΔNp63 and p53 or ΔNp73 and p53 had a significant reduction in the thymic lymphomagenesis compared to the p53-/- mice (Figure 5a). The ΔNp63+/-

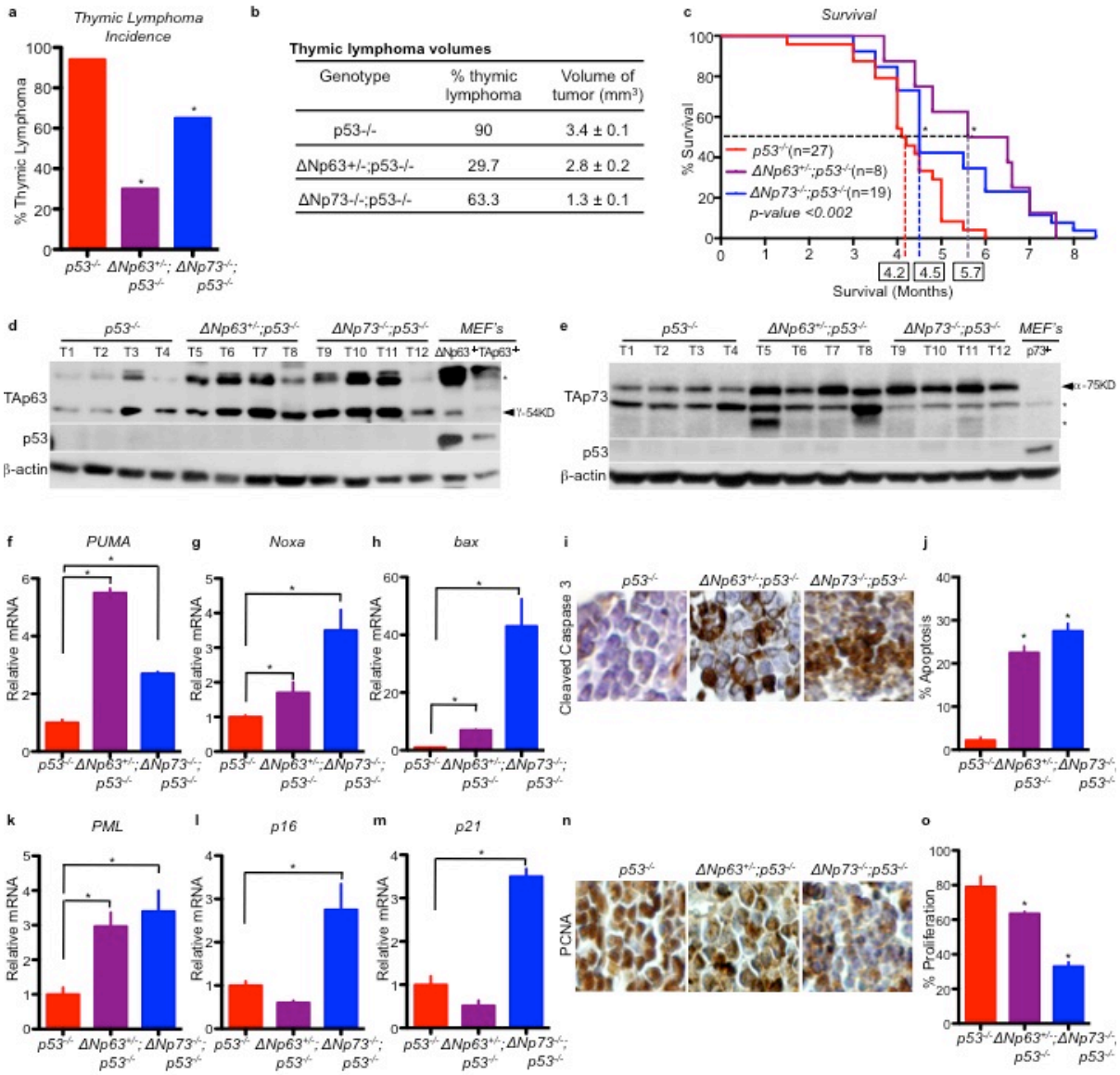

Figure 5: **Decreased thymic lymphomagenesis and increased survival in mice double deficient for Δ*Np63* and *p53* or Δ*Np73* and *p53.*** Quantification of thymic lymphoma incidence (n=30 mice) (**a**). Table showing thymic lymphoma volumes. The difference in tumour volumes between *p53-/-* and Δ*Np63+/-;p53-/-* and *p53-/-* and Δ*Np73-/-;p53-/-* was statistically significant with p values of <0.03 and <0.002 respectively (**b).** Kaplan Meier survival in mice (**c**). Boxed numbers indicate median

survival. Western blot analysis of thymic lymphomas of the indicated genotypes. Arrows indicate specific isoforms. Asterisks indicate non-specific bands (**d & e**).

Q-RT PCR for *PUMA* (**f**), *Noxa* (**g**), and *bax* (**h**) in thymic lymphomas of the indicated genotypes, n=4, $p<0.005$. Immunohistochemistry (IHC) for cleaved caspase 3 in thymic lymphomas (**i**). Quantification of apoptosis as assessed by cleaved caspase 3 staining (**j**), n=20 fields of 3 biological replicates, $p<0.005$. Q-RT PCR for *PML* (**k**), *p16* (**l**), and *p21* (**m**) in indicated thymic lymphomas, n=4, $p<0.005$. IHC for PCNA in indicated thymic lymphomas (**n**). Quantification of the percentage of proliferation as assessed by PCNA staining (**o**), n=20 fields of 3 biological replicates, $p<0.005$. Statistical significance indicated by black asterisks.

;p53-/- mice had a tumor incidence of 29.7% and the ΔNp73-/-;p53-/- mice had a tumor incidence of 63.3% compared to the p53-/- mice which develop thymic lymphomas at a 90% incidence rate. Importantly, I also observed significant differences in the tumor volumes between the double deficient compound mice compared to the p53-null mice (Figure 5b). The thymic lymphomas from the ΔNp63+/-;p53-/- mice measured 2.8mm^3 and the ΔNp73-/-;p53-/- mice measured 1.3mm^3 in volume compared to the p53-/- mice that measured 3.4mm^3 in volume. Interestingly, I also observed that the double deficient compound mice (ΔNp63+/-;p53-/- and ΔNp73-/-;p53-/-) mice had increased survival compared to the p53-null mice which normally die by 4 months of age (Figure 5c). Thus, the *in vivo* analysis from the double deficient mouse cohorts suggests that ΔNp63 and ΔNp73 could have oncogenic roles in p53-deficent thymic lymphomas.

To further characterize the phenotype of reduced thymic lymphoma incidence and decreased tumor volume in the double deficient compound mice, thymic lymphoma tissues from the double deficient compound mice (ΔNp63+/-;p53-/- and ΔNp73-/-;p53-/-) and p53-null mice were collected to perform western blot analysis, quantitative real-time PCR (qRT-PCR) and immunohistochemistry (IHC). Western blot analysis (Figure 5d-e) of the thymic lymphoma tissues from the ΔNp63+/-;p53-/- and ΔNp73-/-;p53-/- mice had increased expression of full-length isoforms of p63 and p73, namely TAp63 and TAp73 compared to the p53-/- thymic lymphoma samples. This suggests that loss of ΔN isoforms of p63 and p73, results in the activation or upregulation of TAp63 and TAp73 in the thymic lymphoma tissues. Since, *TAp63* and *TAp73* are tumor suppressors(65, 120), I hypothesized that

TAp63 and TAp73 could function to mediate the reduced thymic lymphomagenesis in these double deficient mice. Indeed, qRT-PCR analysis of the double deficient thymic lymphoma tissues revealed a significant upregulation of the genes involved in apoptosis like *PUMA*, *Noxa* and *BAX* (Figure 5f-h). This correlated with an increase in apoptosis in the double deficient lymphomas compared to the p53-null lymphomas as demonstrated by immunohistochemistry (Figure 5i-j). Also, cell-cycle arrest targets, namely, *p16*, *p21* and *PML* were also upregulated in the double deficient thymic lymphomas compared to the p53-null lymphoma tissues (Figure 5k-m). This correlated with reduced proliferation in the double deficient lymphomas compared to the p53-null lymphoma tissues (Figure 5n-o). This suggests that upon loss of ΔNp63 and ΔNp73 in p53-deficient lymphomas, TA isoforms of p63 and p73 are upregulated and compensate for *p53*-loss of function by activating downstream apoptosis and cell cycle targets mediating tumor regression.

3.2.2. Increased apoptosis and cell-cycle arrest in the ΔNp63+/-;p53-/- and ΔNp73-/-;p53-/- thymocytes after genotoxic stress

TAp63 and *TAp73* are tumor suppressors that are usually activated in response to genotoxic stress and DNA damage(63). Hence, to determine whether TAp63 and TAp73 induce apoptosis and cell cycle arrest in the double deficient thymus tissues, 4 week-old mice were treated with 10Gy gamma radiation, a dose that was previously demonstrated to induce a p53-dependent response. The double deficient thymocytes had an increased expression of TAp63 and TAp73 after DNA

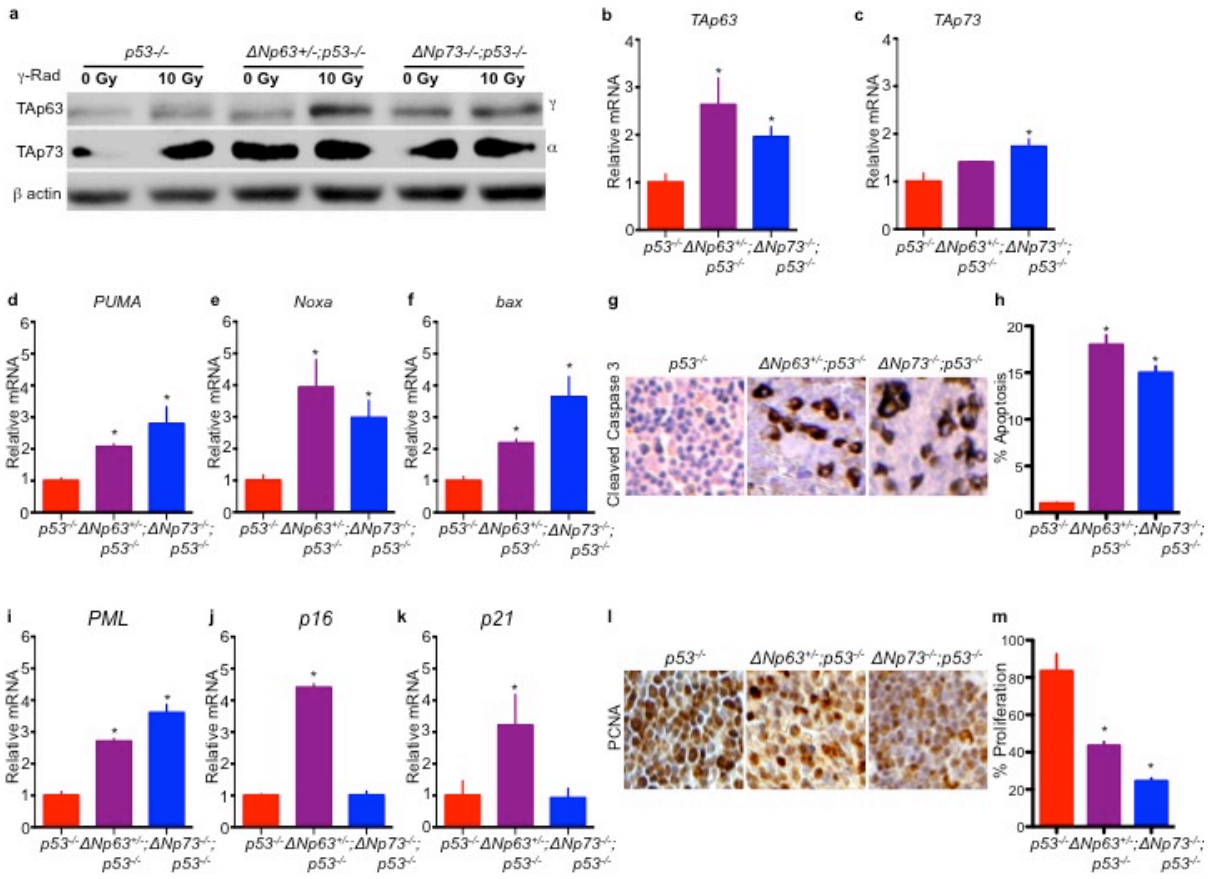

Figure 6: Increased apoptosis and cell cycle arrest in ∆*Np63+/-;p53-/-* and ∆*Np73-/-;p53-/-* thymocytes after genotoxic stress. Western blot analysis in thymocytes derived from mice 6 hours after treatment with 0 Gy or 10Gy gamma irradiation (**a**). Q-RT PCR for TAp63 (**b**), TAp73 (**c**), *PUMA* (**d**), *Noxa* (**e**), and *bax* (**f**) from samples shown in (a), n=4, p<0.005. Q-RT-PCR normalized to samples treated with 0 Gy. Immunohistochemistry (IHC) for cleaved caspase 3 in samples from (a) (**g**). Quantification of the percentage of apoptosis as assessed by cleaved caspase 3 staining (**h**), n=20 fields of 3 biological replicates, p<0.005. Q-RT PCR for *PML* (**i**), *p16* (**j**), and *p21* (**k**) using total RNA from samples shown in (a), n=4, p<0.005. IHC for PCNA in samples shown in (a) (**l**). Quantification of the

percentage of proliferation as assessed by PCNA staining (**m**), n=20 fields of 3 biological replicates, $p<0.005$. Statistical significance is indicated by black asterisks.

damage compared to the p53-null thymocytes (Figure 6a-c). This correlated with the increased relative expression of the apoptosis targets *PUMA, Noxa* and *BAX* (Figure d-f) and increased cell death as denoted by the IHC (Figure g-h) in the double deficient thymic lymphoma tissues compared to the p53-deficient lymphomas. Also, increased relative expression of the cell cycle targets namely *p16, p21* and *PML* (Figure i-k) and reduced expression for cell proliferation (Figure l-m) was observed in the double deficient thymic lymphoma tissues compared to the p53-null samples. These data suggest that TAp63 and TAp73 are upregulated upon genotoxic stress and can compensate for p53 function by activating apoptosis and cell cycle targets.

3.3.3. *In vivo* deletion of ΔNp63 or ΔNp73 in p53-deficient mice suppresses thymic lymphomagenesis

Initial analysis utilizing the ΔNp63+/-;p53-/- and ΔNp73-/-;p53-/- have clearly demonstrated that loss of ΔNp63 and ΔNp73 results in reduced thymic lymphomagenesis in the p53-deficeint mice(74). Additionally, TAp63 and TAp73 are upregulated in the double mutant thymic lymphoma and also upon genotoxic stress in the double deficient mouse thymocytes. Hence to further test whether *TAp63* and *TAp73* can compensate for p53-loss in suppressing lymphomagenesis, a cohort of ΔNp63fl/fl;p53-/- and ΔNp73fl/fl;p53-/- mice were generated. These mice were aged up to 10 weeks and the presence of the thymic lymphoma was determined using a magnetic resonance imaging (MRI). Mice that have a tumor volume ranging from 2.5mm^3 to 5.8mm^3 were selected for further analysis. A cohort of ΔNp63fl/fl;p53-/-

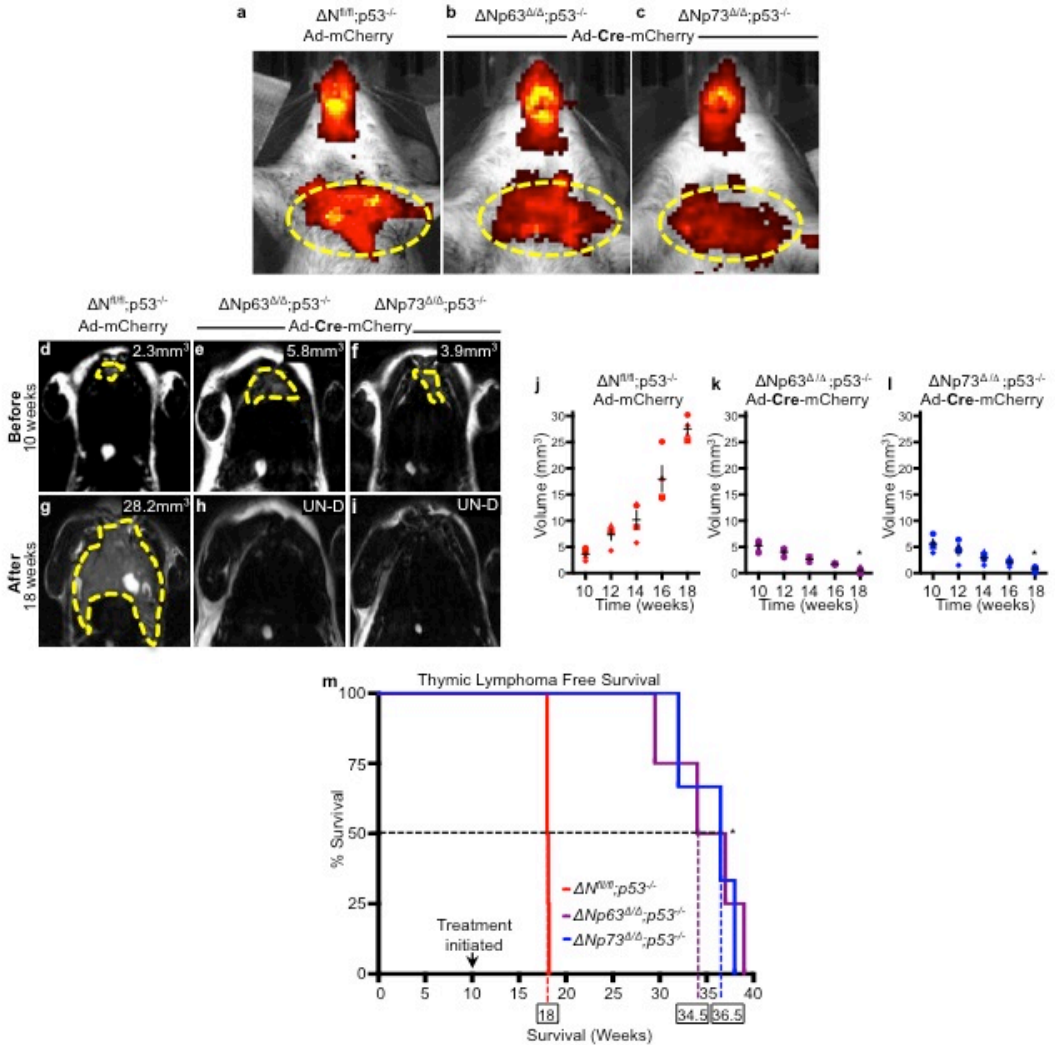

Figure 7: Acute deletion of ΔNp63 or ΔNp73 in p53-deficient thymic lymphomas mediates tumor regression. IVIS Lumina imaging of thymic lymphomas of mice of the indicated genotypes infected with Adenovirus (Ad)-mCherry (**a**) or Ad-Cre-mCherry (**b** & **c**) at 10 weeks of age and 48 hours after adenoviral delivery. Red fluorescence indicates viral delivery to the thymus shown by the yellow dashed ovals. Red fluorescence near the mouth is due to auto-fluorescence of calcium and mineral deposits in the teeth. Magnetic Resonance

Imaging (MRI) of thymic lymphomas of indicated mice (**d-i**). Tumour volume (mm^3) within each panel. UN-D = undetectable. Tumours indicated by the dashed yellow line. Quantification of the indicated thymic lymphomas (**j-l**), n=9 mice. Kaplan Meier curve (**m**), n=9, $p<0.005$. Boxed numbers represent median survival.

and ΔNp73fl/fl;p53-/- mice were administered either adenovirus CRE (Ad-CRE) or adenovirus-mCherry (Ad-mCherry) by intratumoral delivery. The intratumoral adenovirus delivery localization only to the region of the lymphoma was validated by IVIS lumina imaging (Figure 7a). The adenovirus CRE specifically deletes ΔNp63 or ΔNp73 in the p53-deficient thymic lymphomas, generating a ΔNp63Δ/Δ;p53-/- or a ΔNp73Δ/Δ;p53-/- cohort. Interestingly, upon administering Ad-CRE to the ΔNp63fl/fl;p53-/- and ΔNp73fl/fl;p53-/- thymic lymphomas, the mice had a significant reduction in the thymic lymphomas as accessed by the MR images compared to the ΔNfl/f;p53-/- mice administered with Ad-mCherry (Figure 7d-l). By 18 weeks, the thymic lymphoma in the ΔNp63Δ/Δ;p53-/- (Figure 7e, h & k) and ΔNp73Δ/Δ;p53-/- (Figure 7f, I & l) mice were undetectable while the ΔNfl/fl;p53-/- (Figure 7d, g & j) while mice administered with Ad-mCherry had a significant tumor burden. Importantly, the ΔNp63Δ/Δ;p53-/- and ΔNp73Δ/Δ;p53-/- mice had significant survival compared to the ΔNfl/fl;p53-/- mice which died by 18 weeks of age (Figure 7m).

In order to further characterize, the reduction in the thymic lymphoma upon deletion of ΔNp63 or ΔNp73 in the p53-deficent mice, thymic lymphoma tissues from the ΔNp63Δ/Δ;p53-/- and ΔNp73Δ/Δ;p53-/- mice were collected 48 hours after administering Ad-CRE. Since, most of the biological functions like apoptosis or cell-cycle arrest occur transiently, I was interested in understanding the molecular responses that could be activated after deleting ΔNp63 or ΔNp73 in the p53-deficient thymic lymphomas. Interestingly, the ΔNp63Δ/Δ;p53-/- and ΔNp73Δ/Δ;p53-/- thymic lymphoma tissues had increased expression of TAp63 and TAp73 after

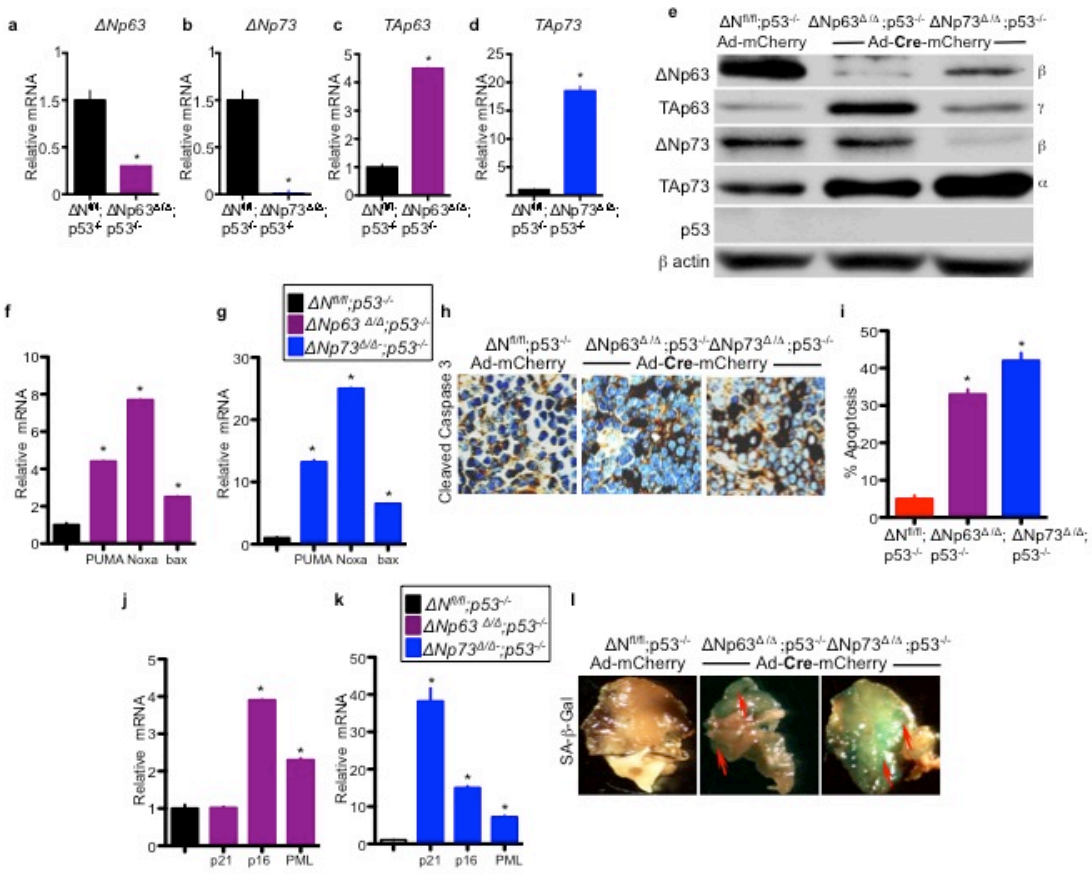

Figure 8: **Loss of ΔNp63 or ΔNp73 in p53-deficient thymic lymphomas results in upregulation of TAp63 and TAp73 with induction of apoptosis and cell cycle arrest.** Quantitative real time (qRT-PCR) (**a-d**). n=4, p<0.005 and western blot analysis using lysates from indicated thymic lymphomas 48 hours after infection with Adenovirus (Ad)-mCherry or Ad-Cre-mCherry (**e**). Quantitative real time (qRT-PCR) of thymic lymphomas 48 hours after infection with Ad-mCherry (Δ*Nfl/fl;p53-/-*) or Ad-Cre-mCherry (Δ*Np63Δ/Δ;p53-/-* or Δ*Np73Δ/Δ;p53-/-*) (**f-g**). n=4, p<0.005. Immunohistochemistry (IHC) for cleaved caspase 3 in thymic lymphomas 48 hours after infection with Ad-mCherry (Δ*Nfl/fl;p53-/-*) or Ad-Cre-mCherry (Δ*Np63Δ/Δ;p53-/-* or Δ*Np73Δ/Δ;p53-/-*) (**h**). Quantification of apoptosis as assessed by cleaved caspase 3 staining of the indicated thymic lymphomas (**i**), n=20 fields of 3 biological

replicates, p<0.005. Q-RT-PCR of thymic lymphomas 48 hours after treatment with Ad-mCherry (Δ*Nfl/fl;p53-/-*) or Ad-Cre-mCherry (Δ*Np63Δ/Δ;p53-/-* or Δ*Np73Δ/Δ;p53-/-*), n=4, p<0.005 (**j-k**). Senescence associated beta galactosidase (SA-β-gal) staining (blue) of thymic lymphomas 48 hours after treatment with Ad-mCherry (Δ*Nfl/fl;p53-/-*) or Ad-Cre-mCherry (Δ*Np63Δ/Δ;p53-/-* or Δ*Np73Δ/Δ;p53-/-*) **(l)**

deleting ΔNp63 and ΔNp73 compared to the ΔNfl/fl;p53-/- lymphoma tissues administered with Ad-mCherry (Figure 8a-e). This suggests that *TAp63* and *TAp73* are activated upon loss of ΔNp63 and ΔNp73 in the p53-deficient thymic lymphomas. Interestingly, the increased expression of TAp63 and TAp73 in the ΔNp63Δ/Δ;p53-/- and ΔNp73Δ/Δ;p53-/- thymic lymphomas correlated with the increased expression of the apoptosis targets *PUMA*, *Noxa* and *BAX* (Figure 8f-g) and an increase in apoptosis (Figure 8h-i) compared to the ΔNfl/fl;p53-/- thymic lymphomas. Similarly, increased expression of cell cycle targets *p16*, *p21* and *PML* (Figure 8j-k) and cellular senescence (Figure l) was observed in the ΔNp63Δ/Δ;p53-/- and ΔNp73Δ/Δ;p53-/- thymic lymphomas. This data suggests that *TAp63* and *TAp73* can compensate for p53-loss of function by activating apoptosis and cell-cycle arrest targets mediating tumor shrinkage.

3.3.4. Loss of ΔNp63 and ΔNp73 in p53-deficient thymic lymphomas accelerates tumor regression

Ablation of ΔNp63 or ΔNp73 in p53-deficient thymic lymphomas mediates tumor regression(74). Importantly, the ΔNp63/ΔNp73 deleted p53-deficient mice have increased survival compared to the p53-deficient mice. Hence, to test whether deleting both ΔNp63 and ΔNp73 in the p53-deficient thymic lymphomas accelerates the tumor regression a cohort of ΔNp63fl/fl;ΔNp73fl/fl;p53-/- mice was generated. At 10 weeks, MR imaging was performed to confirm the presence of a thymic lymphoma. ΔNp63 and ΔNp73 was acutely deleted using adeno-CRE in the p53-deficient thymic lymphomas. Loss of ΔNp63 and ΔNp73 in the p53-deficient thymic lymphomas resulted in rapid reduction in the tumor volume (Figure 9a-t) and

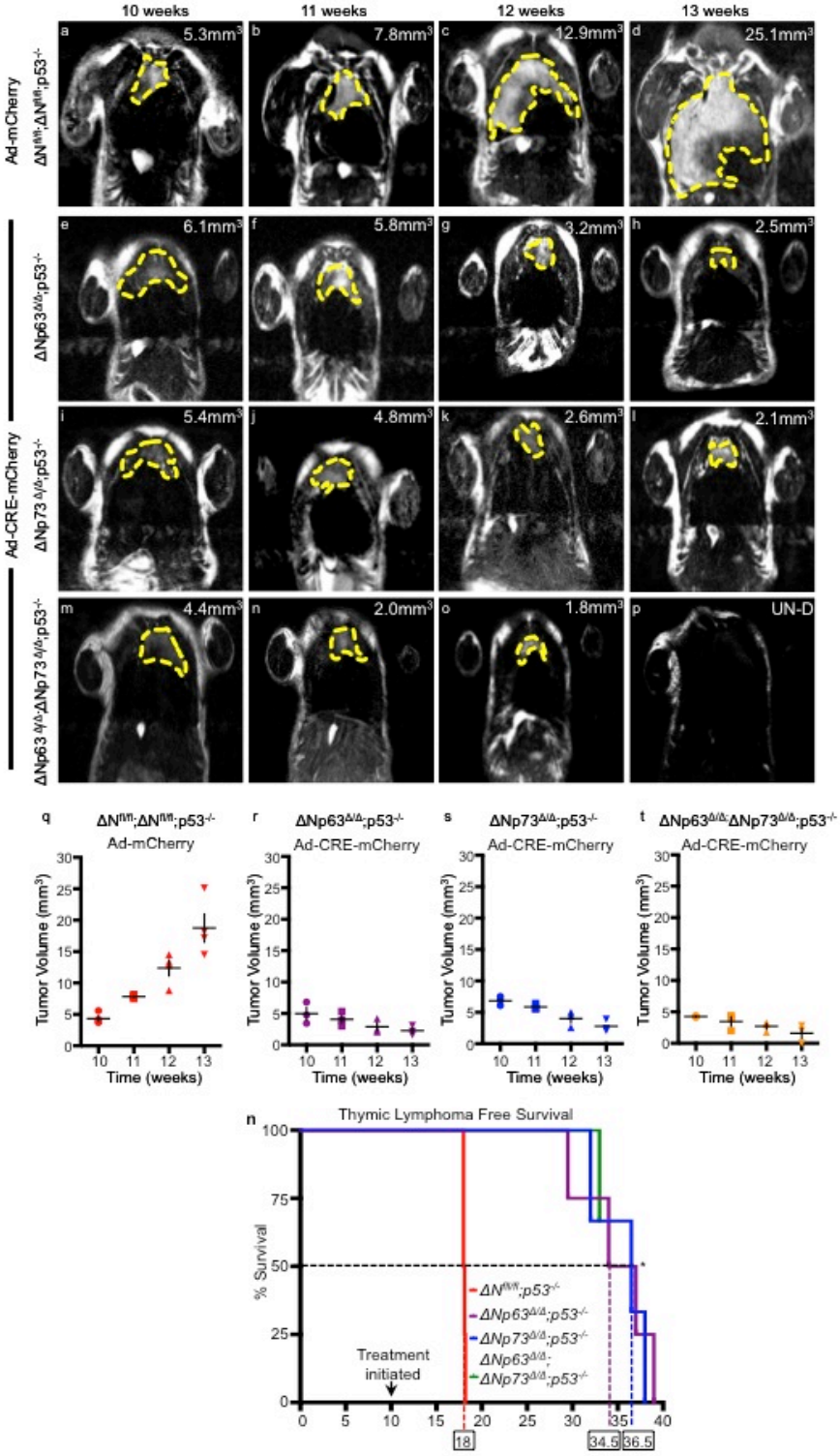
10 weeks
11 weeks
12 weeks
13 weeks
Ad-mCherry
ΔN^fl/fl;ΔN^fl/fl;p53-/-
Ad-CRE-mCherry
ΔNp63Δ/Δ;p53-/-
ΔNp73 Δ/Δ;p53-/-
ΔNp63 Δ/Δ;ΔNp73 Δ/Δ;p53-/-
5.3mm3
7.8mm3
12.9mm3
25.1mm3
6.1mm3
5.8mm3
3.2mm3
2.5mm3
5.4mm3
4.8mm3
2.6mm3
2.1mm3
4.4mm3
2.0mm3
1.8mm3
UN-D
q ΔN^fl/fl;ΔN^fl/fl;p53-/-
Ad-mCherry
r ΔNp63Δ/Δ;p53-/-
Ad-CRE-mCherry
s ΔNp73Δ/Δ;p53-/-
Ad-CRE-mCherry
t ΔNp63Δ/Δ;ΔNp73Δ/Δ;p53-/-
Ad-CRE-mCherry
Tumor Volume (mm3)
Time (weeks)
n
Thymic Lymphoma Free Survival
% Survival
Treatment initiated
ΔN^fl/fl;p53-/-
ΔNp63Δ/Δ;p53-/-
ΔNp73Δ/Δ;p53-/-
ΔNp63Δ/Δ;ΔNp73Δ/Δ;p53-/-
18
34.5
36.5

Figure 9: Ablation of ΔNp63 and ΔNp73 in p53-deficient mice accelerates tumor regression. Magnetic Resonance Imaging (MRI) of mice of the indicated genotypes. **(a-p)** (n=4). Mice were administered with either Adeno-mCherry **(a-d)** or Adeno-CRE-mCherry **(e-p)**. Tumour volume (mm^3) within each panel. UN-D = undetectable. Tumours indicated by the dashed yellow line. Tumor volume quantification of thymic lymphomas (**q-t**), n=4 mice. Kaplan Meier curve (**n**), n=4, $p<0.005$. Boxed numbers represent median survival.

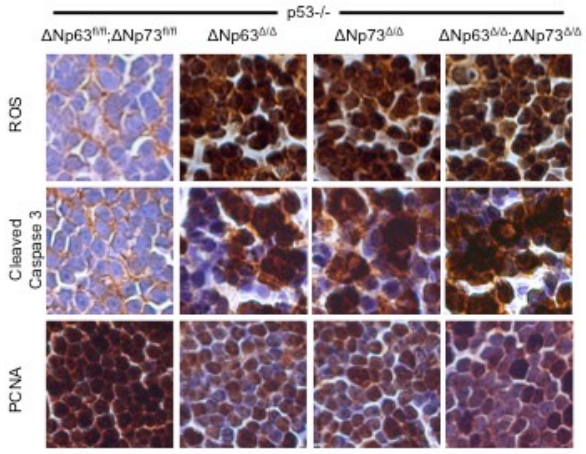

Figure 10: Ablation of ΔNp63 and ΔNp73 in p53-deficient thymic lymphomas results in accumulation of ROS, apoptosis and cell-cycle arrest. IHC panels of the indicated genotypes representing staining for ROS, apoptosis and proliferation. Brown nuclei represent positive cells

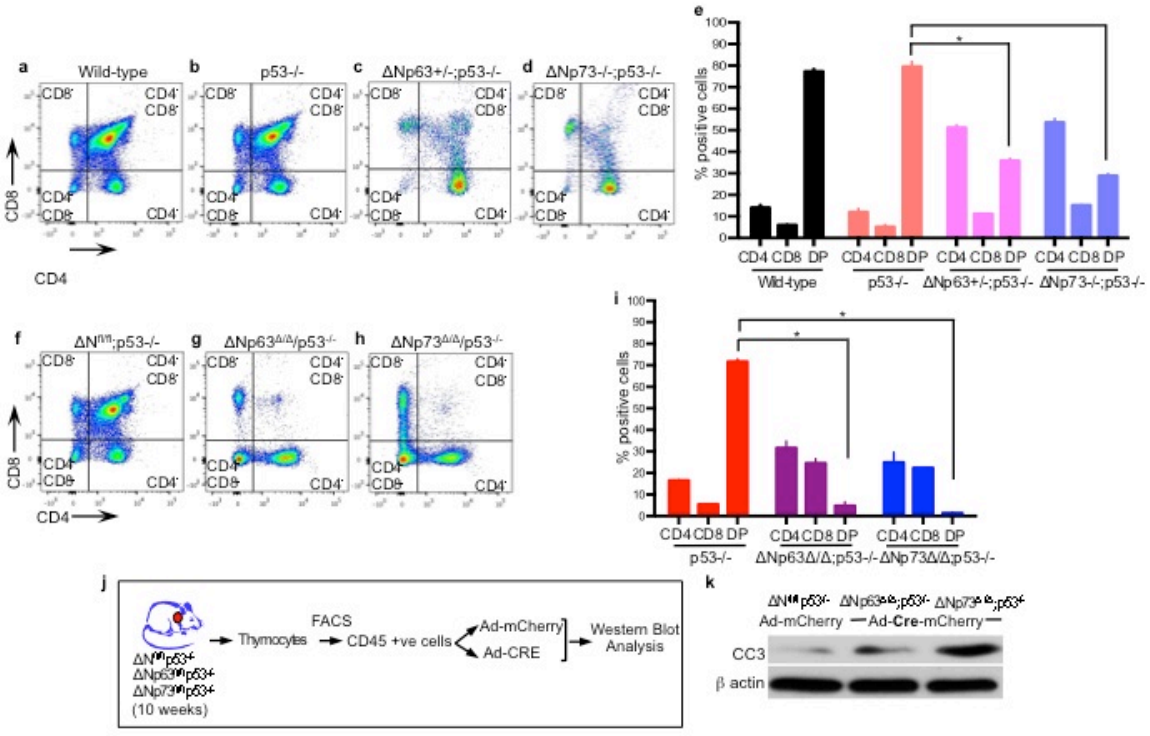

Figure 11: Loss of ΔNp63/ΔNp73 in p53-deficient thymic lymphomas affects the CD4-CD8 double positive cells. Flow cytometry plots of the indicated thymocytes at 4-week of age **(a-d)**. Bar graph showing quantification of CD4, CD8, and CD4/CD8 double positive (DP) cells. n=3 mice per genotype, p<0.005 **(e)**. Flow Cytometry plots of thymic lymphoma cells 48 hours after adenovirus-mCherry or adenovirus-CRE treatment for the indicated genotypes (**f-h**). Bar graph showing quantification of CD4, CD8, and CD4/CD8 double positive (DP) cells in the indicated genotypes. n=3 mice per genotype, p<0.005 (**i**). Cartoon representation of isolation of CD45-postive thymic lymphoma cells from 10 week old mice of indicated genotypes **(j)**. Western blot analysis of CD45-postive thymic lymphoma cells after treatment with Ad-mCherry (ΔNfl/fl;p53-/-) or Ad-CRE-mCherry (ΔNp63Δ/Δ/;p53-/- and ΔNp73Δ/Δ;p53-/-) (**k**). Statistical significance is indicated by black asterisks.

increased survival (Figure 9n). The tumor regression phenotype also correlated with the increase in ROS, cell death and reduction in cell proliferation (Figure 10). This suggests that targeting ΔN isoforms of p63 and p73 could be used as a viable option to treat p53-deficient cancers.

3.3.5. Loss of *ΔNp63* or *ΔNp73* in *p53*-deficient thymic lymphomas affects the CD4-CD8 double positive cells

The p53-deficient mice develop thymic lymphoma, which are of T-cell origin(22). In order to test whether depletion of either ΔN isoforms of p63 and p73 affects the T cells development, a cohort of mice at 4 weeks was established. FACS analysis with the mouse thymocytes was performed using CD3, CD4 and CD8 markers, which label the T-cell receptor complex, T-helper cells and T-lymphocytes respectively. The ΔNp63+/-;p53-/- and ΔNp73-/-;p53-/- mouse thymocytes had decreased number of CD4-CD8 double positive cells compared to the p53-deficient and the wild-type mouse thymocytes (Figure 11a-e). This suggests that reduction in the number of CD4-CD8 double positive cells correlates with the reduced tumor volume and incidence in the double mutant compound mice. Hence, to test whether this is the case, ΔNp63 and ΔNp73 were acutely deleted in the thymic lymphomas of ΔNp63fl/fl;p53-/- and ΔNp73fl/fl;p53-/- mice. Upon analyzing the p53-deficient thymic lymphoma cells, 48 hours after deletion of ΔNp63 or ΔNp73, I observed a significant reduction in the CD4-CD8 positive cells compared to the ΔNfl/fl;p53-/- thymic lymphoma cells (Figure 11f-i). This suggests that loss of ΔNp63 and ΔNp73 in the

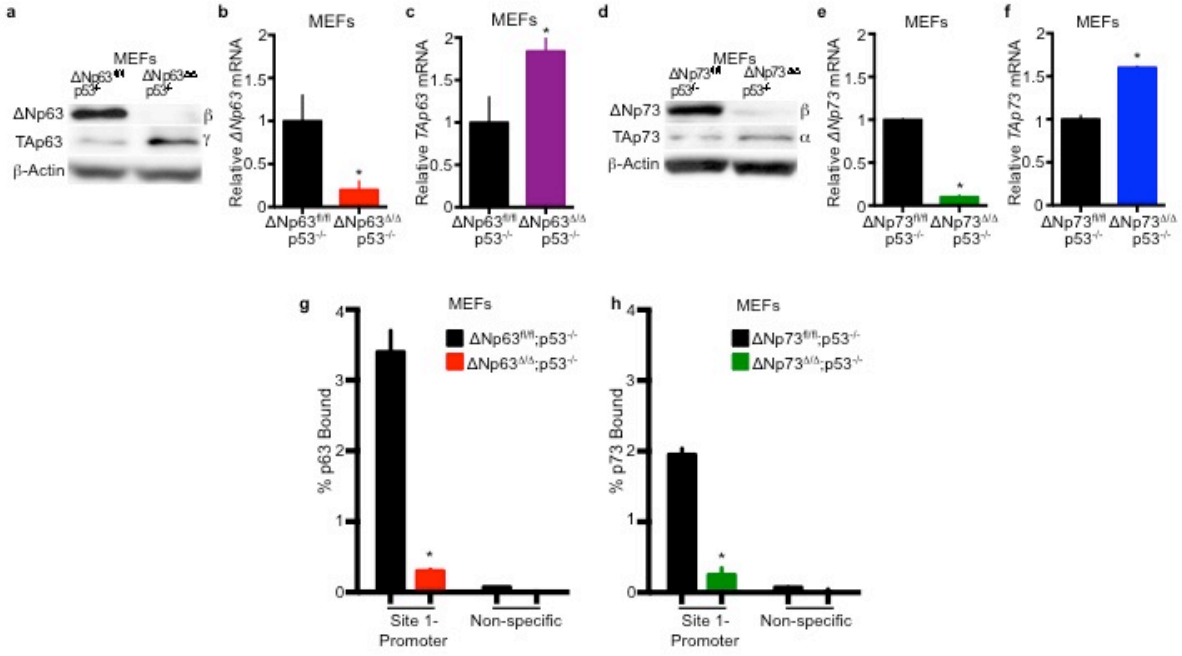

Figure 12: ΔNp63 and ΔNp73 transcriptionally repress TAp63 and TAp73. Western blot analysis in ΔNp63fl/fl;p53-/- MEFs before (ΔNp63fl/fl;p53-/-) and after (ΔNp63Δ/Δ;p53-/-) Ad-cre administration **(a)**. Q-RT-PCR for ΔNp63 **(b)** and TAp63 **(c)** in indicated MEFs. Western blot analysis in ΔNp73fl/fl;p53-/- and ΔNp73Δ/Δ;p53-/- MEFs **(d)**. Q-RT-PCR for ΔNp73 **(e)** and TAp73 **(f)** in indicated MEFs. n=4, p<0.005. Q-RT-PCR of chromatin Immunoprecipitation using indicated MEFs and an antibody for p63 **(g)** or p73 **(h)** n=3, p<0.005.

ΔNp63/ΔNp73 binding sites on TAp63 and TAp73 promoter

Element	Location	Sequence	MM/ Spacer
TAp63-Promoter	-43 to -18	tgaCAGGagc tctca aatCAAGtca	5/5
TAp73-Promoter	-1106 to -1082	cgcCTAGcac acca atcCAAGgaa	8/4

Mismatches are shown in red text.
MM: the number of mismatches in each binding site.
Spacer: number of nucleotides between two half sites.

Table 1: Table showing ΔNp63 and ΔNp73 binding sites on the *TAp63* and *TAp73* promoter regions

p53-deficient thymic lymphomas affects T-cell development, thereby preventing T-cell lymphoma formation.

Addtionally, to determine whether the stromal cells contribute to apoptosis in the p53-deficient thymic lymphoma cells after depletion ΔNp63 and ΔNp73, ΔNfl/fl;p53-/-, ΔNp63fl/fl;p53-/- and ΔNp73fl/f;p53-/- thymic lymphoma cells were FACS sorted for CD45 marker to select for T-lymphocytes. T-Lymphocytes from the indicated genotypes were infected with either Ad-CRE or Ad-mCherry (Figure 11j). Upon, deleting either ΔNp63 or ΔNp73 in the p53-/- T-lymphocytes, I observed increased expression of Caspase 3 compared to the ΔNfl/fl;p53-/- T-lymphocytes (Figure 11k). This suggests that upon loss of ΔN isoforms of p63 and p73, TAp63 and TAp73 induce downstream apoptosis in the T-lymphocytes independently of the stromal cell populations in the thymic lymphomas of the p53-deficient mice.

3.3.6. ΔN isoforms of p63 and p73 function as transcriptional repressors of TAp63 and TAp73

ΔN isoforms function dominant negatively against p53, TAp63 and TAp73(45). Also, ΔNp63 and ΔNp73 function as transcriptional factors activating or repressing certain targets(69). Loss of ΔNp63 and ΔNp73 in the p53-deficient thymic lymphomas resulted in the upregulation of tumor suppressive isoforms, namely TAp63 and TAp73. Hence, to test whether this is the case, ΔNp63fl/fl;p53-/- and ΔNp73fl/fl;p53-/- mouse embryonic fibroblasts (MEFs) were generated. The MEFs were infected with adeno-CRE or Adeno-mCherry. Upon deleting ΔNp63 or

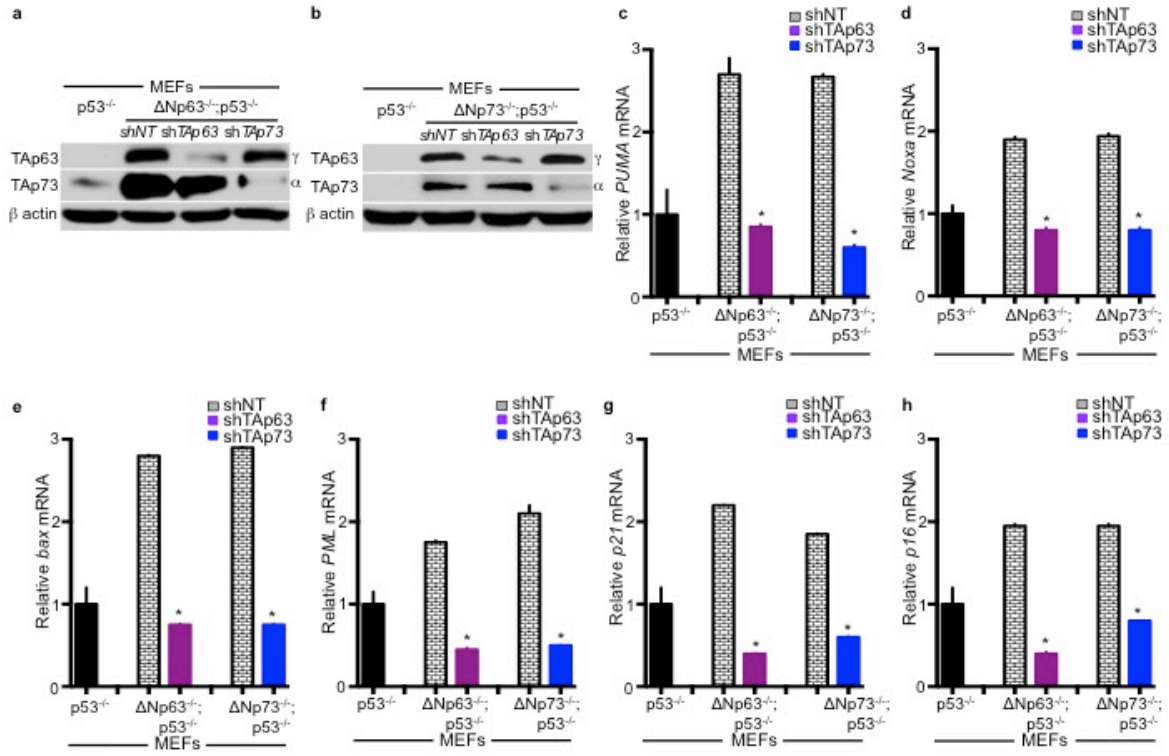

Figure 13: TAp63 and TAp73 are required for activation of apoptosis and cell cycle targets in p53-deficient cells. Western blot analysis in Δ*Np63-/-;p53-/-* (**a**) or Δ*Np73-/-;p53-/-* (**b)** MEFs treated with the indicated shRNAs; (shNT) indicates a non-targeting scramble shRNA. Q-RT PCR for *PUMA* (**c**), *Noxa* (**d**), *bax* (**e**), *PML* (**f**), *p21* (**g**), and *p16* (**h**) in the indicated MEFs expressing the indicated shRNAs, n=5, $p<0.005$. Statistical significance indicated by black asterisks.

ΔNp73 in the p53-deficient MEFs, I observed that TAp63 and TAp73 were significantly upregulated (Figure 12a-f). This suggests that ΔN isoforms could repress transcription of the tumor suppressive isoforms, *TAp63* and *TAp73*. To test whether this is the case, chromatin immunoprecipitation (ChIP) for ΔNp63 and ΔNp73 was performed on the promoter region of *TAp63* and *TAp73* (Table 1). I observed that ΔNp63 and ΔNp73 bind to the promoter region of *TAp63* (Figure 12g) and *TAp73* (Figure 12h), thereby transcriptionally repressing the activity of TA isoforms of p63 and p73. Thus targeting the ΔN isoforms in p53-deficient cells restores the transcriptional function of *TAp63* and *TAp73*. *TAp63* and *TAp73* in-turn compensate for p53-loss by activating downstream apoptosis and cell cycle targets.

3.3.7. TAp63 and TAp73 are required apoptosis and cell cycle arrest in p53-deficient cells

Loss of ΔN isoforms of p63 and p73 results in upregulation of TAp63 and TAp73 in the p53-deficient cells and thymic lymphomas. TAp63 and TAp73 upregulation correlates with the increased expression of downstream apoptosis and cell cycle arrest targets. This suggests that TAp63 and TAp73 compensate for p53-loss. Hence, to test whether this is the case, TAp63 (Figure 13a) and TAp73 (Figure 13b) were knocked down in the ΔNp63-/-;p53-/- and ΔNp73-/-;p53-/- MEFs. Upon down-regulation of TAp63 and TAp73, I observed a reduced expression of apoptosis targets (Figure c-e), *PUMA*, *Noxa* and *BAX* and the cell cycle arrest targets (Figure f-h), *p21*, *p16* and *PML*. This suggests that apoptosis and cell cycle arrest targets are dependent on TAp63 and TAp73 function in the p53-deficient cells and thymic

lymphomas. This further highlights the tumor suppressive role of the TA isoforms of p63 and p73 in treating cancers.

Discussion

TP53 gene is highly mutated in human cancers and therapeutic intervention to reactivate or target the p53-pathway is pivotal due to its tumor suppressive functions(5, 122). Here, we utilized the p53-family members, *p63* and *p73* as an alternative strategy to treat p53-deficient cancers. p63 and p73 are structurally similar to p53 and are less frequently mutated which makes them unique targets for therapeutic intervention(45). Interestingly, p63 and p73 have multiple splice variants, broadly classified as TA (trans-activating) isoforms and ΔN (dominant negative) isoforms of p63 and p73. I have demonstrated that deleting ΔNp63 or ΔNp73 in p53 deficient thymic lymphomas results in rapid tumor regression and increased survival. The loss of ΔN isoforms in these p53-deficient tumor samples correlates with increased expression of TAp63 and TAp73 and downstream apoptosis and cell cycle arrest pathways. This suggests that ΔNp63 and ΔNp73 function dominant negatively against *TAp63* and *TAp73*. Indeed, ΔNp63 and ΔNp73 binds to the promoters of the *TAp63* and *TAp73* preventing their transcriptional function. Upon loss of ΔN isoforms of p63 and p73, TAp63 and TAp73 are activated further inducing downstream apoptosis and cell cycle targets. Interestingly, I was also able to demonstrate that the induction of apoptosis and cell cycle arrest in the p53-deficient cells and thymic lymphomas were dependent on TAp63 and TAp73. This highlights the compensatory tumor suppressive role of *TAp63* and *TAp73* in targeting p53-deficient cancers. Importantly, I have demonstrated that *ΔNp63* and *ΔNp73* function as

oncogenes in the p53-deficient thymic lymphomas and therapeutic targeting of these oncogenic isoforms serves as a novel approach to treat p53-deficient cancers.

4. Chapter 4: *IAPP* driven metabolic reprogramming induces regression of p53-deficient tumors *in vivo* through the calcitonin and RAMP3 receptors

Chapter 4: *IAPP* driven metabolic reprogramming induces regression of p53-deficient tumors *in vivo* through the calcitonin and RAMP3 receptors

Contents of this chapter is based on Venkatanarayan, A., Raulji, P., Norton, W., Chakravarti, D., Coarfa, C., Su, Xiaohua., Sandur, S.K., Ramirez, M.S., Lee, Jaehyuk., Kingsley, C.V., Sananikone, E.F., Rajapakshe, K., Naff, K., Parker-Thornburg, J., Bankson, J.A., Tsai, K.Y., Gunaratne, P.H. and Flores, E.R. IAPP driven metabolic reprogramming induces regression of p53-deficient tumors *in vivo*. *Nature.* 2015; 517(7536),626-630. doi:10.1038/nature13910.

4.1. Introduction and Rationale

ΔNp63 and ΔNp73 function dominant negatively against *p53*, *TAp63* and *TAp73*(47, 60). I have demonstrated that targeting the ΔN isoforms of p63 and p73 in p53-deficient tumors mediates tumor regression in a TAp63 and TAp73 dependent manner(74). This suggests that *TAp63* and *TAp73* function as bonafide tumor suppressors activating apoptotic and cell cycle targets to mediate tumor suppression. Thus TAp63 and TAp73 compensate for p53-loss of function in p53-deficient tumors. This makes *p63* and *p73* as important targets for therapeutic intervention to treat p53-deficient cancers. Hence it is necessary to understand and delineate the global mechanisms by which *TAp63* and *TAp73* mediate its tumor suppressive functions apart from activating apoptosis and cell cycle arrest pathway.

More recently, p53 has been demonstrated to mediate its tumor suppressive functions by activating certain metabolic and immune regulators, suppressing pluripotent factors and also impacting lipid biosynthesis. Given that tumor cells consume increased amounts of glucose and switch to a more aerobic form of respiration, regulation of the glycolytic pathway serves as an important pathway to be targeted. The *p53* tumor suppressor activates two well-known metabolic regulators *GLS2*, *TIGAR* to suppress tumorigenesis. Given the similarity to p53, I was interested in understanding global transcriptional profile or targets activated by *TAp63* and *TAp73* independent of p53 in suppressing tumorigenesis.

4.2. Results

4.2.1. Loss of ΔNp63 and ΔNp73 establishes a novel metabolic gene signature in p53-deficient thymic lymphomas

Loss of ΔNp63 and ΔNp73 in p53-deficient thymic lymphomas mediates tumor regression by induction of apoptosis and cell cycle arrest in a TAp63 and TAp73 dependent manner. To test whether TAp63 and TAp73 could activate other upstream regulators or pathways to mediate tumor suppression, we performed RNA-sequencing using the thymic lymphoma samples from the ΔNp63Δ/Δ;p53-/-, ΔNp73Δ/Δ;p53-/- and ΔNfl/fl;p53-/- 48 hours after adenovirus infection. We observed that ΔNp63Δ/Δ;p53-/- and ΔNp73Δ/Δ;p53-/- lymphoma samples clustered together

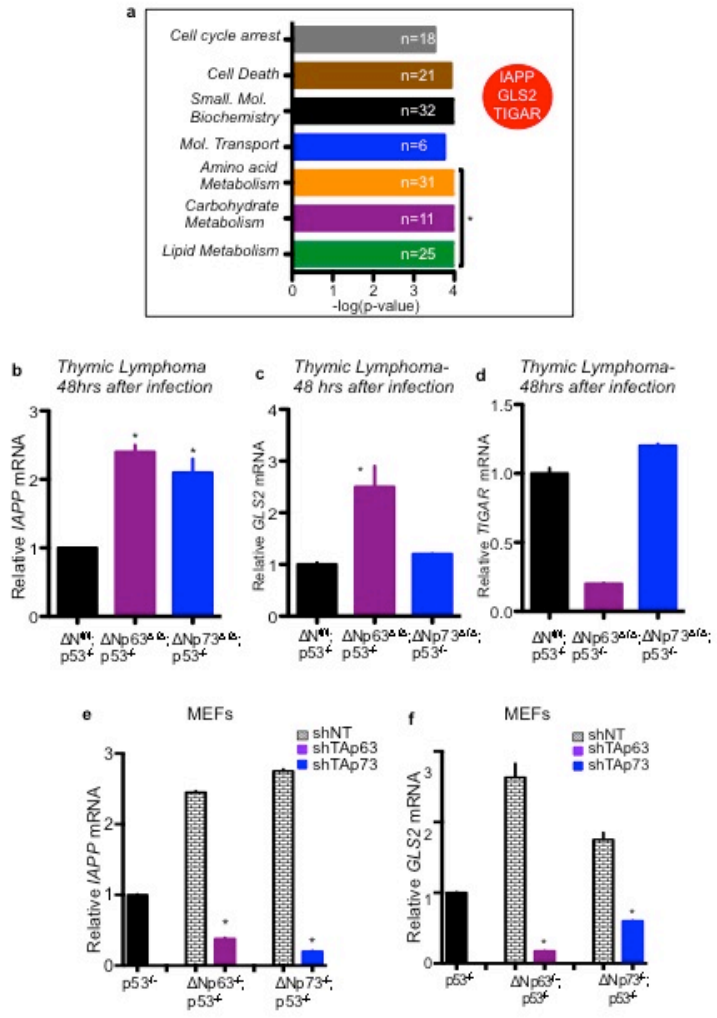

Figure 14: Loss of ΔNp63 and ΔNp73 reveal a novel metabolic gene signature. Ingenuity Pathway Analysis (IPA) of RNA-sequencing from thymic lymphomas 48 hours after infection with adenoviruses (**a**). Red oval indicates significantly upregulated metabolic genes. Q-RT-PCR for *IAPP* **(b)**, *GLS2* **(c)** and *TIGAR* **(d)** in thymic lymphomas or MEFs of the indicated genotypes using a non-targeting shRNA (shNT) or shRNAs for TAp63 (shTAp63) or TAp73 (shTAp73) (**e-f**), n=4, p<0.005.

and separately from the ΔNfl/fl;p53-/- thymic lymphoma samples (Appendix 1). Ingenuity pathway analysis (IPA) (Figure 14a) revealed a novel metabolic gene signature between the ΔNfl/fl;p53-/- versus ΔNp63Δ/Δ;p53-/- and ΔNp73Δ/Δ;p53-/- thymic lymphoma samples. To further determine the TAp63 and TAp73 targets, genes that have a 2-fold mRNA expression in both the ΔNp63Δ/Δ;p53-/- and ΔNp73Δ/Δ;p53-/- thymic lymphomas compared to the ΔNfl/fl;p53-/- tumors were analyzed. Further, genes that shared a p53-consensus binding site were shortlisted. qRT-PCR was performed to determine the fold-change expression levels of these genes in the ΔNp63Δ/Δ;p53-/- and ΔNp73Δ/Δ;p53-/- tumors samples. Based on the relative fold-change expression, three genes were shortlisted, two of which namely, *GLS2* (Figure 14c) and *TIGAR* (Figure 14d), which were previously characterized p53-regulated metabolic targets and another novel less characterized gene called *IAPP(85)*. *GLS2* and *TIGAR* play critical roles in mitochondrial respiration(82) and glycolysis(123). Islet amyloid polypeptide (*IAPP*) is a 37 amino acid polypeptide that encodes for amylin(84). *IAPP* had a >2-fold expression in both ΔNp63Δ/Δ;p53-/- and ΔNp73Δ/Δ;p53-/- samples (Figure 14b). Further, upon downregulating TAp63 and TAp73 in the double mutant MEFs, expression levels of IAPP and GLS2 were significantly downregulated (Figure 14e & f). This suggests that *IAPP* could be activated by TA isoforms of p63 and p73. Since IAPP was expressed at higher levels in the double mutant thymic lymphomas I suspect that IAPP could be functionally implicated in the tumor regression associated with loss of ΔN isoforms of p63 and p73 in p53-deficient cancers.

TAp63 & TAp73 binding sites on IAPP promoter

Element	Location	Sequence	MM/ Spacer
IAPP Site1 Promoter	-1756 to -1736	caaCATGaggctgCATGtca	7/0
IAPP Site2 Intron 2	+706 to +732	gaaCATGttttaggacataCAGGggc	3/6

Mismatches are shown in red text.
MM: the number of mismatches in each binding site.
Spacer: number of nucleotides between two half sites.

Table 2: Table showing TAp63 and TAp73 consensus binding sites on the IAPP promoter

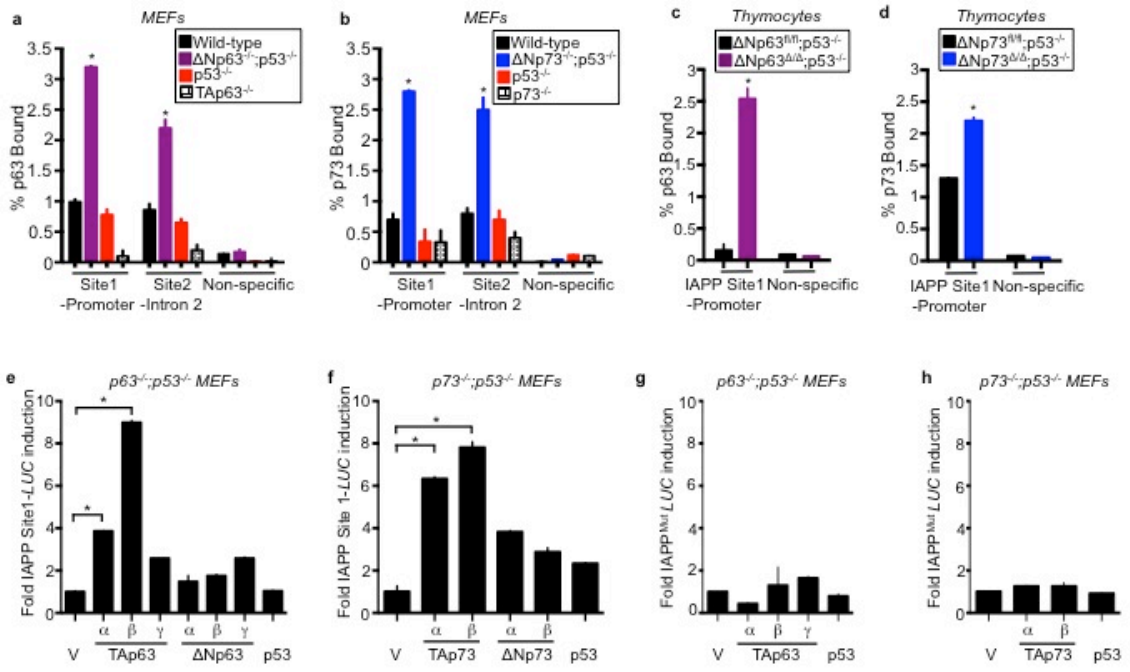

Figure 15: IAPP functions as a downstream target of TAp63 and TAp73.

Q-RT-PCR of Chromatin Immunoprecipitation using MEFs (**a** & **b**) and thymocytes (**c & d**) of the indicated genotypes, n=3, p<0.005. Dual luciferase reporter assay for pGL3-*IAPP* (**e** & **f**) and a mutant version of the *IAPP* reporter gene (pGL3-*IAPP* MUT) (**g** & **h**). Genotypes of MEFs and vectors used are shown. V represents pcDNA3 vector. Western blot analysis of the indicated MEFs expressing IAPP or siRNAs for a non targeting sequence (siNT) or IAPP (siIAPP) (**l** & **m**). Statistical significance indicated by black asterisks.

4.2.2. *IAPP* functions as a downstream target of TAp63 and TAp73

IAPP expression was significantly upregulated in the ΔNp63Δ/Δ;p53-/- and ΔNp73Δ/Δ;p53-/- thymic lymphoma tissues compared to the ΔNfl/fl;p53-/- tumors. Since, ΔNp63Δ/Δ;p53-/- and ΔNp73Δ/Δ;p53-/- tumors have increased expression of

TAp63 and TAp73, I hypothesized that TAp63 and TAp73 could transcriptionally activate *IAPP*. To test whether this was the case, chromatin immunoprecipitation assay was performed (ChIP) on the promoter and intron 2 site of the IAPP gene using MEFs (Figure 15a & b) and thymocytes (Figure 15 c & d) (Table 2). I observed that binding of TAp63 and TAp73 onto the IAPP sites were observed in the ΔNp63-/-;p53-/- and ΔNp73-/-;p53-/- MEFs. Similarly, increased binding of TAp63 and TAp73 on the promoter of *IAPP* was observed upon deleting ΔNp63/ ΔNp73 in the p53-deficient thymocytes. This data suggests that TAp63 and TAp73 bind to the promoter region of *IAPP* and could transcriptionally activate IAPP.

To test whether TAp63 and TAp73 transcriptionally activate *IAPP*, luciferase reporter assay was performed using p63-/-;p53-/- and p73-/-;p53-/- double mutant MEFs. Upon, transfecting the MEFs with indicated plasmids, I observed that TAp63 and TAp73 to be a strong inducer of *IAPP* expression (Figure 15 e & f). However, when the TAp63/TAp73 consensus-binding site on the *IAPP* promoter region was mutated (Figure 15 g-h), no luciferase activity was observed. This suggests that TAp63 and TAp73 transcriptionally activate *IAPP*.

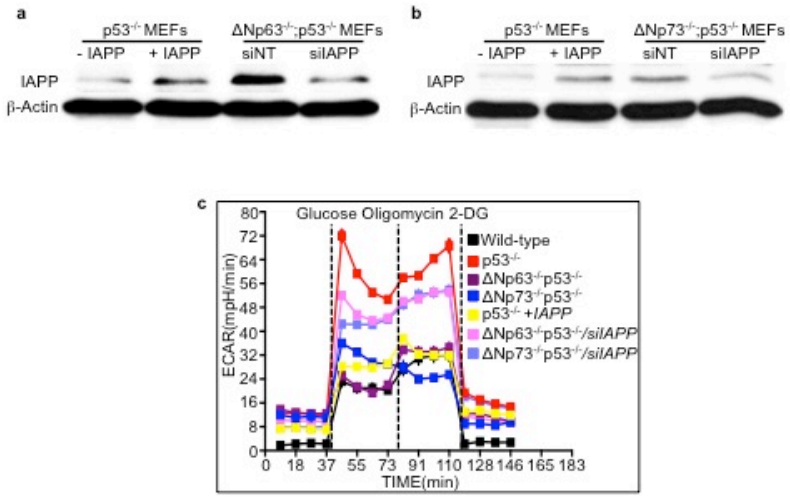

Figure 16: IAPP functions as a regulator of glycolysis in mouse embryonic fibroblasts. Western blot analysis for IAPP in the indicated MEFs and treatment conditions, (n=3) (**a& b**). Seahorse glyocolysis stress assay using the indicated MEFs(**c**) (n=3).

4.2.3. IAPP functions as a critical regulator of glycolysis in mouse embryonic fibroblasts

Majority of the genes in the RNA-sequencing analysis have an enriched metabolic gene signature. Particularly, *TIGAR* and *GLS2* function as regulators of glycolysis(123) and mitochondrial respiration(82). Similarly, IAPP has been previously characterized to play roles in glucose metabolism, apoptosis and autophagy(83). IAPP has been demonstrated to reduce glucose uptake and inhibit glycolysis(84, 124). IAPP inhibits glycolysis by reducing hexokinase activity indirectly by increasing glucose-6-phosphate levels. Hence to test the potential role of IAPP in glycolysis, I performed a glycolysis stress assay using MEFs of the indicated genotypes. The ΔNp63-/-;p53-/- and ΔNp73-/-;p53-/- MEFs have increased expression of IAPP (Figure 16 a & b) and have reduced glycolytic capacity similar to the wild-type MEFs in comparison to the p53-/- MEFs (Figure 16c). Upon, expressing IAPP in the p53-/- MEFs resulted in a shift in the glycolytic capacity closer to the wild-type MEFs (Figure 16c). This suggests that IAPP functions to reduce glycolysis in these p53-deficient cells. To test whether IAPP functions a critical regulator of glycolysis, the IAPP expression was down regulated in the ΔNp63-/-;p53-/- and ΔNp73-/-;p53-/- MEFs (Figure 16 a & b). I observed a significant increase in the glycolytic capacity much closer to p53-/- MEFs (Figure 16c). This highlights the role of IAPP as a critical regulator of glycolysis.

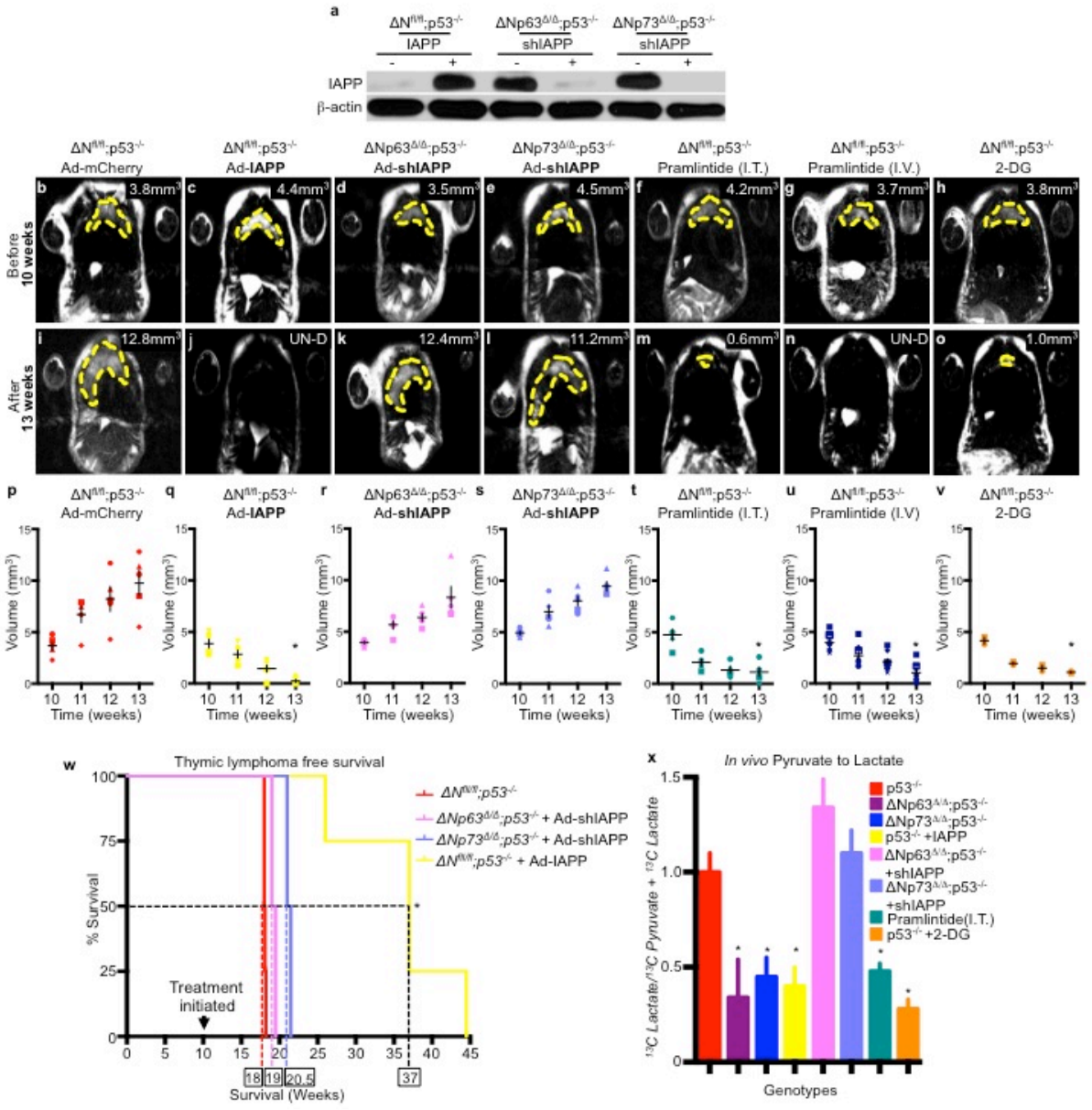

Figure 17: IAPP functions as a tumor suppressor *in vivo*. Western blot analysis showing IAPP expression in the indicated thymic lymphomas, n=5 mice (**a**). Thymic lymphomas were infected with Adenovirus (Ad)-mCherry (**b & i**), Adenovirus (Ad)-IAPP-mCherry (+IAPP)(**c & j**), Ad-shIAPP-mCherry (**d, e, k & l**), or treated with pramlintide intratumoural (I.T.) (**f & m**) or intraveneous (I.V.) (**g & n**), or 2-DG (**h &**

o). Yellow dashed lines indicate tumour. Volume of tumour shown. UN-D = undetectable. Quantification of the indicated thymic lymphomas (**p-v**). n=7 mice per group. Significance indicated by the asterisks, $p<0.005$. Kaplan Meier survival indicating thymic lymphoma free survival (**w**). n=8 mice per group, $p<0.005$ Quantification of *in vivo* pyruvate to lactate conversion using dynamic magnetic resonance spectroscopy as a measurement of glycolysis, n=3 mice, $p<0.005$ (**x**)

4.2.4. IAPP functions as a tumor suppressor *in vivo*

IAPP has been demonstrated to inhibit glycolysis by blocking hexokinase activity(84). Also, I have observed that expressing IAPP in p53-deficient MEFs reduces glycolytic capacity in these cells highlighting the role of IAPP as a regulator of glycolysis. Since, cancer cells and tumors support the notion of Warburg's hypothesis with increased glycolytic rates(75, 76), I wanted to test whether IAPP can inhibit glycolysis in the p53-deficient tumors *in vivo*. Hence, IAPP was expressed in the p53-deficient thymic lymphomas (Figure 17a). Interestingly, upon expressing IAPP, the p53-deficient thymic lymphomas had a massive tumor regression and increased survival compared to the p53-deficient thymic lymphomas that do not express IAPP (Figure 17 b-c, i-j, p-q & w). To test whether IAPP could function as tumor suppressor by itself, IAPP expression was down regulated in the ΔNp63Δ/Δ;p53-/- and ΔNp73Δ/Δ;p53-/- thymic lymphomas in which IAPP expression is high (Figure 17a). Upon down regulating IAPP expression in these thymic lymphomas, the tumors continued to progress similar to the p53-deficient thymic lymphomas (Figure 17 d-e, k-l, r-s & w). Importantly, IAPP expressing p53-deficient mice had increased survival compared to the p53-deficient or ΔNp63/p53 and ΔNp73/p53 double deficient mice in which IAPP was down regulated. This suggests that IAPP functions as bonafide tumor suppressor in p53-deficient cancers.

To further determine whether IAPP mediates the tumor regression in the p53-deficient thymic lymphomas by glycolytic inhibition. We performed an *in vivo* dynamic magnetic hyper-sense resonance spectroscopy to measure the total amount of pyruvate getting converted into lactate, which serves as a proxy for

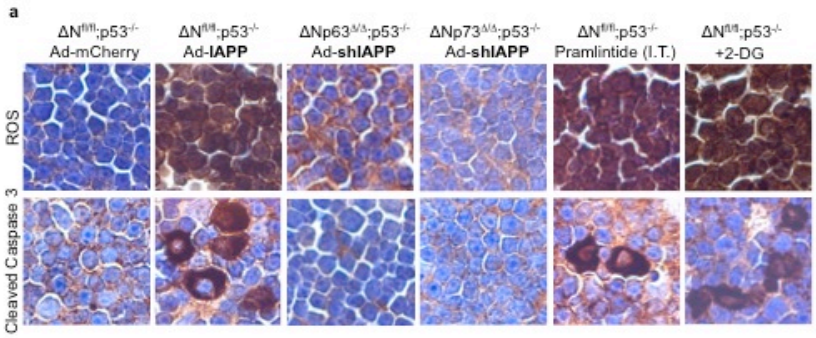

Figure 18: IAPP expression induces ROS accumulation and apoptosis in the p53-deficient thymic lymphomas. Immunohistochemistry for reactive oxygen species (ROS) or cleaved caspase 3 (**a**). Positive nuclei are brown.

glycolysis(110) within the tumor (Figure 17x). We observed that in the ΔNp63/p53 and ΔNp73/p53 double deficient tumors and p53-deficient tumors expressing IAPP, lactate levels were significantly down regulated indicative of reduced glycolysis compared to the p53-deficient tumors. Conversely, when IAPP was down regulated in the ΔNp63/p53 and ΔNp73/p53 double deficient tumors lactate levels were significantly higher and similar to the p53-deficient tumors suggesting increased glycolytic activity (Figure 17x). This suggests that IAPP functions a critical regulator of glycolysis *in vivo*. Importantly, IAPP mediated metabolic inhibition results in tumor regression in p53-deficient mice.

4.2.5. IAPP mediates tumor regression in p53-deficient mice through induction of ROS and cell death *in vivo*

IAPP functions as a bonafide tumor suppressor in p53-deficient mice by glycolytic inhibition. I wanted to delineate the mechanism by which glycolytic inhibition in the tumors results in tumor regression. Previous studies have reported that tumor cells are particularly sensitive to metabolic stress(125). Metabolic stress encountered by the tumor cells correlate with intracellular reactive oxygen species (ROS) levels(125). In general, ROS levels are maintained at low levels and promote tumor cell proliferation. However, under increased metabolic stress in the tumor cells, ROS levels tremendously increase resulting in cell death or cellular senescence(125). Recently, p53 has been demonstrated to induce metabolic stress inhibiting glycolytic pathway resulting in ROS mediated cellular senescence(126).

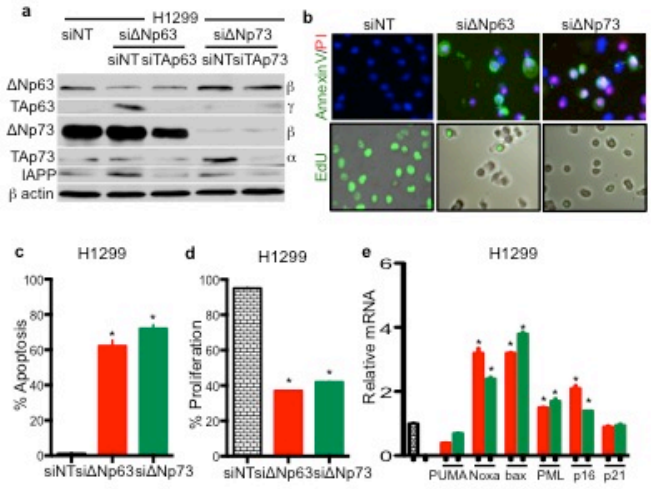

Figure 19: ΔNp63/ΔNp73 ablation induces apoptosis and cell-cycle arrest in p53-deficient human cancer cells. Representative western blot analysis (**a**), n=4. Immunofluorescence (IF) for apoptosis and EdU incorporation (**b**). Quantification of apoptosis (**c**) and proliferation (**d**), n=20 fields of 3 biological replicates, $p<0.005$.

Q-RT-PCR for the target genes indicated on the x-axis in the indicated H1299 cells expressing the indicated siRNAs (**e**), n=4. Asterisks indicate statistical significance ($p<0.005$) relative to siNT.

Interestingly, IAPP functions to inhibit glucose uptake and block glycolysis. This results in increased nutrient related stress for the tumor cells probably leading to intracellular accumulation of ROS and apoptosis (Figure 18a). Indeed, in the ΔNp63/p53 and ΔNp73/p53 double deficient tumors and p53-deficient tumors expressing IAPP, had increased accumulation of ROS that correlated with increased apoptosis compared to the p53-deficient tumors. On the contrary, ΔNp63/p53 and ΔNp73/p53 double deficient tumors in which IAPP was down regulated had no accumulation of ROS or cell death (Figure 18a). This suggests that IAPP mediates tumor regression in p53-deficient mice through the induction of ROS and cell death.

4.2.6. TAp63 and TAp73 compensate for p53-loss by metabolic reprogramming in p53-deficient human cancer cells

By targeting the oncogenic isoforms of p63 and p73, I have demonstrated a novel approach to treat p53-deficient tumors in mice. The tumor regression observed in the p53-deficient thymic lymphomas is through the activation of tumor suppressive isoforms, TAp63 and TAp73. Interestingly, TAp63 and TAp73 transactivate *IAPP*, a metabolic regulator that functions to mediate tumor regression in p53-deficient mice. However, ~50% of the human cancers exhibit either deletions or mutations in the p53 gene. Since, therapeutic approaches to treat p53-altered human cancers are ineffective, I wanted to test whether tumor regression mediated by loss of ΔNp63 and ΔNp73 could be extended to p53-deficient cancers. To test this hypothesis, I extended my analysis to a panel of p53-deficient and mutant cancers. p53-deficient human lung adenocarcinoma cells were co-transfected with siRNA's targeting either ΔNp63 or ΔNp73 in combination with siRNA's for TAp63 and TAp73. I observed that

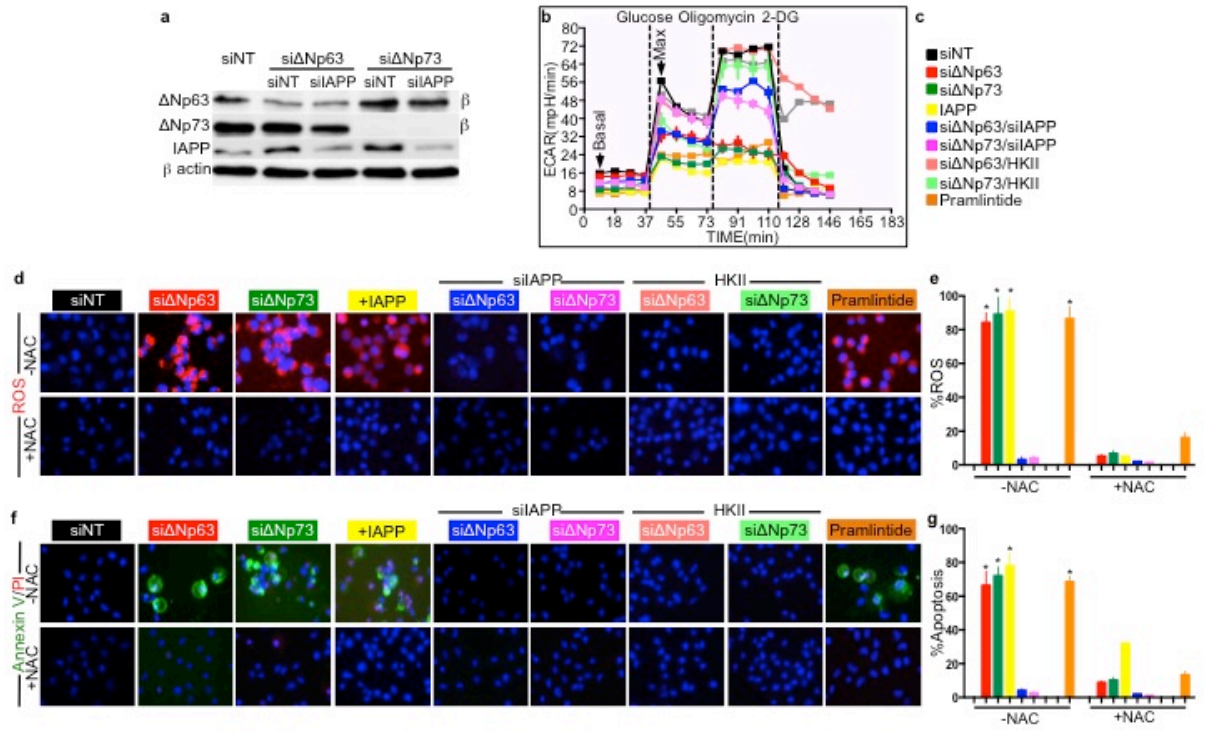

Figure 20: IAPP mediated glycolytic inhibition results in ROS-induced cell death in p53-deficient cancer cells. Western blot analysis of H1299 cells treated with the indicated siRNAs (**a**). Extracellular acidification rate as a measure of glycolysis (**b**), n=3, $p<0.005$. Legend in **c** is color-coded and corresponds to panels **b, d-g**. Immunofluorescence (IF) (**d**) and quantification (**e**) for ROS (red) or apoptosis (green or green/red) (**f & g**)

upon down-regulation of ΔNp63 or ΔNp73, TAp63 and TAp73 upregulation correlated with the increase in IAPP expression in these p53-deficient human cancer cells (Figure 19a). The increase in expression of TA isoforms of p63 and p73 also resulted in the upregulation of apoptosis and cell-cycle arrest targets which in-turn results in the induction of apoptosis and cell cycle arrest (Figure 19b-e).

4.2.7. IAPP directs p53-deficient human cancer cells to a ROS-induced cell death through metabolic reprogramming

IAPP expression was upregulated in p53-deficient human cancer cells after down-regulation of ΔNp63 and ΔNp73 (Figure 20a). This suggests that IAPP could have functional implications in targeting p53-deficient cancer cells to undergo apoptosis. Hence, to test whether IAPP functions as a metabolic regulator in p53-deficient human cancer cells. p53-deficient lung adenocarcinoma cells were transfected with siRNA's for ΔNp63, ΔNp73 individually or in combination with siRNA's for IAPP. Also, IAPP was expressed directly in the p53-deficient cancer cells as well. I observed that after down regulation of ΔNp63/ΔNp73 or expressing IAPP there was significant reduction in the glucose uptake and glycolytic capacity in the p53-deficient human cancer cells compared to the non-targeting treated cells. (Figure 20b). Conversely, upon down regulating ΔNp63/ΔNp73 in combination with IAPP the glycolytic capacity was very similar to the p53-deficient human cancer cells treated with non-targeting siRNA's (Figure 20b). This suggests that IAPP functions as a critical regulator of glycolysis in p53-deficient human cancer cells.

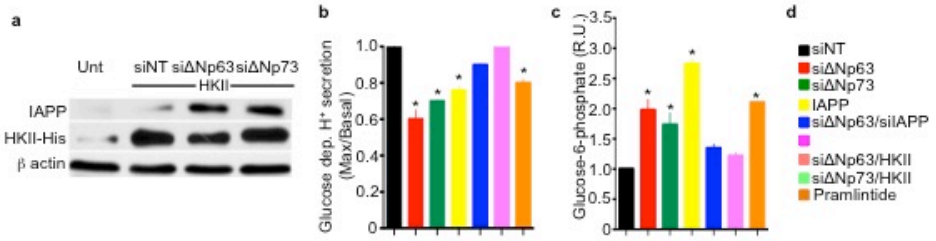

Figure 21: IAPP suppresses glycolysis by inhibiting hexokinase. Western blot analysis of H1299 cells expressing the indicated siRNAs and expression of HKII (**a**). Bar graph indicating glucose dependent proton secretion as a measure of glucose uptake (**b**) and intracellular levels of glucose-6-phosphate in H1299 cells with the indicated siRNAs and treatments (**c**). Color coded legend for panels b & c (**d**).

To test whether IAPP mediated glycolytic inhibition resulted in ROS accumulation and cell death, the p53-deficient human cancer cells were treated with the different indicated siRNA's. Upon knockdown of ΔNp63/ΔNp73 or expression of IAPP, a significant accumulation of intra-cellular ROS (Figure 20d & e) that correlated with the cellular apoptosis (Figure 20f & g) was observed. This effect was completely rescued upon treating the cells with siRNA's for ΔNp63/IAPP and ΔNp73/IAPP or by using an anti-oxidant like N-acetyl cysteine (NAC), functions as a scavenger reducing cellular ROS. This suggests that targeting ΔNp63/ΔNp73 or expressing IAPP can be used as a viable option to treat p53-deficient cancers.

4.2.8. IAPP functions as a metabolic regulator by inhibiting hexokinase

IAPP functions as a bonafide tumor suppressor in p53-deficient human cancer cells. However, the mechanism by which IAPP exhibits its tumor suppressive functions remains unclear. Previous biochemical analysis has revealed that at physiological levels, IAPP functions to inhibit glucose uptake and also increase glucose-6-phosphate (G-6-P) levels(84). Subsequent increase in G-6-P levels results in a feedback inhibition of hexokinase, the rate-limiting enzyme in the glycolytic pathway. Hence to test whether IAPP mechanistically functions in the similar manner in p53-deficient human cancer cells, I measured glucose uptake and gluose-6-phosphate accumulation in the p53-deficient cancer cells. I observed that upon down regulating ΔNp63/ΔNp73 or expressing IAPP there was a significant reduction in the glucose uptake (Figure 21b) and accumulation of the glucose-6-phosphate levels (Figure 21c) in the p53-deficient cancer cells. However, this effect

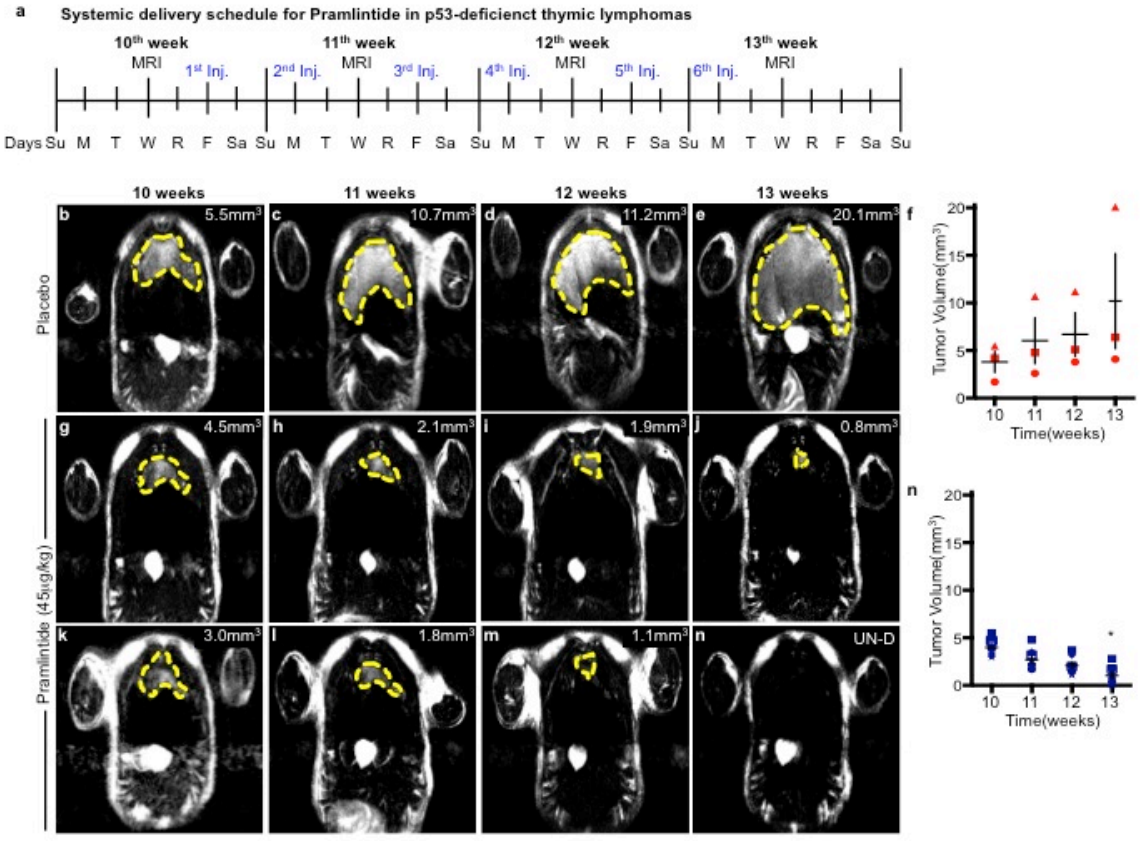

Figure 22: Systemic delivery of pramlintide mediates tumor regression in p53-deficient mice. Cartoon indicating schedule of MRI imaging and injection (Inj.) of pramlintide in mice with *p53* deficient thymic lymphomas (**a**). MRI imaging at 10, 11, 12 and 13 weeks after treatment with placebo (**b-e**) or pramlintide (**g-n**). Quantification of tumour volumes in placebo (n=3) **(f)** and pramlintide treated mice (n=7) **(o)**, $p<0.005$. Statistical significance indicated by black asterisk.

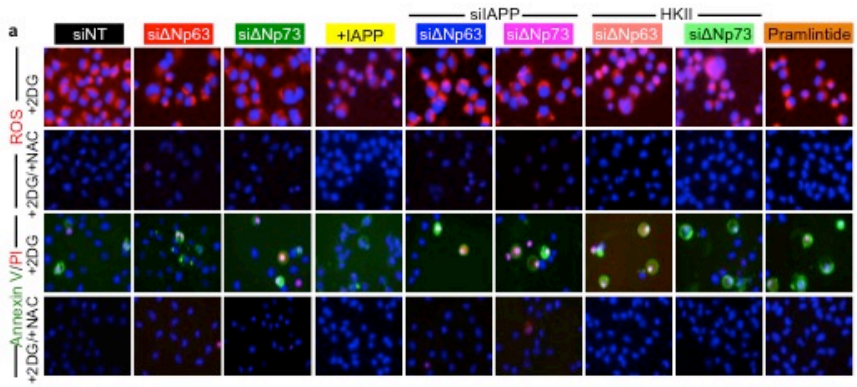

Figure 23: 2-deoxy-D-glucose functions as potent glycolytic inhibitor. Immunofluorescence analysis for ROS (red) or apoptosis (green or green/red) in H1299 cells expressing the indicated siRNAs and treated with 2DG and/or NAC (**a**).

was rescued after treating the cells with siRNA's for either ΔNp63/IAPP or ΔNp73/IAPP.

Additionally, to further validate whether IAPP suppresses glycolysis through inhibition of hexokinase, Hexokinase II (HKII) was expressed after knockdown of either ΔNp63 or ΔNp73 in the p53-deficient human cancer cells (Figure 21a). A significant increase in the glucose uptake (Figure 20b & 21b) and the glycolytic capacity (Figure 20b) and reduction in the G-6-P levels (Figure 21c) in the p53-deficient cancer cells similar to the cells treated with NT siRNA's was observed. This further correlated with very less or no intra-cellular ROS accumulation (Figure 20d & e) and no induction of apoptosis (Figure 20f & g). This suggests that IAPP functions to suppress glycolysis by inhibiting hexokinase activity in the p53-deficient cancer cells.

4.2.9. Pramlintide, a synthetic analog of IAPP: as a glycolytic inhibitor to treat p53-deficient cancer cells

IAPP encodes for amylin, a 37-amino acid peptide secreted from the beta cells in the pancreas. I have demonstrated that IAPP functions as a bonafide tumor suppressor in a p53-deficient model of thymic lymphoma and also in p53-deficient cancer cells. IAPP exhibits its tumor suppression through metabolic reprogramming and inhibiting glycolysis. Interestingly, a synthetic analog of amylin called pramlintide(89) is used in the treatment of diabetes type I and II. Hence, I was interested to test whether pramlintide could be used as an anti-cancer drug to treat p53-deficient tumors and human cancer cells.

Hence, to test the use of pramlintide as an anti-cancer drug, p53-deficient mice that had a significant thymic lymphoma at 10 weeks were administered a single dose of pramlintide intratumorally. By 13 weeks, I observed that the pramlintide treated mice had a significant reduction in the tumor volume compared to the p53-deficient mice treated with placebo (Figure f-g, m-n, t-u). This tumor regression correlated with the reduction in the lactate production as measured by the *in vivo* conversion of C13-pyruvate to lactate suggesting that pramlintide also functions to inhibit glycolysis (Figure 17x). Additionally, pramlintide treatment resulted in the accumulation of intracellular ROS and induction of apoptosis in the p53-defcient tumors highlighting the mechanism of tumor regression (Figure 18a). To test whether pramlintide functions similar to other known glycolytic inhibitors, I treated the p53-deficient mice with 2-deoxy D-glucose (2-DG), a known glycolytic inhibitor (Figure 17h, o & v). I observed similar phenotype of reduction in the lactate production, accumulation of ROS and apoptosis in the p53-deficient tumors upon treating the mice with 2-DG suggesting that pramlintide functions as a glycolytic inhibitor mediating tumor regression. Finally, to test whether systemic *in vivo* delivery of pramlintide mediates tumor regression in the p53-deficient mice, a bi-weekly dose of pramlintide was administered for a period of 3 weeks intravenously to the p53-deficient mice with significant thymic lymphoma (Figure 22a). I observed that, systemic *in vivo* delivery of pramlintide resulted in rapid tumor regression in the p53-deficient mice compared to the placebo treated mice (Figure b-n). This highlights the use of pramlintide as an anti-cancer drug to treat p53-deficient tumors.

To further test the effect of pramlintide in treating p53-deficient human cancer cells, human lung cancer cells were treated with pramlintide. Upon administration of pramlintide, I observed a significant reduction in the glucose uptake and glycolytic capacity (Figure 20b & 21b)) and an increase in the G-6-P levels (Figure 21c) of the p53-deficient human cancer cells. This further correlated with the accumulation of intracellular ROS and cell death in the p53-deficient cancer cells, which was further rescued upon treatment with the N-acetyl cysteine (Figure 20c-f). This suggests that pramlintide, a synthetic analog of amylin, functions to suppress glycolysis by inhibiting hexokinase II (HKII). Importantly, I have also demonstrated the use of a diabetic drug as a potential anti-cancer drug to treat p53-deficient cancers.

Discussion:

Deletion of ΔNp63/ΔNp73 in the p53-deficient mouse tumors, mediates tumor regression in a TAp63 and TAp73 dependent manner. Interestingly, TA isoforms of *p63* and *p73*, which function as transcriptional regulators mediate tumor suppression through activating multiple pathways like apoptosis and cell-cycle arrest. In the p53-deficient thymic lymphomas, I observe that TAp63 and TAp73 induce metabolic reprogramming by recruiting a metabolic regulator IAPP, upon deleting ΔNp63 and ΔNp73. IAPP, which encodes for amylin is a 37-amino acid peptide that functions to maintain glucose homeostasis(84). In the p53-deficient tumors and p53-deficient cancer cells, IAPP functions as tumor suppressor inhibiting glucose uptake and suppressing glycolysis. IAPP, mediates its tumor suppressive function by inhibiting hexokinase (HKII) rate-limiting enzyme in the glycolysis pathway. IAPP mediated glycolytic inhibition results in the accumulation of intracellular ROS resulting in

apoptosis in the cancer cells. Additionally, pramlintide, a synthetic analog of IAPP, used in the treatment of diabetes(89), mediates tumor regression and tumor cell death in p53-altered cancers. Pramlintide mediates tumor cell death in p53-altered cancers by glycolytic inhibition resulting in ROS accumulation and apoptosis whose functions are very similar to known glycolytic inhibitor, 2-DG (Figure 23). However, unlike 2-DG which is highly toxic, pramlintide is less toxic and is also commercially available. Thus, this chapter highlights the identification of a novel metabolic regulator, IAPP and potential use of pramlintide to treat p53-deficient cancers

Chapter 5: IAPP functions through the Calcitonin and RAMP3 receptors to suppress tumorigenesis

Chapter 5: IAPP functions through the calcitonin and RAMP3 receptors to suppress tumorigenesis

Contents of this chapter is based on Venkatanarayan, A., Raulji, P., Norton, W., Chakravarti, D., Coarfa, C., Su, Xiaohua., Sandur, S.K., Ramirez, M.S., Lee, Jaehyuk., Kingsley, C.V., Sananikone, E.F., Rajapakshe, K., Naff, K., Parker-Thornburg, J., Bankson, J.A., Tsai, K.Y., Gunaratne, P.H. and Flores, E.R. IAPP driven metabolic reprogramming induces regression of p53-deficient tumors *in vivo*. *Nature.* 2015; 517(7536),626-630. doi:10.1038/nature13910.

5.1. Introduction and Rationale

IAPP that encodes amylin functions as a secreted protein mediating glucose clearance at physiological conditions(84). *IAPP* functions as a tumor suppressor inhibiting glycolysis in p53-deficient cancers. Since, IAPP is a secreted protein it is still unclear the mode of action of IAPP to execute its tumor suppressive functions. Previous studies have demonstrated that IAPP requires and binds to the calcitonin and RAMP family of receptors(127). Since, IAPP could execute its functions both intrinsically and extrinsically, it is important to understand and determine the role of the receptors in IAPP-mediated tumor suppression in p53-deficient cancers. Additionally, the activity of the receptors could serve as a biomarker in identifying a subgroup of patients responding to pramlintide-based therapies.

5.2. Results

5.2.1. Calcitonin and RAMP3 receptors are required for secreted IAPP function in p53-deficient cancer cells

Since, IAPP is a secreted protein and has been previously demonstrated to show sensitivity to the Calcitonin and RAMP3 receptors(127), I wanted to determine whether IAPP requires the activity of the receptors to execute its tumor suppressive functions. To test whether this is the case, media enriched for IAPP was concentrated after treating the p53-deficient cancer cells with siRNA's for ΔNp63 (siΔNp63^{M}) and ΔNp73 (siΔNp73^{M}). This concentrated media (siΔNp63^{M} or siΔNp73^{M}) was added to the p53-deficient cancer cells in which expression of the Calcitonin and RAMP3 receptors were downregulated after siRNA treatment or to the cells treated with NT siRNA (Figure 24a-c). I observed a significant reduction in glycolysis (Figure 24d) and increase in intra-cellular ROS (Figure 24f) and cell death (Figure 24g) upon addition of IAPP (siΔNp63^{M}/ siΔNp73^{M}) enriched media to the p53-deficient cancer cells treated with NT siRNA's. However, this effect was not observed in the p53-deficient cancer cells in which calcitonin receptor and RAMP3 receptor was downregulated (Figure 24 d,f-g). This suggests that IAPP requires the activity of the calcitonin and RAMP3 receptors to execute its tumor suppressive functions.

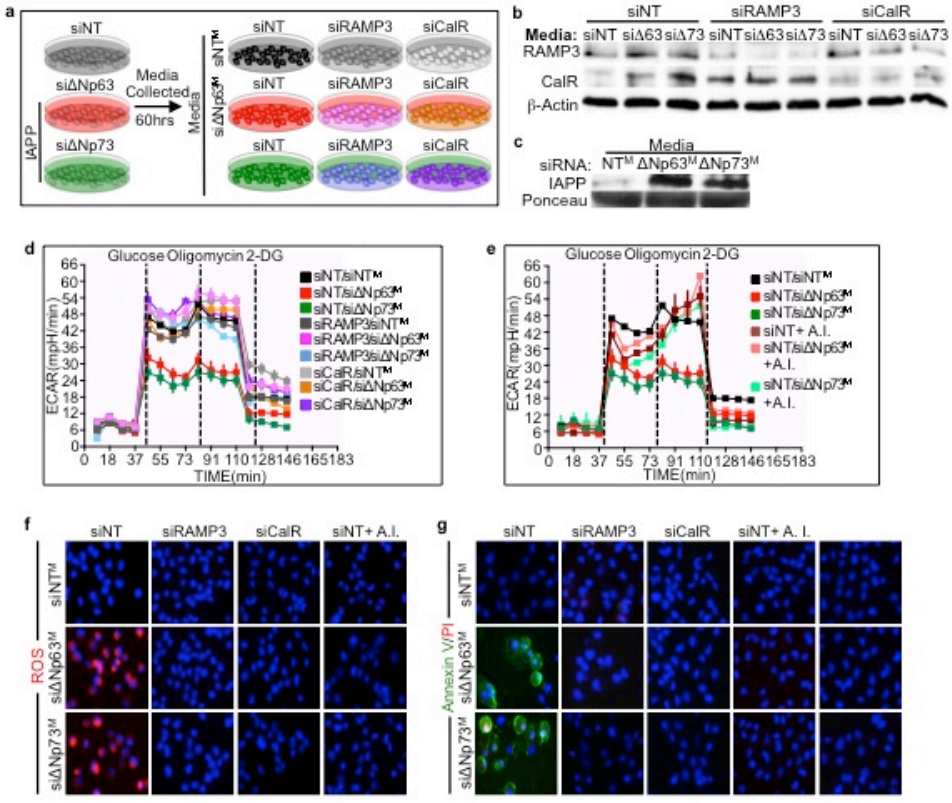

Figure 24: IAPP functions through the activity of the calcitonin and RAMP3 receptors. Cartoon depicting treatment of cells expressing the indicated siRNAs and treated with media from the cells secreting IAPP on the left (**a**). Western blot analysis of H1299 cells expressing the indicated siRNAs (**b)** or concentrated media derived from H1299 cells expressing siNT, siΔNp63, or siΔNp73 (**c**). Extracellular acidification rate (ECAR) in H1299 cells (**d**). Extracellular acidification rate (ECAR) using H1299 cells expressing the indicated siRNAs and treated with the indicated media containing secreted IAPP and treated with the indicated Amylin Inhibitor (A.I.) (**e**)Immunofluorescence (IF) for ROS (**f**) and apoptosis (**g**)

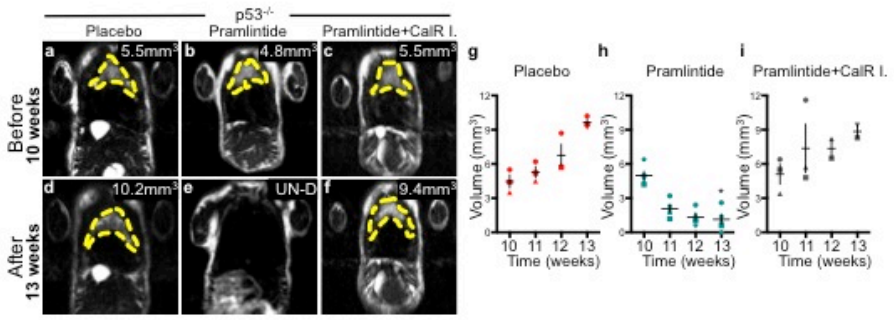

Figure 25: Calcitonin and RAMP3 receptor are required for IAPP/Pramlintide function *in vivo.* MRI and quantification of thymic lymphomas treated with placebo (**a, d, & g**), pramlintide (**b, e, & h**), or pramlintide plus calcitonin inhibitor (CalR I) (**c, f, & i**), n=5 mice

To test whether glycolytic inhibition in the p53-deficient cancer cells is mediated through the IAPP enriched in the media, the NT siRNA treated cancer cells were further treated with amylin inhibitor (A.I.). The amylin inhibitor functions as an agonist and prevents secreted IAPP binding to the receptors. Upon addition of media enriched with IAPP (siΔNp63^{M} or siΔNp73^{M}) to p53-deficient cells treated with A.I. I did not observe any differences in the glycolytic capacity (Figure 24e) or accumulation of ROS (Figure 24f) and apoptosis (Figure 24g). This suggests that secreted IAPP is required to induce glycolytic inhibition, ROS accumulation and apoptosis p53-deficient cancer cells. Further, to test whether, cell death observed in the p53-deficient cancer cells upon IAPP induction is through the intrinsic cell death pathway, siNT treated p53-deficient cells were treated with caspase inhibitor. The treatment with caspase inhibitor completely rescued the effect of IAPP on induction of cell death (Figure 24g). This suggests that IAPP activates cell death machinery to mediate its tumor suppressive function in the p53-deficient human cancer cells.

5.2.2. Pramlintide therapy requires the activity of the calcitonin and RAMP3 receptors

IAPP requires the activity of the calcitonin and RAMP3 receptors to perform its tumor suppressive function in the p53-deficient human cancer cells. To further determine the importance of the receptors *in vivo*, p53-deficient mice with thymic lymphoma at 10 weeks of age were treated with pramlintide by itself or in combination with calcitonin receptor inhibitor (Figure 25). The calcitonin receptor inhibitor prevents binding of IAPP/pramlintide to the calcitonin receptor. Upon pramlintide treatment, the p53-deficient tumors regressed as previously

demonstrated (Figure 25 b, e & h). However, upon inhibition of the calcitonin receptor, pramlintide treatment was ineffective and the tumors progressed to grow similar to the placebo treated p53-deficient mice (Figure 25 c,f & i). This suggests that calcitonin and RAMP3 receptors are required the tumor suppressive function exhibited by IAPP/Pramlintide in treating p53-deficient cancers.

Discussion

IAPP is cosecreted along with insulin from the beta cells of the pancreas. Although, IAPP was previously demonstrated to utilize the calcitonin and RAMP-family of receptors, the mode of action of IAPP was still unclear. I have demonstrated that IAPP/pramlintide mediates its tumor suppressive function through the calcitonin and RAMP3 receptors. Abolishing the activity of either calcitonin or the RAMP3 receptor renders IAPP/pramlintide function ineffective. This highlights an important association of IAPP function with its receptors. Since, pramlintide could be used as a potential drug to treat p53-deficient cancers, determining the status of the receptors will enable selecting patient cohorts responding to the pramlintide treatment and also ensure improved drug efficacy.

Chapter 6: Therapeutic approaches to treat p53-mutated human cancers

Chapter 6: Therapeutic approaches to treat p53-mutated human cancers

6.1. Introduction and Rationale:

TP53 functions as well-documented tumor suppressor. However, most human cancers, harbor p53-mutations altering its function(118). Majority of the human cancers carry a common set of mutations commonly referred to as “Hot Spot” mutations. Mutations in the p53-gene have gain of function activities and in many cases promote tumor progression. The oncogenic properties of mutant p53 are carried out by competitive binding to other tumor suppressors or by activating oncogenes. Current therapeutic strategies are aimed towards downregulating the activity of mutant p53 in human cancers and reactivating wild-type p53(128). However, this therapeutic strategy has been challenging due to the multiple interactions of p53 with other pathways. Hence, this necessitates the need to identify other novel mechanisms to treat mutant p53 tumors. In this chapter, I aim to delineate the interaction between mutant p53 and the p53-family members *p63* and *p73*. Additionally, use of pramlintide to therapeutically treat p53-mutated cancers will be tested.

6.2. Results

6.2.1. Interaction between mutant p53 and p53-family members, p63 and p73

Previously, I have demonstrated that targeting the oncogenic ΔN isoforms of p63 and p73, results in tumor regression in p53-deficient cancers. This tumor

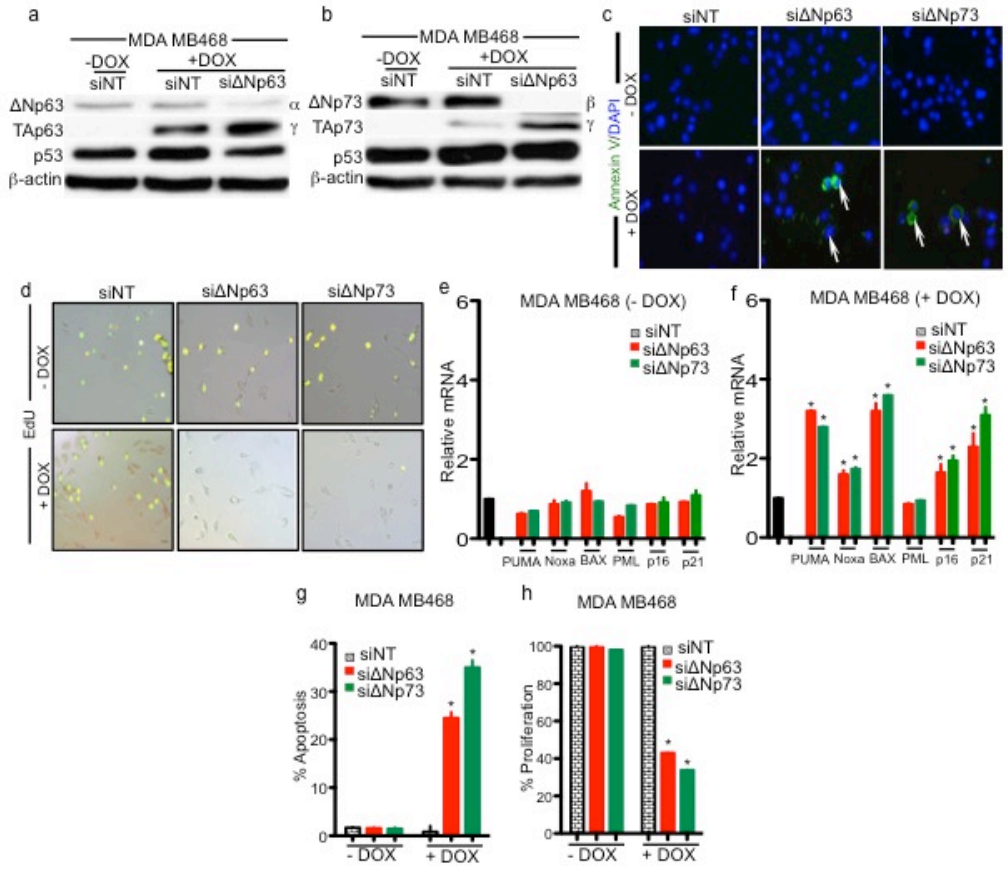

Figure 26: Deletion of ΔNp63/ΔNp73 in combination with genotoxic stress induces apoptosis and cell-cycle arrest in p53-mutant human breast cancer cells. Representative western blots with the indicated genotypes (**a** & **b**) (n=3). Immunofluorescence (IF) and quantifications for apoptosis (**c & e**) and proliferation (**d & f**) for the indicated siRNA's with or without doxorubicin treatment. (n=3) Q-RT PCR analysis for the apoptosis and cell-cycle arrest targets for the indicated siRNA's with of without doxorubicin treatment (n=3, $p<0.0005$). Asterisks represent significance.

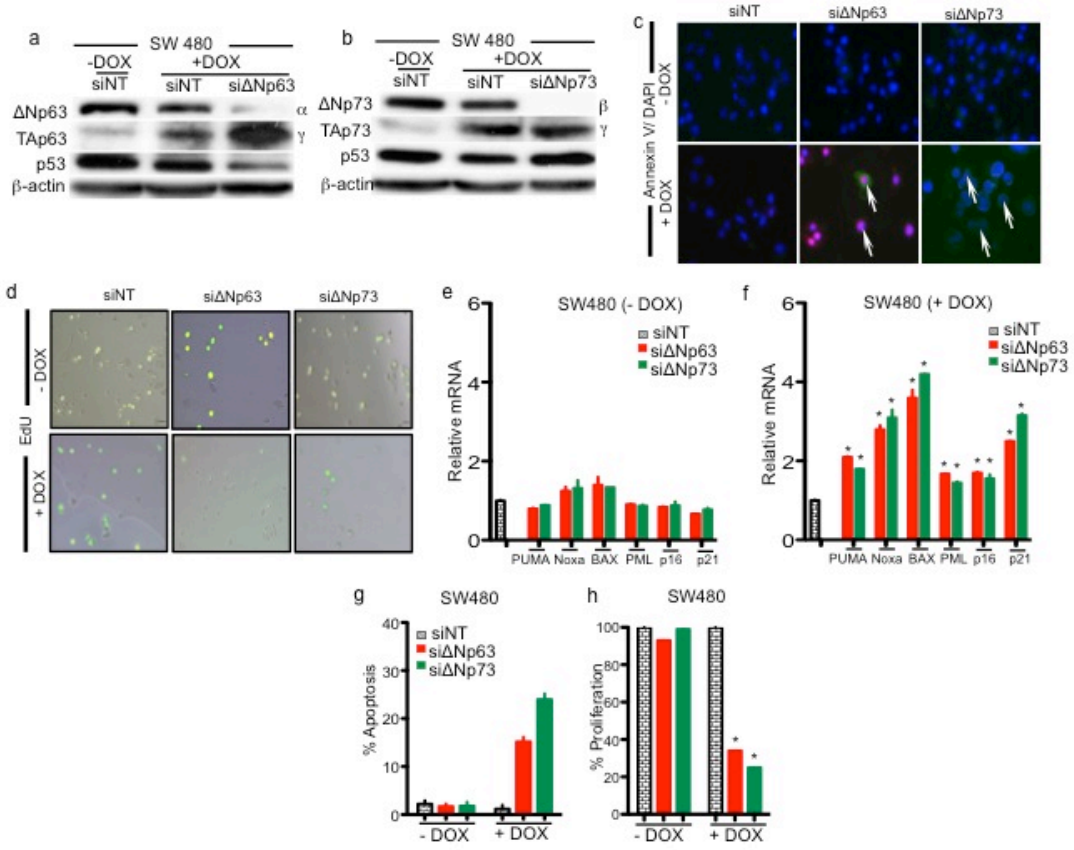

Figure 27: Deletion of ΔNp63/ΔNp73 in combination with genotoxic stress induces apoptosis and cell-cycle arrest in p53-mutant human colorectal cancer cells. Representative western blots with the indicated genotypes (**a** & **b**) (n=3). Immunofluorescence (IF) and quantifications for apoptosis (**c & e**) and proliferation (**d & f**) for the indicated siRNA's with or without doxorubicin treatment. (n=3) Q-RT PCR analysis for the apoptosis and cell-cycle arrest targets for the indicated siRNA's with of without doxorubicin treatment (n=3, $p<0.0005$). Asterisks represent significance.

regression is mediated through the activation of tumor suppressive isoforms of p63 and p73, namely TAp63 and TAp73. Hence, to determine whether targeting ΔNp63 and ΔNp73 could mediate tumor regression in mutant p53 human cancer cells, ΔNp63 and ΔNp73 was downregulated to two mutant human cancer cells namely, MDA MD468 breast adenocarcinoma cells (Figure 26) and SW 480 colorectal adenocarcinoma (Figure 27) that harbor p53 mutations. Upon silencing ΔNp63 and ΔNp73 in the mutant p53 human cancer cells, I observed a significant increase in the expression of TAp63 and TAp73 (Figure 26a & 27a), validating our previous finding that loss of ΔN isoforms of p63 and p73 restores the expression of TAp63 and TAp73 in human cancer cells. To further test whether increased expression of TAp63 and TAp73 correlates with the cell death and cell cycle arrest, qRT-PCR for apoptosis and cell cycle targets and an apoptosis assay and EdU incorporation assay was performed in the mutant p53-cancer cells after downregulating either ΔNp63/ΔNp73. Interestingly, no increase in expression levels of the targets (figure 26e & 27e), cell death (Figure 26c,g & 27c,g) or decrease in cell cycle arrest (Figure 26d,h & 27d,h) was observed in the ΔNp63/ΔNp73 downregulated p53-mutant cancer cells compared to the cells treated with the NT siRNA's. This suggests that although loss of ΔN isoforms of p63 and p73, restores the expression of TAp63 and TAp73 in mutant human cancer cells, the TA isoforms of p63 and p73 could not execute its tumor suppressive function in the mutant p53-cancer cells. One of the reasons for TAp63 and TAp73 to not execute its tumor suppressive function in mutant p53-human cancer cells could be due the gain-of function effect of mutant

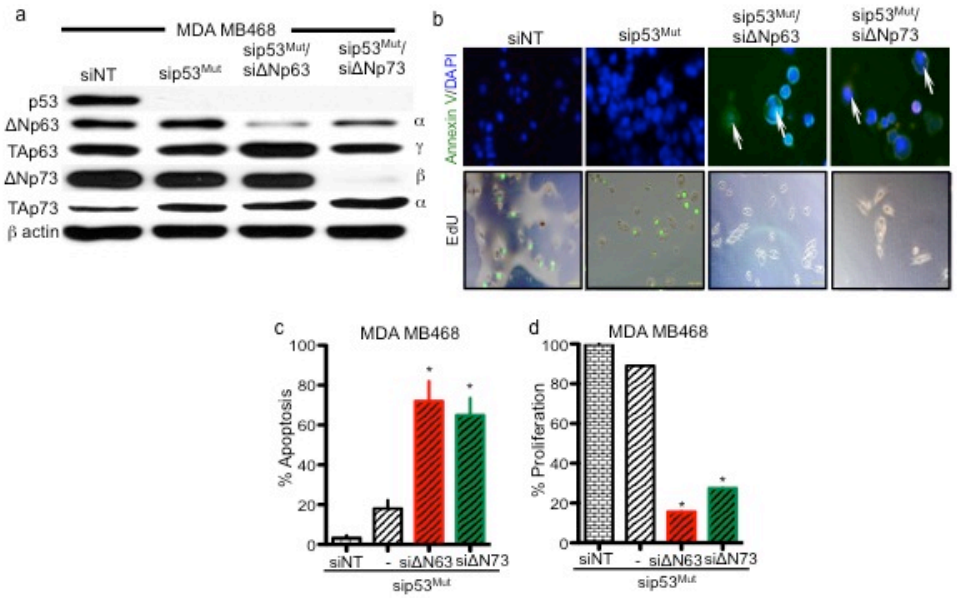

Figure 28: Deletion of ΔNp63/ΔNp73 in combination with mutant p53 induces apoptosis and cell cycle arrest in p53-deficient human breast cancer cells. Representative western blot analysis with the indicated siRNA's (**a**) (n=3). Immunofluorescence (IF) and quantification for apoptosis (**b** & **c**) and for cell-cycle arrest (**b** & **d**) for the indicated siRNA treatment conditions.

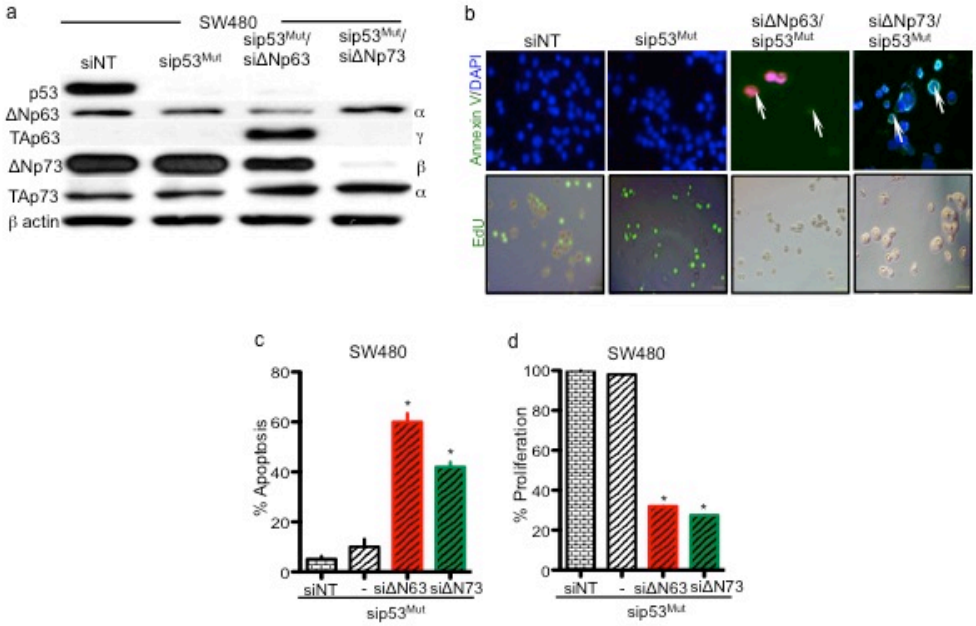

Figure 29: Deletion of ΔNp63/ΔNp73 in combination with mutant p53 induces apoptosis and cell cycle arrest in p53-deficient human colorectal cancer cells. Representative western blot analysis with the indicated siRNA's (**a**) (n=3). Immunofluorescence (IF) and quantification for apoptosis (**b** & **c**) and for cell-cycle arrest (**b** & **d**) for the indicated siRNA treatment conditions.

p53 which could form tetramers with TA isoforms of p63 and p73, preventing its transcriptional function(129).

6.2.2. Targeting the ΔN isoforms of p63 and p73 combined with genotoxic stress induces cell death and cell-cycle arrest in mutant p53 human cancer cells

Gain of function effects of mutant-p53 prevents TAp63 and TAp73 from executing their tumor suppressive function after ablation of ΔNp63 or ΔNp73 in the p53- mutant human cancer cells. However, a significant increase in the expression TAp63 and TAp73 after ablation of ΔNp63/ΔNp73 in the mutant p53-cancer cells was observed. Since, TAp63 and TAp73 also respond to genotoxic stress, I wanted to determine whether loss of ΔN isoforms of p63 and p73 in combination with genotoxic stress would mediate cell death or cell-cycle arrest in the mutant p53 cancer cells. Interestingly, loss of ΔNp63/ΔNp73 in combination with genotoxic stress resulted in a significant increase in the expression of TAp63/TAp73 (Figure 26b & 27b), which further correlated with the increase in expression of apoptosis and cell cycle targets (Figure 26f & 27f), induction of cell death (Figure 26 c,g & 27 c,g) and cell cycle arrest (Figure 26d,h & 27d,h) in the mutant p53-human cancer cells. This suggests that significantly increasing the expression of TAp63 and TAp73 in the mutant p53 cancer cells could function to overcome the gain-of function effect of mutant p53 resulting in cancer cell death and cell-cycle arrest.

6.2.3. Mutant p53 inhibits TAp63 and TAp73 mediated tumor suppression in human cancer cells

Targeting ΔNp63 and ΔNp73 in mutant p53 human cancer cells restores expression of TAp63 and TAp73. However, due to the gain of function effects of mutant p53, TAp63 and TAp73 tumor suppressive function is inhibited. Hence, to test whether this is the case, siRNA's targeting p53 was used by itself or in combination with siRNA's for ΔNp63 and ΔNp73 in the mutant p53 human cancer cells (Figure 28a & 29a). An increase in apoptosis (Figure 28b-c & 29b-c) and decrease in proliferation (Figure 28b,d & 29b,d) in the mutant p53 human cancer cells was observed upon downregulating both ΔNp63/p53 and ΔNp73/p53 in comparison to downregulating only p53. Induction of apoptosis and cell cycle arrest correlated with the increased expression of TAp63 and TAp73 in the p53-mutant human cancer cells. This suggests that mutant p53 inhibits TAp63 and TAp73 from mediating its tumor suppressive functions. Hence, targeting ΔN isoforms of p63 and p73 in combination with mutant p53, serves as novel approach to treat these cancer types.

6.2.4. Pramlintide based therapy to treat p53-mutant cancers

Previously, I have demonstrated that Pramlintide, synthetic analog of amylin/IAPP mediates cancer cell death in p53-deficient cancer cells. Pramlintide mediates its tumor suppressive function by suppressing glycolysis through the inhibition of hexokinase activity. Importantly, the function of Pramlintide is mediated

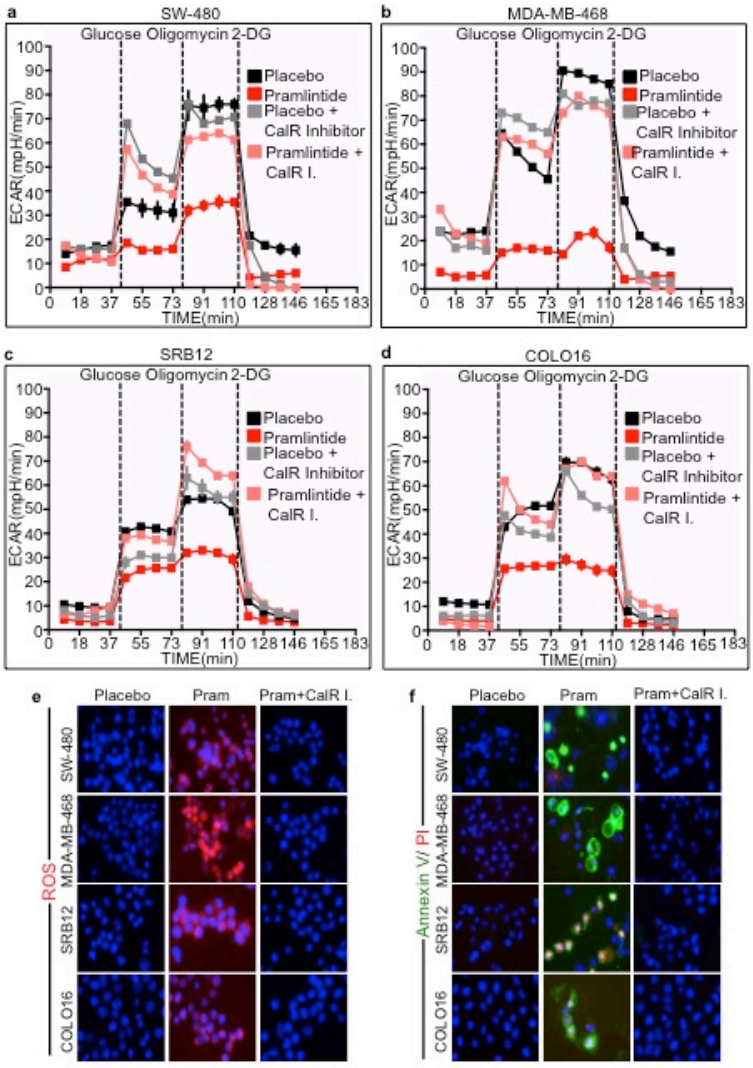

Figure 30: Pramlintide treatment suppresses glycolysis and results in ROS-induced apoptosis in p53-mutant human cancer cells. Extracellular acidification rate (ECAR) as a measure of glycolysis in SW480 **(a)**, MDA- MB-468 **(b)**, SRB12 **(c)** and COLO16 **(d)** human cancer cell lines after treatment with placebo, pramlintide, or pramlintide and a calcitonin receptor inhibitor (CalR I.), n=3, p< 0.005. Glucose, oligomycin, and 2-Deoxy-D-Glucose (2-DG) were supplied to the media at the indicated time points shown on the x-axis. Immunofluorescence for ROS (red) **(h)** and apoptosis (green) **(i)** on the indicated cells, n=3.

downstream of the transcriptional activity of p53 and its family members. This highlights a novel approach to treat p53-mutated cancers as the pramlintide mediates its function independently of p53-status. Hence, to test whether pramlintide could be used to treat p53-mutant cancers, a panel of mutant p53 human cancer cell lines that include, SW480 (colorectal adenocarcinoma) (Figure 30a), MDA- MB-468 (breast adenocarcinoma) (Figure 30b), COLO16 and SRB12 (squamous cell carcinoma) (Figure 30c&d) were selected. Upon treating the mutant p53 human cancer cells with pramlintide, significant reduction in the glycolytic capacity that correlated with an increase in intracellular ROS (Figure 30e) and cell death (Figure 30f) compared to the cell lines treated with the placebo was observed. To test whether apoptosis observed in the mutant p53 cancer cells is due effect of pramlintide, the cancer cells were treated with pramlintide by itself or in combination with calcitonin receptor inhibitor. The p53-mutant human cancer cells treated with calcitonin receptor inhibitor did not respond to pramlintide treatment suggesting that pramlintide mediated inhibition of glycolysis mediates tumor cell death in the p53-mutant human cancer cells. Importantly, the use of Pramlintide serves as a novel approach to treat hard to treat p53-mutant human cancer cells.

6.2.5. Pramlintide based therapy to treat squamous cell cancers (SCC)

Squamous cell cancers (SCC) are a type of skin cancer. SCC is caused primarily due to the multiplication of the epithelial cells of the skin, head and neck, linings of the digestive tract, lungs and genitals(106, 130). One of the factors that promote SCC formation is the exposure to UV skin light over an extended period of

Immunocompetant	Renal Transplant	RDEB	Other Cell lines	Normal KC
SCC 1C1	SCC T1	RDE B2	COLO16	WT
	SCC T2	RDE B3	SRB12	HaCaT
	SCC T3	RDE B4	SRB1	
	SCC T8			

Table 3: Table representing a panel of patient derived human squamous cell carcinomas cells with alterations in p53.

High Glycolysis	Medium Glycolysis	Low Glycolysis
COLO16	SCC 1C1	SCC T1
SRB12	SRB 1	SCC T3
RDE B2	SCC T8	SCC T8
RDE B3		
RDE B4		

Table 4: Table representing a classification of human SCC cells based on the basal glycolytic profile

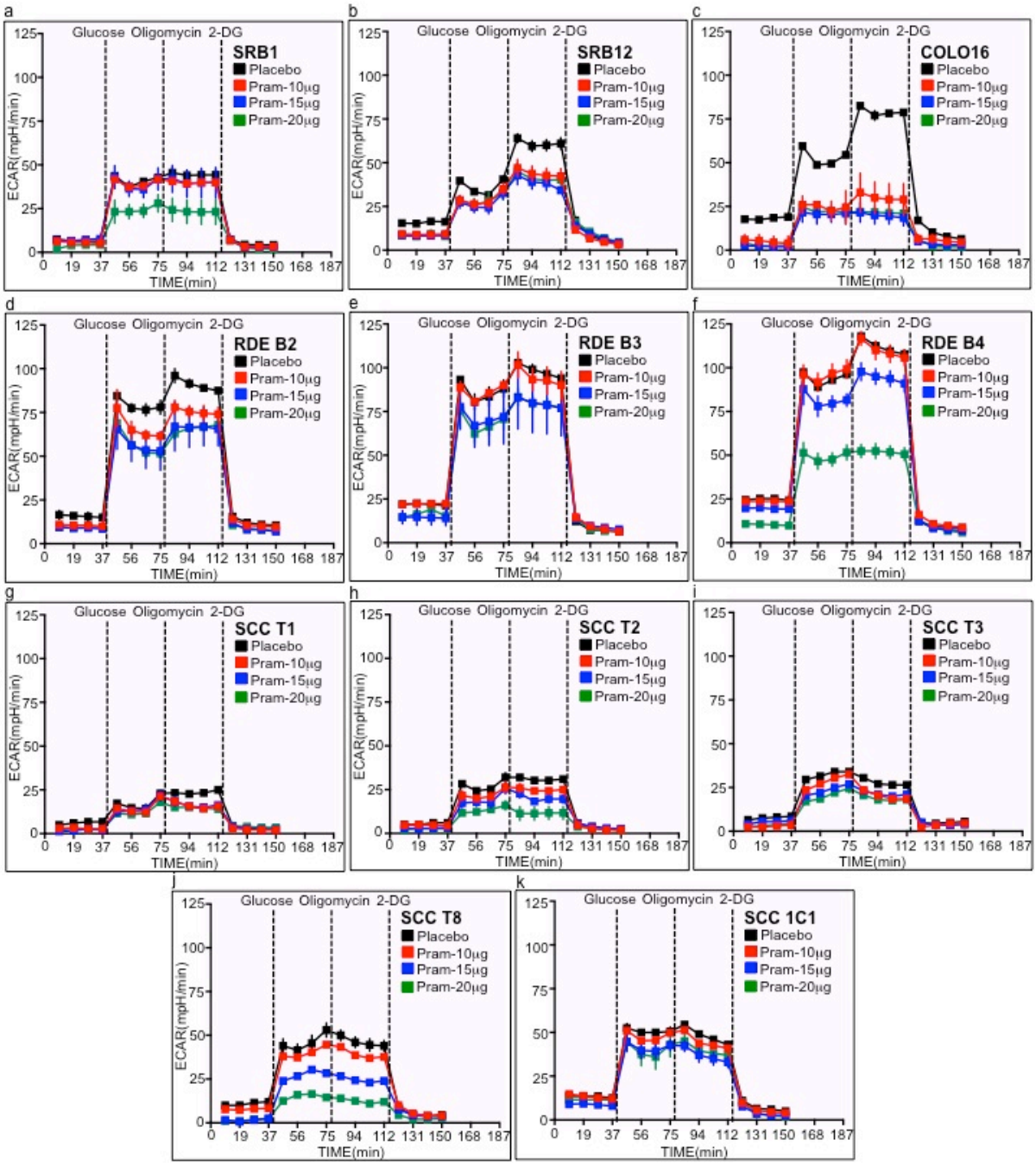

Figure 31: Pramlintide treatment suppresses glycolysis in human SCC cells. Extracellular acidification rate as a measure of glycolysis in a panel of human SCC cells SRB1 (**a**), SRB12 (**b**), COLO16 (**c**), RDE B2 (**d**), RDE B3 (**e**), RDE B4 (**f**), SCC T1 (**g**), SCC T2 (**h**), SCC T3 (**i**), SCC T8 (**j**) and SCC 1C1 (**k**) subjected to indicated doses of pramlintide treatment.

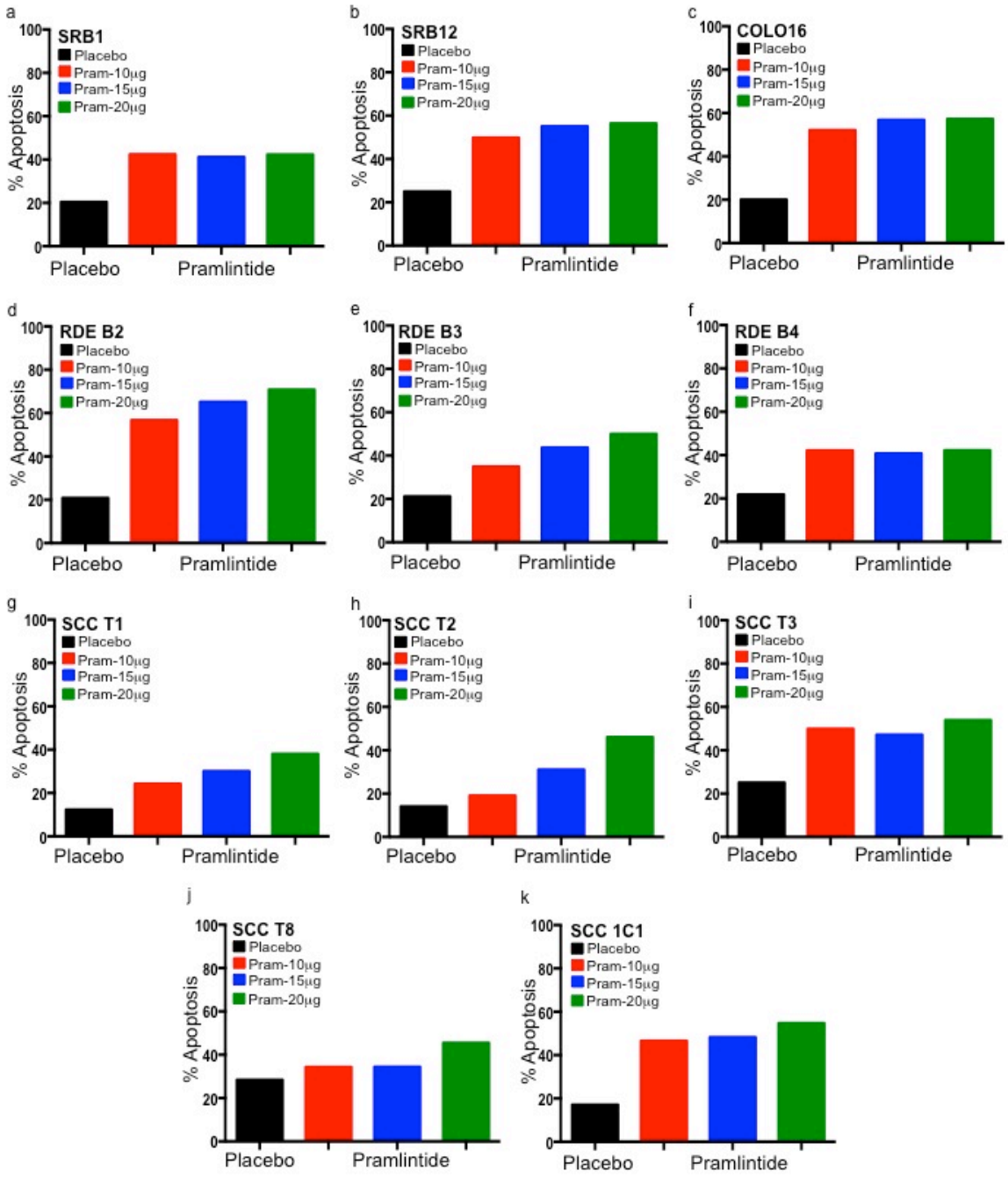

Figure 32: Pramlintide treatment induces apoptosis in human SCC cells. Quantification of apoptosis (Annexin V and PI) in a panel of human SCC cells SRB1 (**a**), SRB12 (**b**), COLO16 (**c**), RDE B2 (**d**), RDE B3 (**e**), RDE B4 (**f**), SCC T1 (**g**),

SCC T2 (**h**), SCC T3 (**i**), SCC T8 (**j**) and SCC 1C1 (**k**) subjected to indicated doses of pramlintide treatment.

time promotes loss of elasticity and pigmentation of the cells. Approximately, 700,000 cases of SCC have been diagnosed every year(130). There are multiple gene alterations that drive tumor formation and one of the alterations occur in the TP53 gene due to point mutations and truncating mutations(113, 114). Currently, therapeutic approaches to treat SCC are limited. Since, pramlintide treatment has shown tremendous potential in treating p53-mutant human cancer cells, I was interested in determining the therapeutic efficacy of treating SCC human cancer cells with pramlintide. Hence a panel SCC human cancer cells with mutations in p53 gene were selected (Table 3). Since, pramlintide functions by inhibiting glycolysis, the basal glycolytic capacity of these SCC panel of cells was determined to classify the cells based on their glycolytic profile (Table 4). The SCC human cancer cells were classified into three types, highly glycolytic, medium glycolytic and less glycolytic based on their glycolytic prolife (Table 4). I suspect that SCC cells with higher glycolytic rate would respond with better efficacy to pramlintide treatment.

6.2.6. Pramlintide treatment inhibits glycolysis and induces cell death in the human SCC cells

To test whether pramlintide mediates glycolytic inhibition in the human SCC cells, the glycolytic capacity of the cells was measured with increasing concentrations of pramlintide. I observed differences in the response to pramlintide depending on the basal glycolytic profile of the SCC cells (Figure 31). However, in most of the SCC cells, I observed an increased suppression of glycolysis at a higher concentration of pramlintide. Additionally, the glycolytic inhibition correlated with a increase in cell death in the SCC cells as measured by the Annexin V and propidium

iodide staining (Figure 32). This highlights the importance to using pramlintide-based therapy to treat human SCC cancers. Currently, I am testing the use of pramlintide in the patient derived models (PDX) using the human SCC cells. Also, I am interested in determining whether pramlintide affects mitochondrial respiration in the SCC cells.

Discussion

Approximately, 50% of human cancer harbor mutations in the *p53* gene(122). Mutant p53 functions as a proto-oncogene promoting tumorigenesis. Further, because of its gain of functions effects, targeting mutant p53 in human cancers has been challenging. In this chapter, I have demonstrated that mutant p53 inhibits TAp63/TAp73 mediated tumor suppression in p53-mutated human cancers. Targeting the oncogenic isoforms of p63 and p73 in combination with genotoxic stress could result in significant accumulation of TAp63 and TAp73, thereby overcoming mutant p53 effect. However, administration of genotoxic stress results in non-specific activation multiple other pathways.

As a novel approach to treat p53-mutant cancers, I have proposed the use of pramlintide, a synthetic analog of IAPP. Pramlintide functions by inhibiting glycolysis and functions independently of the status of the p53-family members. Preliminary data from my thesis has shown great promise in mediating tumor cell death in a panel of mutant p53 human cancer cells. Currently, I have expanded my analysis to human squamous cell cancers and their treatment with pramlintide. Initial *in vitro* results have demonstrated that pramlintide functions effectively in highly glycolytic tumor cells by blocking glycolysis and inducing apoptosis.

Chapter 7: Therapeutically targeting the oncogenic isoforms of p63 and p73 to treat p53-deficient human cancers

Chapter 7: Therapeutically targeting the oncogenic isoforms of p63 and p73 to treat p53-deficient human cancers

7.1. Introduction and Rationale

ΔNp63 and ΔNp73 have been demonstrated to function as oncogenes in p53-deficient human cancers. Importantly, ablation of these oncogenic isoforms of p63 and p73 has identified a new therapeutic approach to treat p53-deficient cancers. Previously, I have demonstrated that ablation of ΔNp63 and ΔNp73 mediates tumor regression through the activation of TAp63 and TAp73, the tumor suppressive isoforms of p63 and p73. Hence, by therapeutically targeting ΔNp63/ΔNp73 in p53-defcient cancers will activate the tumor suppressive properties of TAp63 and TAp73. Additionally, we have also performed a miRNA-sequencing on the p53-deficient thymic lymphoma tissues in which either ΔNp63/ΔNp73 was ablated.

To therapeutically target ΔN isoforms of p63 and p73 in p53-deficient cancers, *in vivo*, I have adopted a DOPC liposomal nanoparticle(131, 132) delivery approach of utilizing siRNA's targeting ΔNp63. These liposomal coated nanoparticle siRNA's could be delivered to the site of the tumor and are not phaogcytosed. This enables us to develop a novel approach to treat p53-deficient tumors by targeting the oncogenic isoforms of p63 and p73.

7.2. Results

7.2.1. Liposomal siRNA delivery of ΔNp63 mediates tumor regression in p53-deficient mice

Ablation of ΔNp63 mediates tumor regression through the activation of TAp63. To therapeutically target ΔNp63 in p53-deficient tumors, I performed a liposomal delivery of siRNA targeting ΔNp63 into the p53-deficient thymic lymphoma at 10 weeks. Administration of liposomal coated siRNA's was specifically localized only to the region of the thymic lymphoma as visualized by the IVIS lumina imaging (Figure 33a-i). ΔNp63 expression was downregulated 48 hours after administration of the DOPC liposomal siRNA in the p53-deficient thymic lymphoma. This correlated with the increase in the expression of TAp63 and also downregulation of DGCR8, another downstream target of ΔNp63 (Figure 33j). Additionally, the downregulation of ΔNp63 expression in the p53-deficeint thymic lymphoma tissues correlated with the increase in apoptosis and cell-cycle arrest 48 hours after treatment with siRNA's. (Figure 33k) This suggests that therapeutically targeting ΔNp63 in p53-defcient tumors *in vivo*, induces cell death and cell cycle arrest.

Since, targeting ΔNp63 in p53-deficient cancers *in vivo* was therapeutically feasible, I wanted to test whether siRNA mediated knockdown of ΔNp63 would mediate tumor regression in p53-deficient mice. To determine the stability of the siRNA's *in vivo*, a single does of siΔNp63 was administered into the p53-deficient thymic lymphoma. The thymic lymphomas tissues treated with siΔNp63 were

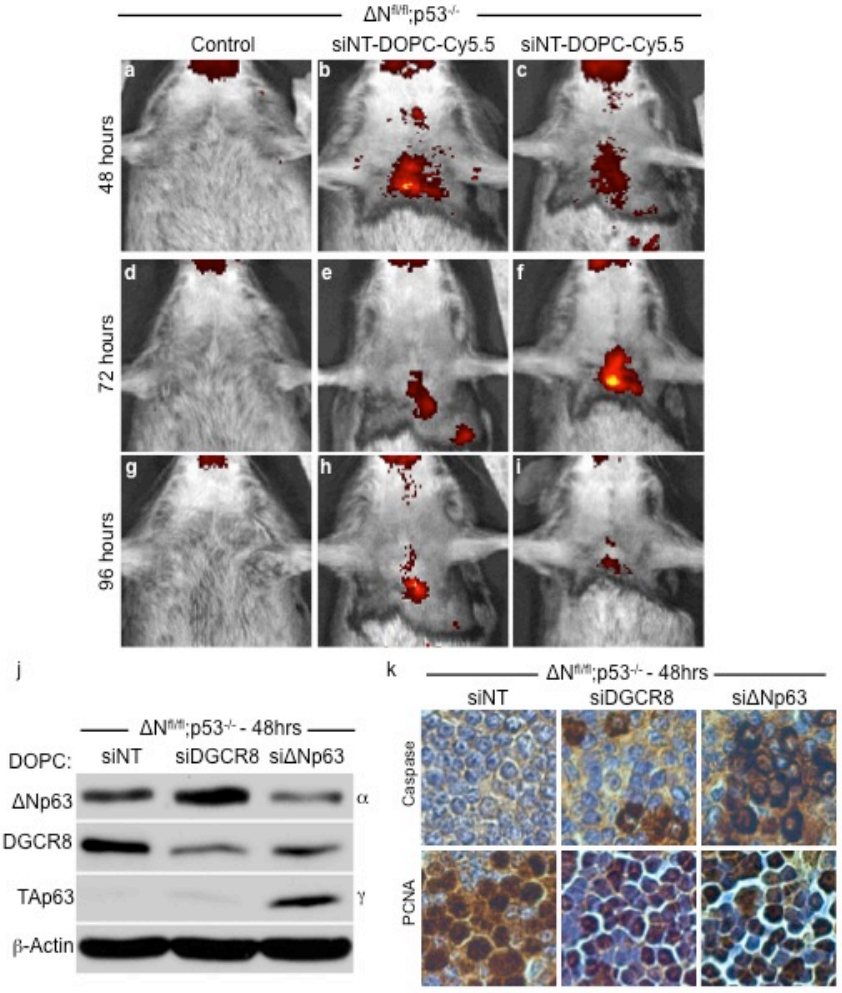

Figure 33: Liposomal siΔNp63 administration in p53-deficient thymic lymphomas induces apoptosis and cell cycle arrest. IVIS Lumina imaging of p53-deficient thymic lymphomas administered with DOPC liposomal nanoparticle coated siRNA's. Presence of the red color marks the region of the siRNA administration which is localized to the thymic lymphoma **(a-i)**. Representative western blot analysis of p53-deficient thymic lymphoma tissues 48 hours after treatment with indicated siRNA's **(j)** (n=3). Immunohistochemistry (IHC) panel of for apoptosis and proliferation in p53-deficient thymic lymphoma tissues 48 hours after treatment with indicated siRNA's. Brown nuclei labels the positive cells.

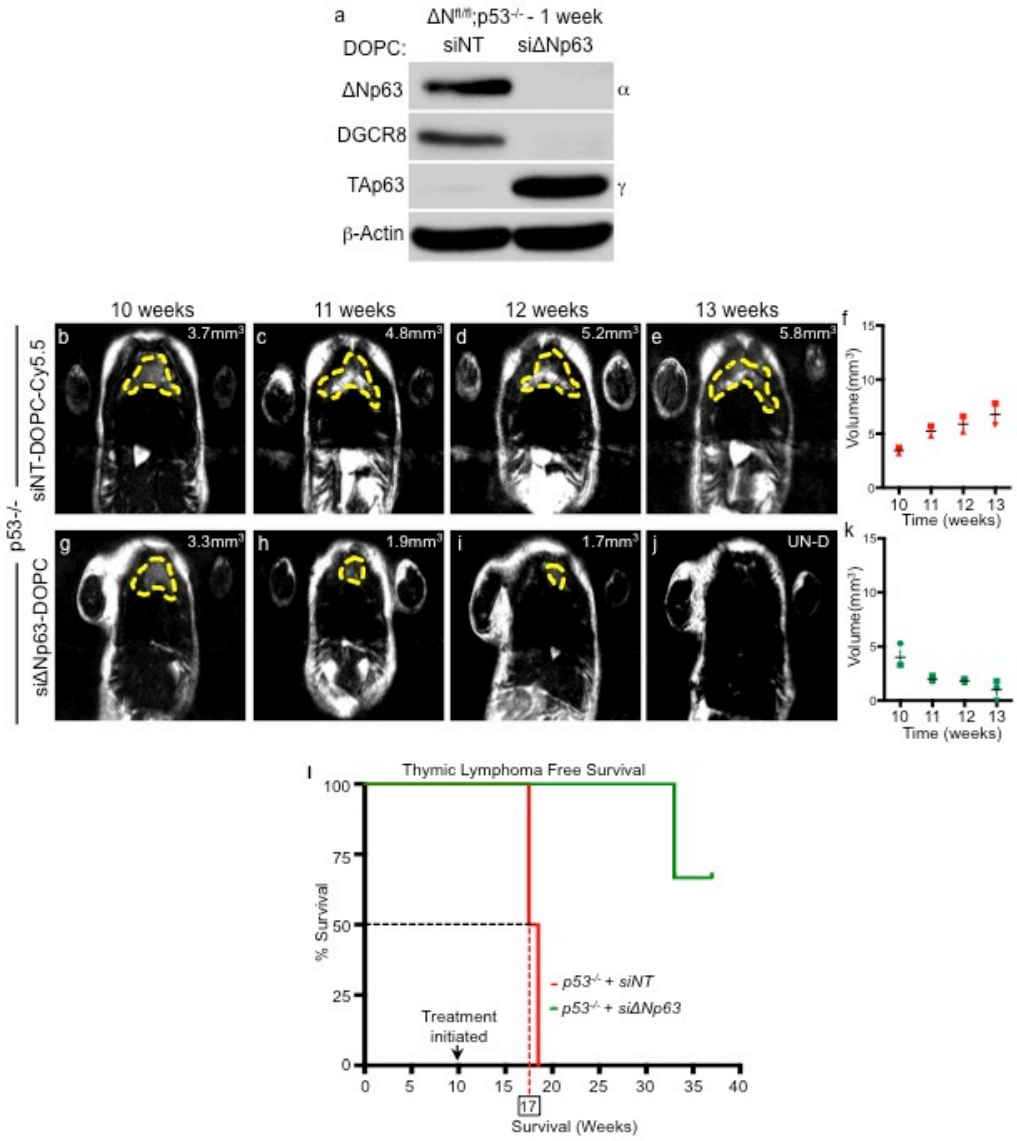

Figure 34: Therapeutically targeting ΔNp63 by liposomal siRNA's in p53-deficient thymic lymphomas mediates tumor regression. Representative western blot analysis of p53-deficient thymic lymphomas treated with indicated siRNA's **(a)**. Magnetic resonance imaging (MRI) of p53-deficient thymic lymphoma treated with siNT **(b-f)** or siΔNp63 **(g-k)**. Tumor volumes (mm^3) included in each panel. Yellow dashed line marks region of the tumor. UN-D refers to undetectable.

Tumor volume measurements for siNT treated **(l)** and siΔNp63 treated **(j).** Kaplan Meier (KM) plots indicating thymic lymphoma free survival, n=3 mice per group, $p<0.0005$.

collected 1 week after dose administration to determine the expression of ΔNp63. Interestingly, even 1 week after administering siΔNp63 into the p53-deficient thymic lymphoma, a significant downregulation of ΔNp63 expression and upregulation of TAp63 expression was observed (Figure 34a). Based on this analysis, a single dose of siΔNp63 was administered into the p53-deficeint thymic lymphoma at 10 weeks of age for period of 3 weeks. A significant reduction the tumor volume (Figure 34b-k) and increase in the life-span (Figure 34k) as observed in the p53-deficient mice upon treatment with siΔNp63 compared to the mice treated with non-targeting (NT) siRNA's. This highlights an important therapeutic approach to treat p53-deficient tumors.

Discussion

Current therapeutic approaches to treat p53-deficient human cancers are aimed towards reactivating wild-type p53 by inhibiting MDM2, negative regulator of p53(128). Although this approach is currently entering clinical trials some challenges remain in reactivating wild-type p53 across multiple cancers. However, by utilizing the function of p53-family members, I have demonstrated a novel approach to treat p53-deficient cancers *in vivo*. ΔNp63 and ΔNp73 are expressed in all epithelial cancers and not mutated making them unique targets for therapeutic intervention. I have demonstrated that by therapeutically targeting ΔNp63 using liposomal-coated siRNA's in p53-deficient model of thymic lymphoma results in tumor regression and increased survival. Currently, I am expanding my analysis to target ΔNp73 and other downstream targets of ΔNp63/ΔNp73 that might promote tumor formation.

Chapter 8. Investigating the roles of p63 and p73 regulated lncRNAs in the context of genotoxic stress and in p53-deficient cancers

Chapter 8. Investigating the roles of p63 and p73 regulated lncRNAs in the context of p53-deficient cancers

8.1. Introduction and Rationale

Long non-coding RNAs (lncRNAs) are similar to mRNAs but do not code for protein(95, 97). RNA molecules that are generally >200nt in length and those that do not code for protein are classified as lncRNAs. In general, lncRNAs are not evolutionary conserved, but have been implicated in disease and development. Particularly, lncRNAs are involved in multiple diseases from neurodegeneration to cancer. In cancer, lncRNAs could function as oncogenes or tumor suppressors depending on the cancer type and tissue context. Particularly, lncRNAs could mediate its function by either regulating the activity of certain mRNA genes which could be tumor suppressors or oncogenes. p53 functions to regulate the expression of multiple downstream targets and prevent tumor suppression(100-102). Interestingly, p53 could also regulate lncRNA function as in the case of linc-p21, PANDA or H19. Alternatively, expression of p53 could be regulated by lncRNAs as well as in the case of MALAT1, MEG3(99). The functions of these lncRNAs are executed by recruiting other cofactors to mediate tumor suppression or suppressing the effect of a mRNA like a tumor suppressor and acting as “sponge” through competitive endogenous mRNA (ceRNA). Since, lncRNA can also function as a predictor of disease status in human cancers, I was interested in determining the regulation of these lncRNA by the p53-family members, p63 and p73. Understanding the lncRNAs regulated by p63 and p73 would enable us to predict disease outcome and also unravel new pathways of regulation in p53-altered cancers.

To determine regulation of lncRNAs by p63 and p73, we performed RNA-sequencing using two different cellular systems in a p53-deficient condition. In the first analysis, since p63 and p73 respond to DNA damage, I was interested in identifying lncRNA that could respond to genotoxic stress. In the second approach, to identify lncRNA that could play critical roles in the progression of p53-deficient lymphomas, analysis was performed using the ΔNp63Δ/Δ;p53-/- and ΔNp73Δ/Δ;p53-/- thymic lymphoma samples. By identifying and characterizing the function of these lncRNAs by the p53-family members, p63 and p73, I aim to delineate novel regulatory pathways that might help design better therapies to treat p53-altered cancers.

8.2. Results

8.2.1. p63 and p73 regulated lncRNAs that are responsive to genotoxic stress

p63 and *p73* function as transcription factors and similar to p53 and respond to genotoxic stress and protect the genome by recruiting DNA repair genes. Unlike p53, which is often mutated in human cancers, *p63* and *p73* are less frequently mutated making them unique targets, which could possibly perform DNA repair even under diseased states. To determine the non-coding regulatory network of p63 and p73 upon genotoxic stress, mouse embryonic fibroblasts (MEFs) of the indicated genotypes were treated with or without doxorubicin to induce DNA damage. RNA-sequencing was performed using the MEFs treated with or without DOX. A total of 2094 lncRNAs were mapped using the mouse mm9 database. Since, I was

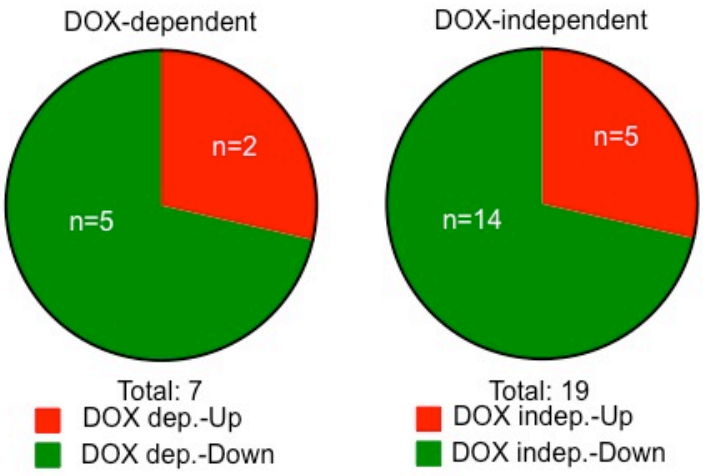

Figure 35: Pie chart representing the differentially expressed lncRNAs either dependent or independent of genotoxic stress. lncRNAs that are DOX dependent (n=7) and lncRNAs that are DOX independent (n=19). Red represents upregulated and green represents downregulated lncRNAS

p63 & *p73* regulated lncRNAs: DOX dependent

LincRNA ID	Ensemble ID	Chr Location
Gm16278*	ENSMUSG00000084862	chr17:25919088-25935745
4931415C17Rik	ENSMUSG00000054910	chr8:12672185-12679229
Gm16170	ENSMUSG00000086245	chr11:48843647-48853493
1810019D21Rik	ENSMUSG00000086390	chr8:106135399-106138525
2010001A14Rik	ENSMUSG00000087165	chr11:57795498-57801417

* - Validated p53-binding site

p63 & *p73* regulated lncRNAs: DOX independent

LincRNA ID	Ensemble ID	Chr Location
Gm13986*	ENSMUSG00000087203	chr2:117857290-118111202
Igf2as	ENSMUSG00000086266	chr7:142659692-142670356
Hoxa11as	ENSMUSG00000086427	chr6:52244392-52249799
F730043M19Rik	ENSMUSG00000052125	chr12:33111710-33147597
Gm20440	ENSMUSG00000092315	chr2:74683445-74694194
Gm9929	ENSMUSG00000053925	chr1:170868644-170881721
A830082K12Rik	ENSMUSG00000087143	chr13:78198016-78236564

* - Validated p53-binding site

Table 5: List of differentially expressed lncRNAs that are either dependent or independent of genotoxic stress

interested in identifying lncRNA that are regulated by p63 and p73, we overlapped the RNA-sequencing data with a ChIP-sequencing to mark all the lncRNAs that encode a p53-consensus binding site. Since, p53, p63 and p73 share a consensus binding site on the target genes, categorizing the lncRNAs based on the consensus increases stringency and provides more confidence.

By bioinformatic analysis, p63 and p73 lncRNAs were classified under two groups, lncRNAs that are doxorubicin dependent and lncRNAs that are doxorubicin independent. Upon, doxorubicin treatment a total of n=7 lncRNA were differentially expressed in which n=5 had a p53-consensus binding site. Interestingly, I observed n=4 lncRNAs to be downregulated and n=2 were upregulated. Similarly, upon analyzing the lncRNAs that are doxorubicin independent a total of n=19 were identified of which n=7 had a p53-consensus binding site. I observed, n=7 to be downregulated and n=2 to be upregulated. Currently, I am planning to perform further stringency analysis based on the expression pattern and develop assays to test and characterize the function of these novel lncRNAs.

8.2.2. Identification of differentially expressed lncRNAs upon ablation of ΔNp63 and ΔNp73 in p53-deficient mouse tumors

ΔNp63 and ΔNp73 deletion in p53-deficient cancers results in tumor regression *in vivo.* I have identified a novel metabolic reprogramming mechanism through the recruitment of *IAPP*, which mediates this tumor regression. However, IAPP is activated by the tumor suppressor isoforms, TAp63 and TAp73, highlighting

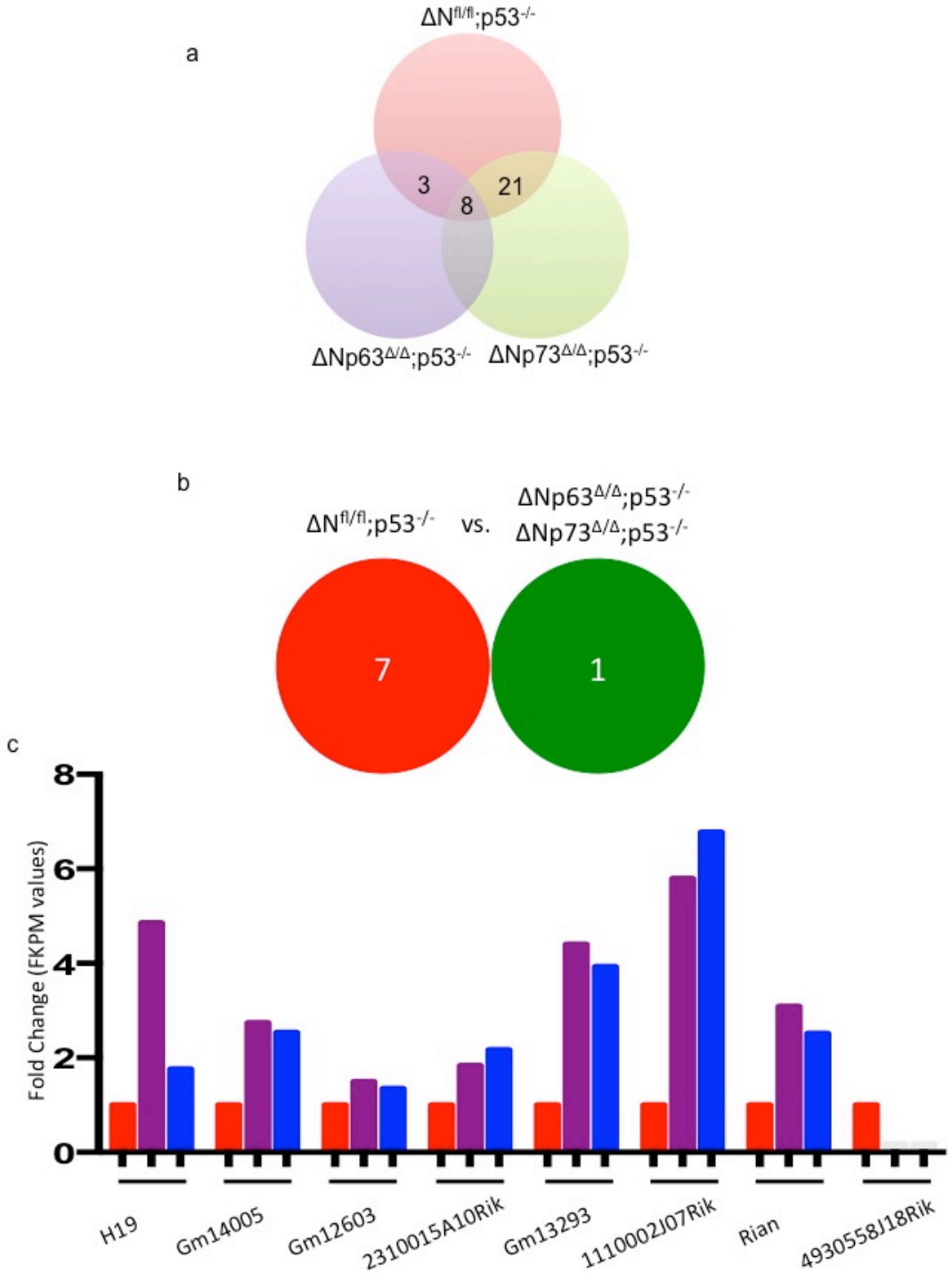

Figure 36: Differentially expressed lncRNAs upon ablation of ΔNp63 and ΔNp73 in p53-deficient thymic lymphomas. Piechart representing number of differentially expressed lncRNAs **(a)**. Pie chart representing lncRNA up and

downregulated in the thymic lymphoma samples **(b).** Graph representing the FKPM fold change values for the selected lncRNAs in the thymic lymphoma samples (**c**).

Ensemble ID	lincRNA	Chromosomal Location
ENSMUSG00000000031	H19	chr7:149761433-149764048
ENSMUSG00000074813	Gm14005	chr2:128015722-128255085
ENSMUSG00000085183	Gm12603	chr4:88696211-88730518
ENSMUSG00000085644	2310015A10Rik	chr12:81221534-81233831
ENSMUSG00000086006	Gm13293	chr2:11261115-11264239
ENSMUSG00000087275	1110002J07Rik	chr10:66375236-66383006
ENSMUSG00000091793	Rian	chr12:110842154-110899919
ENSMUSG00000084958	4930558J18Rik	chr1:57416065-57434348

Table 6. List of differentially expressed lncRNA with ensemble ID and chromosomal location

the global role played by these genes in tumor suppression. Additionally, loss of ΔN isoforms of p63 and p73 could have restored the tumor suppressive role of non-coding genes or suppressed the activity of certain oncogenes. Hence, to further expand our understanding on the p53-deficient tumor regression phenotype and identify biomarkers for disease prediction we utilized the RNA-sequencing data obtained by comparing the ΔNp63Δ/Δ;p53-/- and ΔNp73Δ/Δ;p53-/- versus the ΔNfl/fl;p53-/- tumors (Appendix 1).

Using bioinformatic analysis, a total of n=32 lncRNAs were identified to be differentially expressed between the ΔNp63Δ/Δ;p53-/-, ΔNp73Δ/Δ;p53-/- and ΔNfl/fl;p53-/- thymic lymphoma samples. Since, loss of both ΔNp63 and ΔNp73 accelerates tumor regression in p53-deficient tumors, I focused on the n=8 lncRNAs that are differentially expressed. Of the n=8 lncRNAs, one lincRNA was downregulated and the remaining lncRNAs were all upregulated. Currently, I am performing experiments to determine a phenotypic characterization of these lncRNAs.

Discussion

lncRNAs do not code for proteins, however, are implicated in diseases like cancer. Multiple lncRNAs are significantly expressed in cancer potentiating their roles as oncogenes. However, some lncRNAs that are regulated by tumor suppressors like p53 function to prevent cell proliferation and induce cell death. The gene regulation of lncRNAs is complex and sufficient *in vivo* models have not been developed. In an attempt to understand the regulation of p53-family members, p63

and p73, we mined the database for lncRNA using two distinct approaches. In the first approach, I aim to identify lncRNA that respond to genotoxic stress which may help in recruiting DNA repair genes and also induce cell-cycle arrest in a diseased state. In the second approach, I aim to identify lncRNAs that may play critical roles in p53-deficient tumor regression upon loss of ΔNp63 and ΔNp73.

Since, lncRNAs do not code for proteins, determining the function of the lncRNAs is challenging. Normally, from the bioinformatic analysis of the RNA-sequencing data, a cluster of differentially expressed lncRNAs is obtained. To specifically determine the function of a select few lncRNA, I plan to apply the Guilt by association method (GBA) in which the function of the lncRNA is predicted depending upon the function and the direction of the mRNA genes. This assessment will help design assays depending on the predicted function to characterize the function of lncRNA. Additionally, a few criteria's like determining the chromatin marks for activation or repression or the common consensus binding motifs on the lncRNA promoter will provide leads on determining the function of these lncRNA.

Chapter 9: Discussion, Conclusions and Future Directions

9. Discussion

9.1. p53 mediated tumor suppression in human cancers

TP53 gene's tumor suppressive properties are well documented in multiple cancer types. At physiological conditions, p53 expression is under tight regulation. Upon genotoxic stress, p53 expression levels increase to perform its cellular functions, thereby protecting the genome(133). p53 executes its cellular functions through the recruitment of multiple downstream targets which induce apoptosis or cell-cycle arrest(133). p53 expression is regulated by its own target, MDM2, an E3 ubiquitin ligase that functions as an negative regulator of p53. When p53 is expressed at higher levels, MDM2 inhibits p53 transcriptional activity through its negative feedback mechanism(134). In normal cells, p53 functions to maintain cellular homeostasis. p53 functions to protect the genome from cellular insults and DNA damage. Upon, DNA damage or any form of stress, p53 levels are tremendously increase and direct the damaged cells to undergo cell death or cell cycle arrest. The downstream function if p53 is performed by the recruitment of known p53-targets like *PUMA*, *Noxa* or *BAX* for induction of apoptosis(2, 13)and *p21*, *p16* and *PML* for the induction of cell cycle arrest or cellular senescence(17, 135). More recently, the roles of p53 in multiple cellular pathways like metabolism(79), pluripotency(136), aging(137) etc. are being delineated and this represents the identification unique and novel targets regulated by p53. These functions of the TP53, highlight the importance of this gene in maintaining cellular homeostasis and tumor suppression.

Unfortunately, in a majority of human cancers TP53 function is altered. TP53 gene undergoes a mutation or deletion in most human cancers(118). This results in either gain of function or loss of function of p53. p53 loss corresponds to no activity of the p53 gene resulting in tumor progression upon cellular insults, as p53 is not functional and cannot execute its function of protecting the genome. However, approximately, 50% of human cancers harbor mutations in the *p53* gene that are commonly referred to as “Hot Spot” mutations, which commonly occur in the DNA binding domain of *p53* gene. As a result of these mutations, p53 exhibits gain of function properties promoting tumor growth(8, 23, 138). Mutant p53, because of the mutations in the DNA binding domain cannot be regulated by its negative regulator MDM2, as a result is constantly active. Further, mutant p53 promotes tumor growth by forming heterodimers with known tumor suppressors and preventing their function or by activating oncogenes(26).

In the context of cancer, the status of p53 is critical because one mechanism by which chemotherapy functions is to induce DNA damage which illicits a p53 response which targets the cells to die. Since, p53 expression is altered in most cancers, this raises a concern in therapeutically treating p53-altered human cancers. Hence, the current therapeutic strategy to treat p53-altered cancers has been to reactivate wild-type p53 in p53-deficient human cancers, as this approach has shown promise in p53-deficient mouse models(32). In the case of p53-mutated human cancers, the aim has to been downregulate the expression of mutant p53 through the activation of E3 ubiquitin ligases or other small molecule inhibitors(139). All these approaches have shown great promise but have been a challenge to

therapeutically execute them. This raises an unmet need to develop and identify alternate approaches to treat p53-deficient human cancers.

p53 family members: p63 and p73

In a need to develop alternate approaches to treat p53-deficient human cancers, we have focused on understanding the role of the p53-family members, p63 and p73 in tumorigenesis. p63 and p73 are structurally similar to p53(45). However, unlike p53, both p63 and p73 are less frequently mutated making them unique targets for therapeutic intervention. p63 and p73 were initially identified as developmental regulators and their roles in tumorigenesis were controversial. This is because studies based on *in vivo* mouse models targeting p63 and p73, had a broad tumor spectrum highlighting the indispensable roles of these genes in tumor suppression(46) while some human cancers, expressed higher levels of p63 and p73, suggesting that they could be oncogenic in nature(49, 60, 140). These differences are primarily due to the multiple splice isoforms of p63 and p73. The splice variants of p63 and p73, are broadly classified into N-terminal isoforms and C-terminal isoforms. The major N-terminal isoforms are classified as ones which have an acidic transactivation domain (TA) isoforms or the ones without a transactivation domain (ΔN) isoforms(45). The ΔN isoforms of p63 and p73, function as dominant negatively against p53, TAp63 and TAp73. Previous studies have demonstrated that the TA isoforms function as bonafide tumor suppressors(65, 120) while the role of the ΔNp63 and ΔNp73 in tumorigenesis is still unclear. Hence, in this thesis I aimed to determine the role of the ΔNp63 and ΔNp73 in tumorigenesis.

ΔNp63 and ΔNp73 conditional knockout mice

To determine the roles of the ΔNp63 and ΔNp73in tumorigenesis, we generated ΔNp63 and ΔNp73 conditional knockout mice were generated. These mice were crossed to a Zp3-CRE mouse to generate a ΔNp63+/- and ΔNp73-/- mice. In order to determine the role of the ΔN isoforms of p63 and p73, in the context of p53-deficiency and also to accelerate tumorigenesis, I generated a cohort of ΔNp63+/-;p53-/- and ΔNp73-/-;p53-/- mice, henceforth referred to as double mutant mice.

ΔNp63/p53 and ΔNp73/p53 double deficient mice had reduced thymic lymphomagenesis

ΔNp63/p53 and ΔNp73/p53 double mutant mice had a significant reduction in the thymic lymphoma incidence and increased survival compared to the p53-deficient mice, which develop thymic lymphoma at a 90% incidence rate. This suggests that loss of ΔNp63/ΔNp73 in the p53-deficient thymic lymphomas reduces tumor incidence. Upon analysis on the thymic lymphoma tissues of the double mutant mice, I observed a significant increase in the expression in the TAp63 and TAp73, the tumor suppressive isoforms of p63 and p73. This correlated with the induction of apoptosis targets and increase in cell death and also, induction of cell-cycle targets and increase in cell-cycle arrest in the double mutant thymic lymphomas. This suggests that loss of ΔN isoforms of p63 and p73, results in the upregulation of tumor suppressive TAp63 and TAp73 isoforms mediating cell death and apoptosis. Since, TAp63 and TAp73 respond to genotoxic stress, 4 week old

double mutant mice were subjected to gamma radiation. I observed a significant increase in the expression of the TA isoforms of p63 and p73 that correlated with the induction of apoptosis and cell cycle targets. This further resulted in the induction of apoptosis and reduction in proliferation in the double mutant thymus tissues. This suggests that loss of ΔNp63/ΔNp73 in the p53-deficient thymic lymphomas restores the tumor suppressive functions of TAp63 and TAp73 thereby suppressing lymphomagenesis.

Acute deletion of ΔNp63/ΔNp73 in p53-deficient mice reveals a novel metabolic gene signature that suppresses lymphomagenesis

Total loss of ΔNp63/ΔNp73 in the p53-deficient mice suppresses thymic lymphomagenesis. To test whether this is the case and also determine the molecular determinants that mediate this tumor suppression, ΔNp63 and ΔNp73 were acutely deleted from the p53-deficient thymic lymphoma. The ΔNp63/p53 and ΔNp73/p53 deficient tumors had a significant reduction in the tumor volume and increased survival. This correlated with the increased expression of TAp63 and TAp73 and also induction of cell death and cellular senescence through the activation of targets. I reported that ΔN isoforms of p63 and p73, bind to the promoters of TAp63 and TAp73 preventing its transcriptional function. Further, TAp63 and TAp73 are required for the activation of the apoptosis and cell-cycle targets to mediate tumor regression in the p53-deficient mice.

Since, apoptosis or cellular senescence are downstream functions, I was interested in determining the global role of TAp63 and TAp73 in suppressing

tumorigenesis. RNA-Sequencing analysis of ΔNp63/p53 and ΔNp73/p53 tumors revealed that novel gene signature enriched with metabolic genes compared to the p53-deficient tumors. Ingenuity pathway analysis revealed a cluster of gene involved in glycolysis pathway, which includes known metabolic regulators like *TIGAR*(123) and *GLS2*(82) and novel target called *IAPP*. IAPP expression was significantly upregulated in the ΔNp63/p53 and ΔNp73/p53 deficient tumors suggesting that both TAp63 and TAp73 could activate IAPP. Indeed, I reported that TAp63 and TAp73 bind and transcriptionally activate *IAPP*, which functions as its downstream target (Figure 35). Although, *TIGAR* and *GLS2* were differentially regulated, I found that GLS2 was expressed at higher levels in the ΔNp63/p53 tumors suggesting that GLS2 could function as a TAp63 target. Similarly, TIGAR was significantly expressed at higher levels in the ΔNp73/p53 tumors suggesting that TAp73 could regulate TIGAR. For the purpose of this study, I focused on the combined tumor suppressive roles of TAp63 and TAp73. However, exploring the individual tumor suppressive functions of TAp63 and TAp73 could provide more mechanistic evidence of the interplay among the family in tumorigenesis.

IAPP functions as bonafide tumor suppressor in p53-deficient tumors

IAPP encodes amylin, a 37 amino acid peptide secreted from the beta cells in the pancreas(83). IAPP has been demonstrated to play functional roles in glucose metabolism and apoptosis(84, 124). Interestingly, I reported that IAPP functions as a critical metabolic regulator in p53-deficient mouse embryonic fibroblasts (MEFs) upon ΔNp63/ΔNp73 loss or expressing IAPP. Since, IAPP is expressed at higher

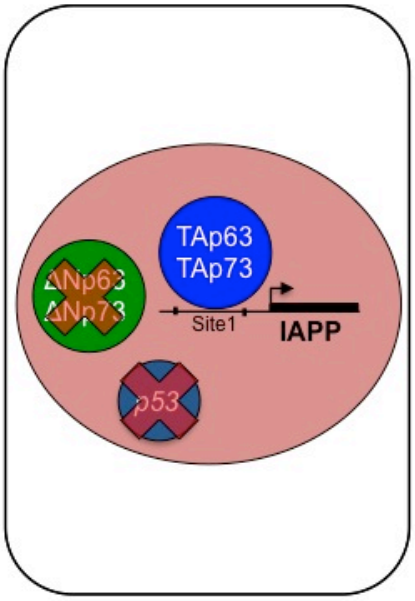

Figure 37: TAp63 and TAp73 compensate for p53-loss by IAPP driven metabolic reprogramming. Model depicting loss of ΔNp63 & ΔNp73 in p53-deficient cancers results in the upregulation of TAp63 and TAp73. TAp63 and TAp73 recruit IAPP to mediate tumor regression in p53-deficient tumors

levels in the ΔNp63/p53 and ΔNp73/p53 double deficient tumors, I suspect the role of IAPP in suppressing thymic lymphomagenesis. However, the role of IAPP in tumor suppression is relatively less characterized. To determine the role of IAPP in tumorigenesis, IAPP was expressed *in vivo* in the p53-deficient thymic lymphomas. This resulted in significant tumor regression and increase in life span. Conversely, when IAPP was downregulated in the ΔNp63/p53 and ΔNp73/p53- deficient thymic the tumors continued to grow very similar to p53-deficient mice. This correlated with the decreased lactate production and also increased accumulation of intracellular ROS and cell death. These findings confirm that *IAPP* functions as a bonafide tumor suppressor in p53-deficient thymic lymphomas.

Ablation of ΔNp63 and ΔNp73 induces IAPP mediated metabolic reprogramming in p53-deficient human cancer cells

Loss of ΔNp63/ΔNp73 in a p53-deficient mouse model of thymic lymphoma induces IAPP mediated metabolic reprogramming that results in suppression of thymic lymphomagenesis. To extend my analysis, to human cancers, ΔNp63/ΔNp73 was knocked down or IAPP was expressed in p53-deficient human cancer cells. I observed a significant reduction in the glycolytic capacity that correlated with the accumulation of ROS and cell death upon ΔNp63/ΔNp73 deletion or IAPP expression. Previous studies have reported that IAPP at physiological levels, functions to inhibit the glycolysis pathway by indirectly inhibiting hexokinase through increasing the levels of glucose-6-phosphate. I observed a similar accumulation of glucose-6-phosphate upon ablation of ΔNp63/ΔNp73 or expression of IAPP in the p53-defiicent cells. Indeed, expression of hexokinase II in these p53-deficient cells,

completely restored glycolysis and reduced ROS levels and rescued cell death in the p53-deficient cells. This suggests that IAPP mediates its tumor suppressive function by inhibiting hexokinase the rate-limiting enzyme in the glycolysis pathway (Figure 36).

IAPP requires the activity of the Calcitonin and RAMP3 receptors to perform its tumor suppressive functions

IAPP is a secreted protein from the pancreas. Previous studies have reported that IAPP functions through the activity of the calcitonin and RAMP family of receptors(127) to perform its physiological functions. Since, IAPP functions as a metabolic regulator mediating tumor suppression in p53-deficient mouse tumors and p53-deficient human cancer cells, I wanted to determine whether IAPP requires the activity of the receptors. Interestingly, I demonstrated that IAPP, requires the activity of both the calcitonin and RAMP3 receptors to perform glycolytic inhibition, induction of ROS and cell death in the p53-deficient human cancer cells and also p53-deficient mouse tumors (Figure 36). Importantly, loss of function of any one of the receptor activity renders IAPP function ineffective. To test whether the expression of IAPP and its receptors correlate with patient survival, we performed a TCGA analysis of patient survival data. In a select group of patients harboring p53-mutations, we observed increased survival when IAPP, RAMP3 and calcitonin receptors are expressed at higher levels (Figure 37). This analysis proved true across a panel of human breast (Figure 37a), colorectal (Figure 37b) and lung squamous (Figure 37c) cell cancers. This data provides important information about selecting a patient group who might serve as better responders for pramlintide, synthetic analog of

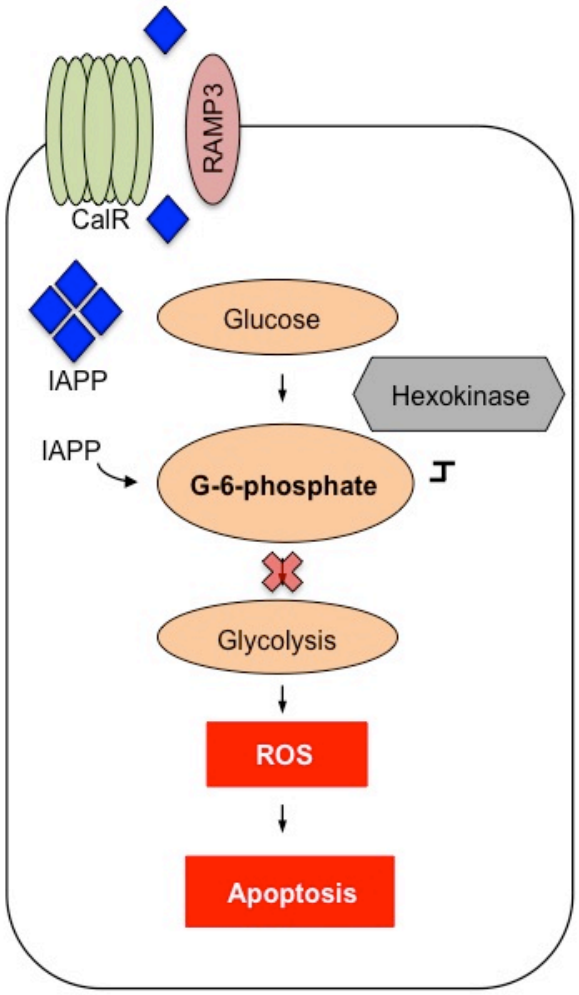

Figure 38: IAPP mediated mechanism of glycolytic inhibition in p53-altered cancers. IAPP functions through the calcitonin and RAMP3 receptors to inhibit glycolysis by suppressing hexokinase activity. IAPP mediated glycolytic inhibition results in ROS accumulation and apoptosis.

IAPP, for treatment. Importantly, the patient populations, could be classified based on the receptor status which could serve as a biomarker. I would suspect that patients with less alterations in the calcitonin and RAMP3 receptor status would respond better to pramlintide based therapies.

Pramlintide based therapy to treat p53-altered cancers

IAPP functions as a bonafide tumor suppressor in p53-deficient cancers. This raises the possibility of using pramlintide as a therapeutic approach to treat p53-altered cancers. Pramlintide is a synthetic analog of IAPP, used in the treatment of Type 1 and Type 2 diabetes. Majority of the human cancers are hard to treat due to alterations in TP53, which makes them less responsive to chemotherapy. In such cases, pramlintide based approach may provide an alternative since IAPP functions by inhibiting glycolysis and does not depend on any alterations or mutations in the genes. Indeed, p53-deficient mice treated with pramlintide intratumorally and systemically had a significant thymic lymphoma regression compared to the placebo treated mice. Further pramlintide treatment in the p53-deficient human cancer cells, resulted in inhibition of glycolysis that correlated with increases in ROS and cell death. This suggests that pramlintide functions similar to IAPP in p53-defcient human cancer cells. Since, pramlintide also functions by inhibition of glycolysis and metabolic reprogramming, I suspect that pramlintide could be used to treat p53-mutant cancer, which are generally hard to target. Indeed, a panel of mutant p53-human cancer cells harboring different p53-hotspot mutations where subjected to pramlintide therapy and I observed an inhibition of glycolysis and significant

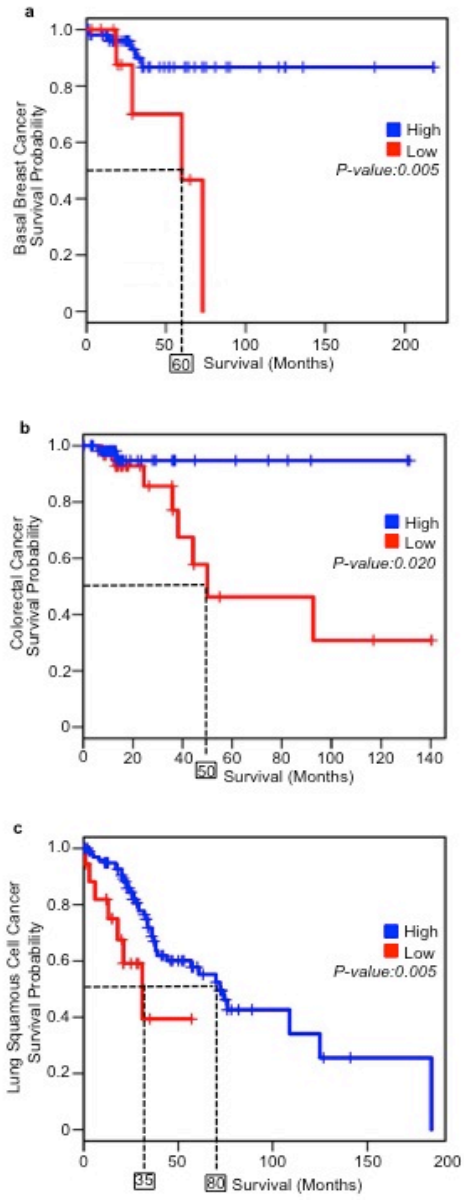

Figure 39: Kaplan Meier Survival plots for expression of IAPP-CALCR-RAMP3 in p53-mutated human cancer patients.

accumulation of ROS and cell death. Interestingly, pramlintide mediated tumor suppression was ineffective when the activity of the receptors was blocked. Currently, I am expanding the possibility of using pramlintide-based therapy to treat squamous cell cancers as a single agent.

Thus far it has become evident that pramlintide treatment mediates tumor suppression in p53-altered human and mouse tumors by inhibiting glycolysis. Since, pramlintide is already used as a diabetic drug, pramlintide use is associated with reduced cellular toxicity. Hence, I was interested in determining whether long term and early dosing of pramlintide could be used to prevent tumor formation. To test whether this is case, a cohort of p53-deficient mice was administered with increasing doses of pramlintide (30μg/kg, 45μg/kg and 60μg/kg body weight) at 4 weeks of age. The mice were administered a biweekly dose of pramlintide for a period of 6 weeks by intravenous (IV) delivery method and tumor progression were monitored by MR imaging. Additionally, blood glucose levels and body weight of the mice were measured every week to monitor the health of the mice upon pramlintide treatment. Interestingly, after 6 weeks of pramlintide treatment, I observed the thymic lymphoma in the p53-deficient mice were smaller in comparison to the placebo treated mice (Appendix 3). Interestingly, some of these treated mice had an extended survival compared to the placebo treated mice. From this initial pilot study, we were able to demonstrate that pramlintide could be used to p53-deficient mice and prevent tumor formation. Our current work is to understand how pramlintide prevents thymic lymphoma progression in these p53-deficient mice and expand our analysis to a larger cohort.

Therapeutically targeting ΔNp63 and ΔNp73 in human cancers

ΔNp63 and *ΔNp73* function as oncogenes in p53-deficient cancers. Importantly, I have demonstrated that targeting the ΔN isoforms of p63 and p73 restores the tumor suppressive function of TAp63 and TAp73. Importantly, TAp63 and TAp73 compensate for p53 loss by activating downstream apoptosis and cell-cycle targets thereby suppressing tumorigenesis. Additionally, targeting ΔNp63 and ΔNp73 also suppresses the expression of oncomiRs that promote tumor formation. Hence, this raises a novel therapeutic opportunity to target ΔNp63 and ΔNp73 to treat p53-deficient cancers. One approach that I have adopted is to deliver small interfering RNAs (siRNA's) through DOPC liposomal nanoparticle based approach. In this case, siRNA's targeting ΔN isoforms of p63 and p73, will be coated with neutral liposomal particles and can be delivered to the site of the tumor either intratumorally or systemically. Upon, delivering siRNA's targeting ΔNp63, I observed a significant reduction in tumor volume of the p53-deficient mice that correlated with the increase in cell death and cell-cycle arrest. This approach of delivering siRNA's targeting ΔNp63 and ΔNp73 can be applied to multiple cancer types and presents a unique opportunity to therapeutically treat p53-deficient cancers.

9.2. Conclusions

TP53 is a highly mutated tumor suppressor gene rendering cancer therapies ineffective. Reactivation of the p53-pathway has been challenging to execute in human cancers. By utilizing the functions of the p53-family members, p63 and p73, I

have identified a novel approach to treat p53-altered cancers. p63 and p73, although structurally similar to p53, exhibit different functions depending on there splice variants. I have demonstrated that the shorter ΔN isoforms of p63 and p73 function in a dominant negative manner against p53, TAp63 and TAp73. Infact, the ΔN isoforms of p63 and p73, function as repressors of transcriptional function of *TAp63* and *TAp73*, preventing their tumor suppressive properties. Therefore, I have demonstrated that ablation of ΔN isoforms of p63 and p73 mediates tumor regression in p53-deficient mice through activation of tumor suppressive isoforms namely, TAp63 and TAp73. Importantly, TAp63 and TAp73 compensate for p53-loss by recruiting IAPP, which induces metabolic reprogramming induced regression of p53-deficient tumors. Additionally, TAp63 and TAp73 can also activate downstream apoptosis and cell-cycle targets mediating tumor suppression.

IAPP, 37-amino acid peptide secreted from the beta cells of pancreas functions as a critical regulator of glucose metabolism. IAPP inhibits glucose uptake and glycolysis by inhibiting hexokinase, the rate-limiting enzyme in the glycolytic pathway. This IAPP mediated glycolytic inhibition results in accumulation of intracellular ROS and cell death resulting in p53-deficient tumor suppression. Interestingly, Pramlintide a synthetic analog of IAPP, is used in the treatment of Type I and II diabetes also functions to inhibit glycolysis and result in ROS induced cell death in the p53-deficient cancer cells. This raises the possibility of utilizing Pramlintide based therapy to treat p53-deficient cancers. Upon administering pramlintide, p53-deficient mice showed significant reduction in thymic lymphomagenesis. Importantly, I have also identified that IAPP/Pramlintide mediates

its tumor suppressive function through the activity of the calcitonin and RAMP3 receptors which could be used as biomarkers to classify patients for pramlintide based therapy.

Further, to expand my understanding of treating p53-mutant cancers, I have demonstrated that mutant p53 binds and inhibits TAp63/TAp73 mediated tumor suppression upon ablating ΔNp63/ΔNp73 in p53-mutant human cancer cells. Hence, two approaches to treat p53-mutant cancers, is to overcome the effect of mutant p53, by ablating the oncogenic isoforms of p63 and p73 and treating the cells with DNA damaging agent like doxorubicin. This results in increased accumulation of TAp63 and TAp73, which could possibly overcome mutant p53 effect. Second approach is to target the downstream glycolysis pathway using pramlintide based therapies. Treatment of mutant p53 human cancer cells with pramlintide has resulted in inhibition of glycolysis and ROS-induced cell death through the activity of the calcitonin and RAMP3 receptors. Since cancer cells are in general highly glycolytic supporting Warburg's hypothesis, pramlintide based therapy would work as novel approach to treat these cancer types. Further, the only other available glycolytic inhibitor is 2-deoxy glucose (2-DG), which has potent effect in inhibiting glycolysis, however, 2-DG is highly toxic and cannot be used for therapeutic intervention. On the contrary, Pramlintide functions similar to 2-DG and is less toxic and is already used in the treatment of diabetes. Thus the use of pramlintide highlights a novel approach to treat p53-mutant cancers.

Finally, since I have demonstrated that ΔNp63 and ΔNp73 function as oncogenes in p53-deficient cancers, targeting these oncogenic isoforms has raised

a novel therapeutic opportunity to treat p53-deficient cancers. To therapeutically target ΔNp63/ΔNp73 in p53-deficient cancers, I delivered liposomal nanoparticle coated siRNA's targeting ΔNp63 in vivo in to a p53-deficient thymic lymphoma. This resulted in a significant reduction in the thymic lymphomagenesis highlighting the therapeutic applications of targeting the oncogenic isoforms of p63 and p73 to treat p53-deficient cancers.

Thus far, my work has presented a novel and unique approach to treat p53-deficient and mutant cancers. Importantly, understanding the interplay among the p53-family members has enabled us to delineate the intricate and individual functions of each of the isoforms in tumorigenesis. Further, by characterizing the tumor suppressive role of IAPP, I have proposed the possibility of repurposing an existing diabetic drug with less toxicity towards cancer treatment.

9.3. Future Directions

My thesis thus far has identified the intricate regulations among the p53-family members, p63 and p73 and their role in tumor suppression. Importantly, I have identified novel therapeutic approaches to treat p53-deficient cancers by multiple approaches, one of which is through metabolic reprogramming induced by IAPP which mediates tumor regression and second approach by using DOPC-labeled siRNA's to target the oncogenic isoforms of p63 and p73.

Hence, from this study it is evident that both ΔNp63 and ΔNp73 function as oncogenes in a p53-deficient model of thymic lymphoma. Indeed this has been the trend in human cancers, were expression of ΔNp63 and ΔNp73 is significantly

upregulated. However, in some instances, ΔN isoforms could also function as tumor suppressors (unpublished data). Nevertheless, it is important to further understand and elucidate the larger roles played by ΔNp63 and ΔNp73 in tumorigenesis. ΔNp63 and ΔNp73 function as repressors of gene function. As a result, it is important to test whether ΔNp63 and ΔNp73 could repress other transcription factors or even miRNAs which could function as tumor suppressors. ΔNp63 and ΔNp73 may perform these functions individually or by recruiting other co-repressors. Hence, by performing a ChIP-sequencing analysis we can determine the binding partners of ΔNp63 and ΔNp73.

Additionally, since ΔNp63 and ΔNp73 function as transcription factors, it is possible that these isoforms could transactivate certain oncogenes by activating oncogenic pathways to promote tumor formation. Hence, it is important to identify the transcription related functions of ΔNp63 and ΔNp73 as well. Further to suppress tumorigenesis, we could direct miRNAs that could function as “sponges” to control and limit the function of ΔNp63 and ΔNp73 in tumor formation.

Further, previous work and current work as again attested that *TAp63* and *TAp73* function as potent tumor suppressors. I have demonstrated that TAp63 and TAp73 jointly induce metabolic reprogramming by activating IAPP, a metabolic regulator. However, it is possible that TAp63 and TAp73 do have their individual targets to mediate tumor suppression. Given the possible role of the TA isoforms in regulating lncRNAs, TAp63 and TAp73 could play critical roles in activating lncRNAs to mediate tumor suppression. Also, TAp63 and TAp73 could have distinct tumor suppressive functions depending upon the tissue context. For example, p53

restoration in the thymic lymphomas induces apoptosis, while in the osteosarcomas, induces cellular senescence. Hence, similar to p53, TAp63 and TAp73 could have diverse functions depending on the tissue context and origin. Hence, it would be interesting to clearly delineate the diverse cellular process regulated by TA isoforms of p63 and p73 in tumor suppression.

Finally, metabolic reprogramming is becoming a well-debated topic and even emerged as one of the hallmarks of cancer. This is due to the fact that cancer cells are metabolically active promoting tumor cell proliferation and require large influx of energy to continue this process. Hence, therapeutically inhibiting this pathway seems more feasible and does not depend on the functional status of different genes. However, the metabolic circuitry is far more complex and constantly evolving. I have identified the role of a metabolic regulator called IAPP which functions to mediate tumor suppression by inhibiting glycolysis. Importantly, synthetic analog of IAPP called Pramlintide, a diabetic drug has shown tremendous potential towards the treatment of p53-deficient cancers. Currently, I have tested the use of pramlintide in multiple cancer types and I aim to test the efficacy of the drug using preclinical patient derived xenografts models. Results from this study will enable us to use the drug as a single agent or as a combinatorial drug with other standard of care therapy drugs.

Previously, as per Warburg's hypothesis, mitochondrial oxidation does not contribute to tumor cell proliferation. However, recent evidence has demonstrated the mutations in the mitochondrial oxidation pathway have lead to tumor cell

proliferation. Hence as a therapeutic strategy, we could utilize both pramlintide and a mitochondrial inhibitor to suppress tumor cell proliferation.

Appendix 1: Mouse thymic lymphoma mRNA heat map.

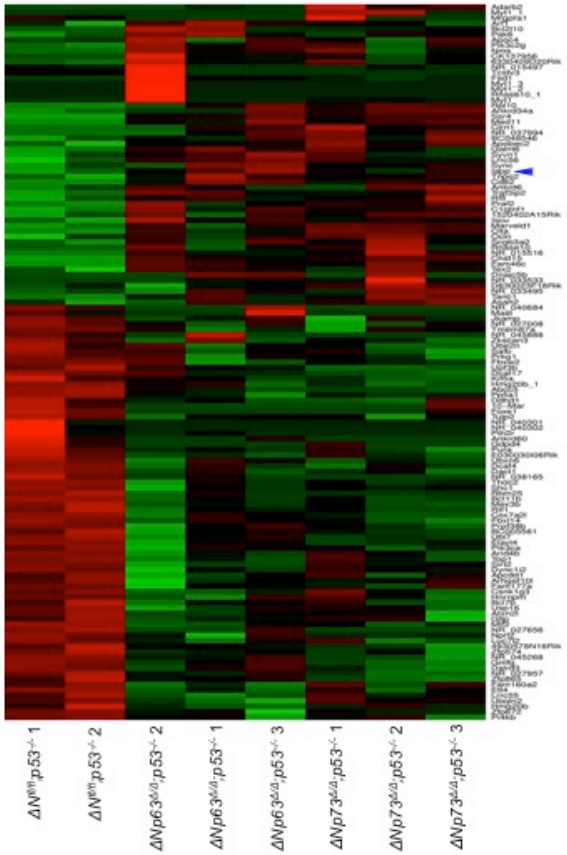

Appendix 2: List of genes differentially expressed in ΔNfl/f;p53-/- vs ΔNp63Δ /Δ;p53-/- and ΔNp73Δ/Δ;p53-/- thymic lymphoma samples

Gene Name	ΔNfl/fl; p53-/-	ΔNp63Δ/Δ;p53-/- ΔNp73Δ/Δ;p53-/-	t-value	p-value
Lce6a	0.50623477	0.8510781	3.2239006	0.014574393
Upp1	0.7964159	0.6226899	3.1032262	0.026755208
Ssr4	0.58017164	0.30428436	5.612081	0.004953332
Dph5	0.8363405	0.6458249	2.8655672	0.035176527
Kcnj10	0.6928598	0.8021817	2.8215833	0.025714781
Rplp1	0.89320916	0.40704307	3.2561753	0.047268085
Chst15	0.34172666	0.39977396	7.654346	1.21E-04
AI118078	0.70577794	0.823888	2.684871	0.0313175
1700029J07Rik	0.80049235	0.41755116	3.6963458	0.020902188
NR_033629	0.7805456	0.61027247	3.2125351	0.02366173
Gpr55	0.8152403	0.50371623	3.3865895	0.027616808
Apobec2	0.39166403	0.55679625	5.6879067	7.45E-04
Tnpo2	0.46795464	0.5575977	5.1519804	0.001321112
C1qtnf1	0.31462026	0.490858	6.9381404	2.24E-04
Sncb	0.68061334	0.62077165	3.6268063	0.011007131
Hemk1	0.7203515	0.7550949	2.9178421	0.026706224
Rps2	0.7302686	0.7622172	2.852749	0.029076638
Mapre2	0.8589156	0.5447324	3.0736532	0.037160475
Fbxw2	0.7842838	0.76749945	2.6384406	0.038620915
Clptm1	0.6981217	0.48885804	4.043158	0.015563355
Cdkn2b	0.759716	0.8135128	2.5456023	0.04374917
Tcstv3	0.27684957	0.5970781	6.0870256	4.97E-04
Lrp4	0.7297057	0.64692396	3.3024392	0.021417892

Gene Name	ΔNfl/fl; p53-/-	ΔNp63Δ/Δ;p53-/- ΔNp73Δ/Δ;p53-/-	t-value	p-value
Snph	0.5002801	0.97959596	2.5421705	0.038541656
Atat1	0.53324264	0.97110534	2.5028503	0.040821623
Ankrd60	0.2085665	0.828321	4.2540317	0.008060685
Fzd3	0.7992467	0.53205603	3.378766	0.027817171
Slc39a10	0.7468975	0.6011655	3.3935597	0.019386165
Pogk	0.79479855	0.80082333	2.4766378	0.04802364
Ssr4	0.67074746	0.58611465	3.8162637	0.012420383
Arf1	0.60844433	0.71573335	3.5322573	0.009568775
Rpl10	0.47247326	0.7212307	4.092963	0.004613714
Glod4	0.58177453	0.9311328	2.5762439	0.036672536
Tmem229b	0.7877702	0.7324492	2.755291	0.033059366
Pcdh12	0.71684206	0.77184725	2.8627381	0.028698595
Cpt1a	0.50031483	0.98236585	2.5269172	0.039410077
Jub	0.8114347	0.75536054	2.5871568	0.04136963
Marveld3	0.6655221	0.9202029	2.384675	0.048547305
Mael	0.09720916	0.6674868	6.0559745	0.001770923
Smoc2	0.6986251	0.6333105	3.4929614	0.012936638
Usp46	0.7022045	0.66434157	3.3539565	0.015343993
Atp5g1	0.741628	0.8482092	2.4646173	0.04317217
Trpc6	0.52749956	0.8119151	3.3625886	0.012041636
NR_040684	0.14194141	0.77539027	4.846768	0.004687081
Acpp	0.6721452	0.8147476	2.839229	0.02507229
Fut4	0.75040406	0.7059895	2.9948723	0.024167644
Abcc1	0.7909167	0.738919	2.7202146	0.034632906
Rragc	0.79355305	0.8044168	2.467177	0.048643574

Gene Name	ΔNfl/fl; p53-/-	ΔNp63Δ/Δ;p53-/- ΔNp73Δ/Δ;p53-/-	t-value	p-value
Rab25	0.60436094	0.87930626	2.7644632	0.027915865
Ror1	0.39281154	1.0071157	2.6372552	0.038682207
Calu	0.61523455	0.9443378	2.4152248	0.046416476
Marveld1	0.47468898	0.7533694	3.8917649	0.00596181
Slc25a21	0.8176421	0.7046145	2.7429042	0.040651474
Fam46c	0.54810005	0.5812634	4.5079803	0.004069225
Gal3st4	0.6925565	0.81971294	2.7475557	0.02860464
Rpl10a	0.69966877	0.8878008	2.4280963	0.045547623
Gm5077	0.79221207	0.74436057	2.6956744	0.035781357
Tpbg	0.8670789	0.57156676	2.9640145	0.041389212
Smarca2	0.5522846	0.91535926	2.7418885	0.028839475
Lrrc56	0.51858276	0.49713963	5.170814	0.002072778
Mrgpra1	0.03466722	0.717363	5.57638	0.002555353
Fam20b	0.59198934	0.89849436	2.7087545	0.030253453
Rtn4	0.585884	0.93577594	2.541162	0.03859846
Pth2r	0.06894411	0.7952146	4.771537	0.005007988
Foxe1	0.06402541	0.7921452	4.804346	0.004864986
Stt3a	0.68839693	0.6226994	3.5824049	0.011609451
Gdpd4	0.05965448	0.775595	4.963919	0.004233855
Prom2	0.29395136	1.0304649	2.683304	0.036375646
Rffl	0.3702356	0.7321335	4.4629426	0.002925672
Asb13	0.51346165	0.8901825	2.9896507	0.02023635
NR_038165	0.06112718	0.7859784	4.864335	0.004615638
10-Mar	0.04384523	0.78105056	4.9238796	0.004382753
Akr1cl	0.586931	0.8700178	2.8650258	0.024163263

Gene Name	ΔNfl/fl; p53-/-	ΔNp63Δ/Δ;p53-/- ΔNp73Δ/Δ;p53-/-	t-value	p-value
Rpn2	0.8236423	0.74626064	2.5763524	0.041974813
Iscu	0.3857484	0.7311601	4.404584	0.003139355
Tacr3	0.40059546	0.88987154	3.322399	0.012723062
Large	0.42922392	0.9303198	3.0033495	0.019847875
Pak6	0.58600616	0.6490751	3.9564848	0.005486284
Tuba4a	0.6070302	0.8479222	2.9073396	0.022746634
Krtcap2	0.54625815	0.8307415	3.1979437	0.015108911
NR_045888	0.03359216	0.76225203	5.1121187	0.003731821
Bmp6	0.52605855	0.8455745	3.1881936	0.015315074
Slc36a3	0.72738564	0.880149	2.3753183	0.04921976
Apoc4	0.4426753	0.7864958	3.817456	0.006563929
Rhox4b	0.49544	0.8362016	3.3415244	0.012393758
Treml4	0.64355266	0.9215	2.4434934	0.04453018
Spic	0.48758885	0.97271717	2.6121955	0.034802
Galnt9	0.47929856	0.8997125	3.0390067	0.018873326
1810046K07Rik	0.4811074	0.8500687	3.3114579	0.01291566
Zkscan3	0.5762213	0.76946473	3.4009442	0.011427785
Sbf2	0.5884245	0.8156363	3.1275332	0.01666711
Ufsp2	0.3882136	0.93116844	3.1038597	0.017228816
Tex2	0.6097382	0.6423541	3.872926	0.008237901
NR_015497	0.046098124	0.7693352	5.0349994	0.003983822
Bcap31	0.74081314	0.71593606	2.9943774	0.024183095
Sync	0.41539133	0.7837205	3.9364207	0.00562912
1520402A15Rik	0.4395788	0.66299117	4.6181703	0.00243139
Fastkd2	0.6023917	0.85377264	2.8944259	0.023169441

Gene Name	ΔNfl/fl; p53-/-	ΔNp63Δ/Δ;p53-/- ΔNp73Δ/Δ;p53-/-	t-value	p-value
Muc15	0.48963168	1.0017498	2.4464188	0.044339523
Tanc1	0.3942968	0.69174206	4.6445045	0.002357065
Efhb	0.64946467	0.826088	2.8665035	0.024112253
Nqo2	0.70100087	0.70463	3.1969662	0.018671393
Ptgs2	0.6398621	0.92783684	2.4242017	0.04580874
Egfr	0.47836643	0.8383031	3.3869758	0.01164735
NR_015516	1.09E-05	0.78030497	4.9450326	0.007788752
Mrpl32	0.7962867	0.80487895	2.4562397	0.04937077
Klrc2	0.6295951	0.68254524	3.5947902	0.01143785
Nfyc	0.42785197	0.8803824	3.3011353	0.013100242
Ocln	0.53484064	0.67174685	4.088315	0.004640799
Sec61g	0.5311733	0.91416025	2.8096251	0.026160005
Manba	0.47241944	0.90458584	3.031675	0.019069478
Pik3c2g	0.5235649	0.77561355	3.572338	0.00906853
Tgfbr2	0.6057456	0.9590669	2.3689172	0.049685277
Med11	0.5247877	0.68585765	4.058766	0.004817104
Mrps6	0.5970628	0.87763494	2.795532	0.026695142
NR_030738	0.5055372	1.0090405	2.3675964	0.049781892
Abcb1b	0.5881341	0.9499241	2.463673	0.04323195
Pla2g4c	0.6487061	0.7689414	3.1268964	0.016681964
Iapp	0.37614614	0.7640406	4.2150292	0.003960948
Zmpste24	0.7017584	0.88372415	2.4395854	0.044786185
Praf2	0.516418	0.7758566	3.5985727	0.00875646
Traf3ip2	0.5621396	0.7359082	3.6270857	0.00843042
Naip7	0.66979957	0.90549463	2.4397695	0.044774093

Gene Name	ΔNfl/fl; p53-/-	ΔNp63Δ/Δ;p53-/- ΔNp73Δ/Δ;p53-/-	t-value	p-value
Adamts14	0.64072967	0.8861263	2.6184433	0.034487177
Clta	0.27749223	0.64808947	5.579663	8.34E-04
Gnas	0.86566114	0.6538075	2.7268248	0.041436642
1300017J02Rik	0.40781325	0.95330995	2.9224846	0.022261126
Ly9	0.60790765	0.957329	2.371578	0.04949123
NR_033567	0.6981446	0.8721835	2.5015848	0.040897276
Galnt6	0.558411	0.7451528	3.5949407	0.008798962
Cab39l	0.67603004	0.76048815	3.0611315	0.018294284
6330409D20Rik	0.2894976	0.87401193	3.7218037	0.009831389
Dhx29	0.6045901	0.9455439	2.43939	0.044799034
Cd151	0.4969481	0.91345584	2.9121544	0.022591082
Pgam2	0.43017796	0.9631706	2.8098369	0.026152052
Rpl38	0.55708057	0.8995604	2.8088906	0.026187617
Cd82	0.5228897	0.7125258	3.919965	0.005749298
Tspan32	0.48725036	0.85251766	3.277781	0.013528376
Extl2	0.671924	0.8576328	2.6498168	0.032950453
Psma5	0.5289441	0.841474	3.2003438	0.015058617
NR_033495	0.45328638	0.8283428	3.5287938	0.009613382
C2cd2	0.60580796	0.82422304	3.0252416	0.019243384
0610010O12Rik	0.5705635	0.9569846	2.4763649	0.042435452
Slc25a12	0.7201853	0.86228335	2.4744027	0.042557597
Ap4m1	0.5918478	0.8213844	3.0874119	0.017630924
Gstp1	0.4371063	0.95067763	2.8648202	0.024170365
Mrpl47	0.5924998	0.95079786	2.447101	0.044295173
Rps24	0.5697426	0.9511336	2.5086052	0.04047941

Gene Name	ΔNfl/fl; p53-/-	ΔNp63Δ/Δ;p53-/- ΔNp73Δ/Δ;p53-/-	t-value	p-value
Ncald	0.5127015	0.94034237	2.7223492	0.02966473
Cacna1f	0.47335693	1.0060757	2.4611814	0.043390118
BC048546	0.33758682	0.7778202	4.260159	0.003745855
Fbxo10	0.49252775	0.9984751	2.4575386	0.04362243
Cryaa	0.5712679	0.94908345	2.5148673	0.0401104
Clnk	0.49137715	0.86753416	3.181155	0.015465769
Fam19a1	0.6111891	0.9431995	2.4322996	0.045267522
Ugt1a1	0.44555384	0.9623292	2.7765749	0.027433163
1810006K21Rik	0.21862034	1.0390533	2.7403898	0.04077316
Eps8l1	0.43315858	1.0194954	2.4765108	0.042426385
Arhgef17	0.61637163	0.84924567	2.8701138	0.023988103
Med22	0.36853078	0.9276793	3.1742754	0.019214507
NR_029468	0.35080907	0.9451299	3.107887	0.020905085
Scgb3a2	0.2620157	0.8053907	4.2967877	0.005110728
Scml4	0.65128565	0.9152222	2.4501765	0.04409585
Asah2	0.46289924	0.8275435	3.5008683	0.009981358
Fam98a	0.62171805	0.9417445	2.4094806	0.04680969
Taz	0.13061292	0.9723755	3.2965355	0.021557627
Fau	0.48894367	0.9964673	2.4774058	0.0423708
NR_045290	0.6946559	0.8758147	2.4966183	0.041195575
Syvn1	0.47107065	0.77000326	3.8079958	0.006645221
Pdlim1	0.6388014	0.91971564	2.4659784	0.04308614
NR_003965	0.6674969	0.89619136	2.4893866	0.041633945
Mup8	0.28921473	1.0305451	2.6907148	0.036018368
Afg3l2	0.47320518	0.9837088	2.587048	0.03609968

Gene Name	ΔNfl/fl; p53-/-	ΔNp63Δ/Δ;p53-/- ΔNp73Δ/Δ;p53-/-	t-value	p-value
4931408A02Rik	0.5731959	0.94342273	2.5383627	0.038756575
Ssu72	0.20708062	1.0556824	2.6451163	0.045694012
Pigu	0.47711998	0.94269335	2.805804	0.026303977
9930012K11Rik	0.7243802	0.88134074	2.3795633	0.0489135
Clrn1	2.46E-05	0.87987256	4.069787	0.00963597
Gm3258	0.33341172	1.0345705	2.588222	0.041310463
Tspan8	0.77924377	0.7922718	2.562129	0.04278586
Nmur2	0.32798997	0.99668837	2.8342068	0.029792687
Lman1	0.26106992	0.92545706	3.4305842	0.013961174
NR_033474	0.34091642	0.8583539	3.6919248	0.010185443
B230217C12Rik	0.41473922	0.88270944	3.325502	0.012669002
Sv2b	0.51376563	0.9290682	2.7799869	0.027298767
Ptp4a2	0.27657467	0.9073741	3.5217657	0.012491772
Ankrd6	0.46388268	0.80018413	3.6573663	0.008098511
Fau	0.46296304	1.0127833	2.4475908	0.04426337
Folh1	0.5174267	0.9502935	2.656049	0.03265377
Arid5a	0.51709694	0.9645196	2.5805302	0.03644415
Mup2	0.47848442	0.9453433	2.7874343	0.027007809
Klra4	0.37658283	0.9900398	2.7747087	0.03222138
Slc40a1	0.1771824	1.0311472	2.8428626	0.036124878
Glrx3	0.5580255	0.8876175	2.8671272	0.024090758
Tbc1d5	0.4829335	0.90015644	3.0259233	0.019224878
NR_045514	4.46E-06	0.9485071	3.5368476	0.0166182
2310008H09Rik	0.010931266	0.9003462	3.9053736	0.011347706

Gene Name	ΔNfl/fl; p53-/-	ΔNp63Δ/Δ;p53-/- ΔNp73Δ/Δ;p53-/-	t-value	p-value
Tnfrsf19	0.1674707	0.93556035	3.5172882	0.016968133
Cfhr2	0.23195125	1.0613495	2.5768409	0.0496218
Llgl1	0.0021698	0.892555	3.9677355	0.010660225
D630023F18Rik	0.37240082	0.8146346	3.8862486	0.006004374
Rpl19	0.079263635	0.9787726	3.2910182	0.021689147
Nsun4	0.4416605	0.91613525	3.0523489	0.018521847
Cnih4	0.39498183	0.95586914	2.938306	0.021765612
Nadk	0.42643613	1.03985	2.372246	0.04944263
Ankrd34a	0.19225873	0.7893165	4.612589	0.00577403
Dhrs1	0.39609712	0.9833172	2.7718215	0.027621552
Hopx	0.5611796	0.9375947	2.601936	0.035325464
Ltb4r2	0.32045794	1.0218899	2.6908607	0.03601137
G630090E17Rik	0.5017128	0.8816087	3.0717993	0.018021865
Ermap	0.100690484	1.0353256	2.881328	0.034534495
Ubac2	0.4101417	0.93958837	2.9980452	0.01999735
Pcdhgb1	0.28273576	0.98378414	3.0019758	0.023947064
Rgs22	0.44141433	1.0208169	2.4505277	0.04407315
Paqr7	0.6668556	0.76181465	3.089987	0.017567312
Klrb1a	0.22580683	1.0472682	2.6770046	0.04397767
Tmsb10	0.17267758	1.0051781	3.023695	0.029292101
Sdr9c7	0.1983991	1.0443401	2.7305067	0.041255385
Dnm2	0.29322225	0.99542636	2.9078968	0.02705447
Cops7a	0.40569085	0.9745358	2.8019078	0.026451634
Ccl19	0.22727525	0.9722433	3.1730046	0.02473142
Ttll11	0.21911533	0.9631975	3.247384	0.02276186

Gene Name	ΔNfl/fl; p53-/-	ΔNp63Δ/Δ;p53-/- ΔNp73Δ/Δ;p53-/-	t-value	p-value
Pold4	0.2391084	0.92063814	3.506603	0.01716284
Gm1987	0.2326995	1.0171548	2.865371	0.035184603
Syn1	0.010146572	0.9074213	3.8498783	0.012002615
Atrnl1	0.42843425	1.0190974	2.4892452	0.04164256
Klk1b8	0.39827925	0.9093671	3.2101076	0.014855861
Tmem87a	0.52063036	0.97502416	2.5148137	0.04011355
5830411N06Rik	0.5213376	0.865152	3.0992453	0.01734063
Eif4a2	0.09404888	1.0454574	2.8158395	0.037290826
Lpcat1	0.16151527	1.0282186	2.8792467	0.03461853
Sec24c	0.34898728	0.91431296	3.3065064	0.016275393
Prl2c5	0.16585448	0.88248074	3.9134727	0.011255602
NR_045551	0.27606234	0.8820939	3.6977692	0.010115091
Slc25a13	0.3427428	0.97040373	2.968056	0.025020428
Spryd4	0.4059689	1.0225371	2.517598	0.045434296
Col6a4	0.42790028	0.99260974	2.6444578	0.033207808
Mrps10	0.19412164	1.0520066	2.6845717	0.043580882
Wwtr1	0.5607859	0.9568985	2.503545	0.040780153
Eml1	0.31955248	1.0166045	2.7256072	0.034385867
Kank3	0.33374676	0.98271513	2.910037	0.026979113
4930579G22Rik	0.24159038	1.0129989	2.8796208	0.03460341
Ptpn3	0.18376632	1.009624	2.9804668	0.030783365
BC068157	0.44300586	1.0300736	2.3934824	0.047922913
Kcnj16	0.1452977	0.9886137	3.1676726	0.02487983
Cubn	0.4371116	0.9212942	3.0348473	0.018984344
C030006K11Rik	0.3596322	1.0092193	2.69375	0.035873126

Gene Name	ΔNfl/fl; p53-/-	ΔNp63Δ/Δ;p53-/- ΔNp73Δ/Δ;p53-/-	t-value	p-value
Wscd1	0.3796186	1.0385841	2.475681	0.048085954
Filip1	0.3174312	1.0554887	2.4859033	0.04742458
Epb4.1l5	0.27832347	1.0483567	2.5945826	0.040959068
Pou2f1	2.04E-04	1.0830048	2.5851943	0.049121927
Hn1l	0.33259466	1.0364295	2.5781753	0.04187205
Naaa	0.3033944	1.0623595	2.4658666	0.048730098
Lrp11	0.4181843	1.0247229	2.4786282	0.04229501
Zp3	0.33273584	1.0134135	2.7208018	0.034605913
BC020535	0.13597594	1.0502218	2.75375	0.040131155
NR_003559	0.31307563	1.0081371	2.7907507	0.031546272
Ap4s1	0.47268093	0.97784877	2.621144	0.034352
Spink8	0.17779204	1.0021979	3.038038	0.02881531
Grhl2	0.33539027	0.9735747	2.9638171	0.025158186
Trim65	0.29378456	1.0665808	2.4543815	0.04949545
1110067D22Rik	0.33296582	1.027188	2.6348464	0.038807075
Kap	0.18033898	0.9351312	3.5023742	0.0172406
Bnip1	0.1973908	1.0033227	3.006044	0.029891029
Higd1b	0.30218932	1.0357987	2.6355996	0.038767986
Lce1a2	0.12076877	0.96750176	3.3405473	0.020540189
Lyplal1	0.30945802	1.0592098	2.4758434	0.04807537
Tmprss2	0.25288934	1.0497423	2.6236742	0.046889488
Hbb-bh1	0.096041106	0.94791174	3.5035288	0.017219327
Gsc	0.15691313	0.9495058	3.4307046	0.018621366
Scube1	0.2076112	1.048915	2.689168	0.043341804
AW551984	1.30E-04	1.0293053	2.9558487	0.031670462

Gene Name	ΔNfl/fl; p53-/-	ΔNp63Δ/Δ;p53-/- ΔNp73Δ/Δ;p53-/-	t-value	p-value
Dab1	0.0501478	0.9338845	3.635904	0.014967592
Kcnk16	0.106278725	0.9433708	3.5284772	0.016766937
Pou5f1	0.21591836	1.0218856	2.857435	0.035512984
NR_040725	0.050579414	1.0547882	2.771202	0.039309315
Serpine3	0.071880594	1.0747625	2.6265485	0.046727255
Triobp	0.001302765	0.95452374	3.4921272	0.01743069
Cpb2	0.17187624	1.0402282	2.7875478	0.03855644
Wdsub1	3.49E-04	1.0074637	3.1093168	0.026571333
Pla2g10	0.08787624	0.9853477	3.238725	0.022981795
Sall3	0.16996822	1.001712	3.0504706	0.028409056
Prss3	0.16676864	1.0712739	2.5847702	0.049147174
B020004J07Rik	0.050596338	0.9881912	3.2372963	0.02301831
Prkg1	0.016211495	1.0360569	2.9079576	0.033479154
NR_045499	0.121789984	0.9866879	3.2035015	0.023901505
Dcst1	0.023635086	0.9728535	3.355415	0.02020886
Hist1h1t	0.12700328	1.0330417	2.8779435	0.034671262
Nr2e3	0.06102681	0.9930714	3.1982481	0.024042198
Ppp1r42	0.10658224	1.0088007	3.0608091	0.028076116
Serpina1a	1.44E-05	1.0836018	2.5811038	0.049366016
Nog	0.064044625	0.9909495	3.211993	0.023676045
NR_045471	0.07664614	1.0190103	3.0081723	0.029818088
Gpr123	0.009730205	0.98342794	3.2806072	0.021939807
NR_045403	0.07147401	1.0313613	2.9248602	0.03282796
Dync1i2	0.066882834	1.0650269	2.6951408	0.043033276
Fam178b	6.77E-06	1.0829573	2.5855205	0.049102522

Gene Name	ΔNfl/fl; p53-/-	ΔNp63Δ/Δ;p53-/- ΔNp73Δ/Δ;p53-/-	t-value	p-value
NR_045139	0.06735169	1.008584	3.085693	0.027292563
Naaladl1	0.053612288	1.0680281	2.6793606	0.043853704
Prkag3	0.06384879	1.0049062	3.1131773	0.026455523
Slc22a20	0.03645663	0.9997913	3.159037	0.025122324
Kcnq2	0.036764227	1.0096254	3.089353	0.027179392
Caps2	0.015649516	0.9968863	3.1835794	0.024440022
Gm5415	0.034550942	1.0045222	3.125965	0.026075933
Hsd17b13	0.03275477	1.0138159	3.06079	0.028076725
Plec	0.045199126	1.0173177	3.0328953	0.028985256
Gpr45	0.012568595	0.99713814	3.182096	0.024480665
Gpr151	0.034017283	1.0244093	2.9862201	0.030580075
Mas1	0.021702003	1.0055172	3.1214514	0.026209213
Ugt2b35	0.015060733	0.9937249	3.2062118	0.02382928
Opn4	0.025556093	1.0219386	3.00519	0.029920353
NR_045633	0.019177223	1.0061882	3.1170616	0.026339568
Sez6l2	0.010578183	1.0408726	2.8749948	0.034790907
Gm15085	0.014337389	1.0038928	3.133896	0.02584359
Nkain2	0.012200879	1.0196103	3.0232098	0.029308382
Dlg5	0.005792228	1.0646698	2.7109206	0.042229768
Fkbp10	0.002660292	1.042329	2.8652275	0.03519051
Kcnq2	0.001736278	1.0002984	3.1601448	0.02509107
Sgce	6.18E-06	1.0689567	2.6815572	0.043738477
Mum1l1	1.76E-06	1.0081193	3.1046782	0.026711244
NR_040301	0.008865041	0	436.87704	5.24E-06
NR_040302	0.06453177	0	59.975018	1.02E-05

Gene Name	ΔNfl/fl; p53-/-	ΔNp63Δ/Δ;p53-/- ΔNp73Δ/Δ;p53-/-	t-value	p-value
Defb19	0.71080106	0	4.9688	0.015658686
Myt1	0	0.001229972	3856.5217	0
Myt1	0	0.012753357	371.91794	2.67E-12
Myt1	0	0.06677306	70.94985	1.05E-08
Ccdc34	0.7565142	0.7743096	2.7106729	0.035074696
NR_038063	0.9059068	0.108112104	3.610451	0.03649204
Hsd3b1	0.9762237	0.1183075	3.242564	0.047757953
NR_045294	0.71784025	0.876197	2.4221497	0.04594694
Rsrc2	0.7443213	0.27466303	4.3815093	0.022009687
Bcl2l10	0	0.17948449	26.190445	1.52E-06
Dnm2	0.7816765	0.7036265	2.8824856	0.027966736
Ccdc73	0.7500891	0.80644923	2.606324	0.04031871
Gast	0.899202	0.49879313	3.0194435	0.039184667
Cnnm3	0.6512607	0.85505253	2.728589	0.029398533
Ssb	0.89562666	0.46026605	3.1269035	0.035290547
Ppfia1	0.17896304	0.4426226	9.011467	4.23E-05
NR_015569	0.8817025	0.6314438	2.7326956	0.04114804
Cspp1	0.9237553	0.30175745	3.3034446	0.04561552
Nr1h2	0.80819005	0.7916678	2.465703	0.048740912
Ccar1	0.7473373	0.33813232	4.2108502	0.024464315
Cd97	0.7391347	0.7507099	2.8657172	0.028586878
Rbm25	0.56713337	0.34691033	5.5523005	0.005149068
Larp7	0.7287209	0.7800584	2.7866962	0.031715456
NR_040337	0.9435602	0.2577174	3.270256	0.046767995
Brd3	0.9159391	0.5309495	2.8696134	0.045486327

Gene Name	ΔNfl/fl; p53-/-	ΔNp63Δ/Δ;p53-/- ΔNp73Δ/Δ;p53-/-	t-value	p-value
Tob2	0.8125718	0.69766694	2.785804	0.03863599
NR_027656	0.4660744	0.40277642	6.213478	0.00157788
Calm2	0.68383205	0.74108434	3.1140285	0.02074208
Fam100b	0.8499497	0.54074174	3.1237369	0.035398606
Celf2	0.8482771	0.6944917	2.662934	0.04472609
Ap1m1	0.8313259	0.30461124	3.7822196	0.03239436
Bod1l	0.8083337	0.27769783	3.9667544	0.028626364
Cdk5r1	0.8614844	0.46018153	3.283664	0.030395865
Brd9	0.88041836	0.30041733	3.5238216	0.038810708
Zfp161	0.9409301	0.5197001	2.7949195	0.04906509
Rnf6	0.44702148	0.908454	3.0818298	0.017769653
Srek1	0.81591403	0.58965653	3.126639	0.026056103
4930578N16Rik	0.59512186	0.44799608	4.8665276	0.004606811
Itgb5	0.73957336	0.3174806	4.313101	0.022953564
Crebzf	0.6561649	0.8002372	2.9595892	0.021117367
Abcc5	0.51673055	0.36533624	5.938121	0.004032765
Btbd6	0.7685415	0.50855094	3.6003833	0.022750376
NR_045578	0.9126684	0.48834902	2.9865665	0.040475197
Arpp21	0.8975752	0.33963913	3.3679037	0.043478187
Asb13	0.51212585	0.8886454	3.0019608	0.019886896
NR_037588	0.7172673	0.7719071	2.860952	0.028765805
Mmadhc	0.75836766	0.47774488	3.7490823	0.01996297
Rps11	0.35408777	0.9651544	2.9759834	0.024764983
Dcaf17	0.5781421	0.69776237	3.7513547	0.007155442
Rtf1	0.5206674	0.43033463	5.5381308	0.002633922

Gene Name	ΔNfl/fl; p53-/-	ΔNp63Δ/Δ;p53-/- ΔNp73Δ/Δ;p53-/-	t-value	p-value
Zrsr1	0.56968236	0.9738193	2.3920841	0.04802149
Mfsd2b	0.93503726	0.53652716	2.7782524	0.049907636
Ube2d2	0.8636002	0.6110902	2.8639185	0.03524445
Ttbk1	0.8831647	0.62915653	2.7337832	0.041094817
Zfp574	0.55221087	0.5197923	4.810299	0.002969328
Dhx30	0.7612478	0.6757851	3.0636566	0.027985187
Ahdc1	0.7171415	0.684632	3.2106376	0.01835228
Pura	0.56960326	0.4479001	5.0545273	0.003918179
Mgat1	0.7375186	0.8573658	2.4397557	0.044775
Wscd2	0.8613684	0.5395813	3.0772598	0.037030213
Csnk1g2	0.83794755	0.6719081	2.7754176	0.039113607
Ssb	0.6503541	0.9072962	2.4900734	0.0415921
Rock1	0.71568114	0.7212333	3.0715823	0.021897644
Kin	0.89099675	0.48331088	3.092922	0.036470704
Hmg20b	0.66140604	0.52969086	4.095439	0.009396655
2-Mar	0.8640084	0.40957704	3.3909113	0.04274617
Cklf	0.7687318	0.72835547	2.8410273	0.029527117
Zc3h14	0.7551423	0.62978643	3.255054	0.022569034
Taf3	0.38079923	0.9247394	3.1617765	0.0158889
Arhgef10l	0.6336453	0.5946082	3.9706135	0.007361795
N6amt1	0.7559443	0.85042006	2.4093246	0.04682041
Rbm17	0.85908145	0.6336144	2.8141544	0.037364904
NR_028577	0.6761663	0.7327598	3.1792881	0.019093057
Fndc1	0.8455971	0.46573249	3.3447828	0.02870774
Syk	0.5447683	0.9641938	2.5088084	0.040467385

Gene Name	ΔNfl/fl; p53-/-	ΔNp63Δ/Δ;p53-/- ΔNp73Δ/Δ;p53-/-	t-value	p-value
Hnrnpm	0.800717	0.46694723	3.561675	0.023550654
NR_030673	0.835641	0.5774963	3.0792713	0.03695779
Uimc1	0.7633097	0.48195842	3.7100184	0.020653702
Shc1	0.44396058	0.68393433	4.4583945	0.002941736
Ing3	0.7795554	0.72993296	2.7948492	0.031376243
Phf14	0.82985073	0.5457115	3.198287	0.03295459
Mex3b	0.6063178	0.43012962	4.864984	0.004613023
Anxa2	0.8367505	0.67850846	2.7584453	0.039908197
Reck	0.6805226	0.69872534	3.3054204	0.016297424
Bptf	0.76309305	0.8378896	2.4369915	0.044956952
Rnf39	0.40021583	1.0008725	2.6583276	0.032546
Raf1	0.8120058	0.4597659	3.5246024	0.024348741
Lrrcc1	0.7895861	0.44642094	3.6763673	0.021271734
Thoc2	0.2576664	0.5756566	6.437475	3.54E-04
4933430H15Rik	0.70253646	0.8906831	2.406515	0.047014035
Pigv	0.794924	0.45385212	3.6278434	0.022202266
NR_030779	0.90529424	0.57521474	2.7983265	0.048894897
E030030I06Rik	0.6243755	0.5619415	4.165929	0.005905252
Snap23	0.84929556	0.524234	3.1724238	0.033779275
Mier2	0.8059555	0.78203076	2.5090163	0.04596432
Cir1	0.7852969	0.5092136	3.5151021	0.024558416
Bcl11b	0.6159637	0.46623135	4.6406145	0.005629563
Cetn4	0.6991679	0.73771614	3.0688279	0.021975018
Cyth2	0.75424033	0.7992667	2.6206896	0.039549675
Palm	0.822884	0.7263186	2.6487508	0.04549472

Gene Name	ΔNfl/fl; p53-/-	ΔNp63Δ/Δ;p53-/- ΔNp73Δ/Δ;p53-/-	t-value	p-value
Vps4a	0.7282406	0.5738591	3.5787551	0.015895769
Kif5a	0.62185764	0.48612505	4.515499	0.00630892
Wrnip1	0.6356815	0.78147686	3.118717	0.01687398
Tulp2	0.54497343	0.7128762	3.8204868	0.006538115
Lmo4	0.66365415	0.8370295	2.7692146	0.027725447
Ppp1r10	0.6500399	0.9239539	2.4127975	0.046582222
Elavl4	0.15755658	0.63556826	6.255576	0.001530557
Fbxl14	0.6255018	0.6577499	3.7264848	0.009777168
Akap5	0.75391114	0.69257015	3.0312917	0.023059575
Igfbp6	0.7547445	0.652518	3.1749818	0.024676641
Csnk1g3	0.6171592	0.5976586	4.04312	0.006778718
Klk5	0.6948286	0.6554953	3.4215493	0.014116849
4930452B06Rik	0.83182234	0.5254681	3.2476401	0.031445812
Csnk1e	0.7655034	0.600903	3.3106167	0.021226026
Ube2n	0.6042501	0.6818456	3.7117028	0.007537909
Ddhd1	0.5254294	0.62025064	4.422035	0.003073707
Ints3	0.68637633	0.56756693	3.810743	0.012490577
Dcaf8	0.6433541	0.9240245	2.4321096	0.045280144
Syf2	0.75671476	0.73409146	2.8644576	0.028634055
Rai1	0.7688361	0.58904004	3.336076	0.020641034
Mlf2	0.55079055	0.5159931	4.8399463	0.002880945
NR_015349	0.8180218	0.7322675	2.6456184	0.038251977
Brd4	0.78793657	0.523612	3.4582684	0.02585857
Axin1	0.6970009	0.743669	3.0525334	0.022438858
Zfp295	0.8054627	0.76213	2.5836973	0.041562386

Gene Name	ΔNfl/fl; p53-/-	ΔNp63Δ/Δ;p53-/- ΔNp73Δ/Δ;p53-/-	t-value	p-value
Top1	0.6067318	0.6072432	4.0532465	0.006701471
Arid4b	0.5123038	0.77038735	3.644609	0.008236586
Rfesd	0.45654958	0.84788245	3.4036427	0.011385886
BC005561	0.5326797	0.6388459	4.2796435	0.003656983
NR_033442	0.6421799	0.7713979	3.1403644	0.01637085
Dbndd1	0.8621894	0.64172083	2.7772841	0.039027292
Adamtsl5	0.79542696	0.5411376	3.368849	0.028073633
Wdr33	0.69219875	0.80477273	2.8128295	0.026039911
Ndufs1	0.7671161	0.7572592	2.7382882	0.033812333
Dact1	0.5049645	0.5545078	4.9262686	0.001701469
Sorbs1	0.72754884	0.62102324	3.4090002	0.019064002
Wdr53	0.56409645	0.978322	2.3835714	0.04862613
Ubl7	0.421326	0.61160135	5.075129	0.001438832
Alx3	0.5302911	0.9404301	2.6734247	0.031841222
Aagab	0.6572083	0.63159823	3.6926894	0.010176208
Zfp672	0.13123523	0.7517969	5.088889	0.003805714
Tbxa2r	0.7575673	0.60550946	3.3301222	0.020776184
Mknk2	0.44224867	1.0299667	2.3957646	0.047762465
Fam177a	0.5899091	0.68773896	3.7481132	0.007185903
NR_027957	0.5725367	0.61177254	4.212026	0.005610548
Tcp11	0.79367644	0.70578396	2.8290186	0.036717057
Gpc3	0.6709766	0.7733604	3.0243428	0.019267814
Rad52	0.5025112	0.9872908	2.494428	0.041327845
NR_027859	0.7378596	0.68268377	3.1330378	0.020246252
Hectd2	0.51094145	0.9664823	2.5860868	0.036150273

Gene Name	ΔNfl/fl; p53-/-	ΔNp63Δ/Δ;p53-/- ΔNp73Δ/Δ;p53-/-	t-value	p-value
NR_027008	0.6537888	0.63087565	3.712074	0.009945159
Dact3	0.6942757	0.8681166	2.5316873	0.03913635
Mtap4	0.657026	0.7007251	3.3952367	0.014581224
Prss53	0.68146247	0.7189174	3.2168279	0.018209754
2310035K24Rik	0.8634628	0.6797194	2.6541584	0.045199968
Dcaf4	0.45337337	0.56417084	5.2055607	0.001245379
Upf3b	0.48036706	0.60581875	4.763459	0.002051215
Fbxo46	0.40984645	0.89562535	3.2615662	0.013834438
Rexo1	0.87334	0.63144875	2.7650402	0.03959734
Srek1ip1	0.8395489	0.6457891	2.8530421	0.03569622
Zkscan3	0.45221916	0.74121994	4.0579915	0.004821822
Etl4	0.17413361	0.6203647	6.3700395	7.03E-04
Dguok	0.7053372	0.89199996	2.392085	0.048021425
Atxn2l	0.4271552	0.76592535	4.0048165	0.0051582
Adarb2	0	0.7746691	4.9992986	0.004107182
Phf21a	0.70575136	0.82782346	2.6682532	0.032080833
1300018I17Rik	0.5401398	0.7832738	3.4681034	0.010432599
Arnt	0.6687846	0.7261573	3.2368786	0.017756354
Angptl1	0.8247388	0.6986858	2.7365696	0.040958814
Cox7a2l	0.23154019	0.6239354	6.0568757	9.18E-04
Cep97	0.5411474	0.93019515	2.696865	0.030778343
NR_045268	0.5481574	0.74986714	3.6121795	0.008599197
Rnase10	0	0.7747412	4.998601	0.004109637
Myt1	0	0.7747441	4.998573	0.004109736
Usp16	0.21065246	0.7395884	4.998531	0.002455932

Gene Name	ΔNfl/fl; p53-/-	ΔNp63Δ/Δ;p53-/- ΔNp73Δ/Δ;p53-/-	t-value	p-value
Anapc11	0.62159806	0.75412816	3.298472	0.013148325
D330028D13Rik	0.81690884	0.6869514	2.8058786	0.03773109
NR_037865	0.6036144	0.8308061	3.0011466	0.01990981
Klc3	0.61332154	0.87530315	2.7555535	0.028276635
CK137956	0	0.7751593	4.9945555	0.004123905
Bcl2l1	0.83993524	0.65894616	2.8096044	0.03756574
NR_045836	0.78177375	0.5636572	3.3609936	0.02008611
Ubxn6	0.49219784	0.72642493	3.976024	0.005350981
Npepps	0.6244869	0.7334903	3.382713	0.011715255
Trp53i13	0.7999554	0.78777355	2.5082364	0.046012808
Rhoa	0.6461705	0.76251376	3.1653295	0.015810406
Shank2	0.89041245	0.5714423	2.8684409	0.045540113
Zfp14	0.7922065	0.65131646	3.024311	0.02927144
NR_037994	0	0.7783602	4.9636917	0.004234684
Map2k7	0.6341646	0.90655434	2.5423002	0.03853436
Cep164	0.87164605	0.66907	2.6570299	0.045044303
Ythdc1	0.76479363	0.67449814	3.0539968	0.028295005
Pi4kb	0.10819078	0.77908874	4.872118	0.004584393
Dnajc5b	0	0.77953666	4.952396	0.004276094
Pptc7	0.7900982	0.79142	2.528216	0.04478743
Phf14	0.44339877	0.8663194	3.3374078	0.012463856
Mta3	0.6046586	0.73495823	3.4565203	0.010597348
4930404N11Rik	0.6045984	0.922098	2.5550313	0.03782484
Celf1	0.510967	0.90942675	2.893551	0.023198381
Wnt11	0.8077902	0.6352808	3.0144293	0.029604806

Gene Name	ΔNfl/fl; p53-/-	ΔNp63Δ/Δ;p53-/- ΔNp73Δ/Δ;p53-/-	t-value	p-value
Pik3ca	0.43003753	0.79575723	3.806954	0.006654241
Dalrd3	0.4499849	0.63253427	4.7649264	0.002047728
Abca6	0.78884876	0.78179115	2.568847	0.042400736
Med10	0.68042433	0.9132144	2.3725033	0.04942393
Rnase10	0	0.7790405	4.9571567	0.004258584
Lrrc55	0.49998307	0.7044652	4.068538	0.004757999
Os9	0.6712847	0.916248	2.3858652	0.048462443
Armcx2	0.5472892	0.9352324	2.65326	0.032786198
AI597468	0.15942389	0.98546755	3.1743722	0.024693517
Nprl2	0.44184563	0.80489534	3.708528	0.007569478
NR_037957	0.64764315	0.8573473	2.729844	0.029345294
Prkg1	0.5095542	0.7167073	3.955685	0.005491902
Dync1i2	0.2762159	0.85682684	3.8763223	0.008205559
Safb2	0.7134781	0.8293146	2.63606	0.033615317
Ppil2	0.07427365	0.9993173	3.1475754	0.0254483
Foxp4	0.71792686	0.7712024	2.861434	0.028747648
Senp8	0.6936455	0.75356686	3.0240614	0.02327509
Galnt1	0.72600716	0.87310547	2.4097717	0.04678968
Bcl7b	0.5419179	0.668453	4.0718465	0.00473817
Cdkn1b	0.6115648	0.86368525	2.8168738	0.025889166
Phf17	0.52273506	0.97663397	2.5007133	0.040949456
Htatsf1	0.7188913	0.66379094	3.2844977	0.016728327
Nms	0	0.7861389	4.88947	0.004515614
Zranb2	0.6593553	0.8404091	2.7683823	0.027758704
Wipf2	0.6554555	0.8603764	2.6906781	0.031055236

Gene Name	ΔNfl/fl; p53-/-	ΔNp63Δ/Δ;p53-/- ΔNp73Δ/Δ;p53-/-	t-value	p-value
NR_045199	0.7937492	0.7310667	2.738319	0.033810955
Dgcr6	0.59782135	0.74148375	3.4529839	0.010648205
Snx15	0.55247813	0.9107759	2.764956	0.027896052
Rps9	0.5673595	0.9254546	2.6464233	0.033113178
Zfp865	0.6092422	0.681453	3.690992	0.007746457
Ubap2l	0.49465027	0.90207225	2.98109	0.020483203
Prpf38b	0.14805315	0.8123992	4.508817	0.006347803
Sema3c	0.6181054	0.9336318	2.4593935	0.04350398
Egfl8	0.5520453	0.9853867	2.3781722	0.049013652
Mex3d	0.771046	0.70845985	2.9057271	0.02713109
Fam76b	0.6104966	0.9041898	2.6249244	0.034163717
Tfap2b	0.6116507	0.7360093	3.4230442	0.011089454
2010109K11Rik	0.542541	0.8724677	2.9934573	0.0201276
Hmg20b	0.3917597	0.67028075	4.811871	0.001939541
Cnot3	0.59446603	0.79876924	3.188295	0.015312916
Map3k1	0.5970785	0.9522292	2.4271564	0.0456105
NR_028296	0.6637605	0.87100047	2.6157708	0.034621477
Abtb1	0.50172323	0.87733525	3.0950723	0.017442416
Abcf3	0.5553815	0.8647535	2.9924054	0.02015759
Sdccag8	0.5323854	0.81639963	3.3214037	0.012740452
Hoxa7	0.5585729	0.8714137	2.9481747	0.021462454
Apcdd1	0.5051843	0.7833241	3.6003404	0.008735855
Zfp653	0.49923918	0.8417716	3.2979968	0.013156923
Stau1	0.4474471	0.94864327	2.8500662	0.0246861
Mylpf	0.50479585	0.81522506	3.425224	0.011056672

Gene Name	ΔNfl/fl; p53-/-	ΔNp63Δ/Δ;p53-/- ΔNp73Δ/Δ;p53-/-	t-value	p-value
Fsd1	0	0.7863221	4.887735	0.004522437
Il11ra2	0.61620104	0.76958287	3.2469985	0.014115741
Safb	0.37423646	0.7603252	4.2480645	0.003802212
Ppm1h	0.6729283	0.8142038	2.8389108	0.025083728
Lrrc58	0.5103216	0.8714947	3.1000147	0.017321933
Jkamp	0.41460916	0.75396657	4.1315413	0.004395489
Psmd8	0.5353771	0.89093375	2.919222	0.02236478
Sirt2	0.14304742	0.78501093	4.7576427	0.005070019
Zxdb	0.47418293	1.0151492	2.4081335	0.046902396
Hnrnpd	0.5728875	0.81935	3.1637008	0.015846336
Ankrd11	0.43313587	0.8988593	3.1767614	0.015560637
Zfand2b	0.39990926	0.94115597	3.0143824	0.019540753
Otud1	0.56800467	0.8183331	3.1859396	0.015363161
Sema4d	0.5153147	0.85833365	3.1551049	0.016037423
Ubqln2	0.4239337	0.83499956	3.586618	0.0088972
Casp7	0.50147617	0.8450988	3.2722661	0.013631649
Pfn1	0.6683331	0.90442926	2.449092	0.04416604
Zfp575	0.53988343	0.9070609	2.821359	0.02572306
Fnbp1	0.68849593	0.8814452	2.4909873	0.0415365
Polr3gl	0.4477471	0.90510195	3.099109	0.017343946
Gm1965	0.42112926	0.9808967	2.7284148	0.029405933
Pias1	0.4457344	0.8892454	3.1966069	0.015137001
Fbxw2	0.15463954	0.81758016	4.4528923	0.006684369
Kif5b	0.43570784	1.0276177	2.4237242	0.045840863
Tnrc6c	0.66337115	0.87159204	2.6143215	0.034694538

Gene Name	ΔNfl/fl; p53-/-	ΔNp63Δ/Δ;p53-/- ΔNp73Δ/Δ;p53-/-	t-value	p-value
Gltp	0.38288268	0.82021946	3.8148606	0.006586124
Zcchc9	0.5295479	0.8421459	3.1947608	0.015175884
Zfp746	0.55000275	0.986537	2.3774047	0.049068995
Luc7l2	0.4103945	0.7733772	4.0217533	0.005048355
Mbd6	0.6565342	0.8940796	2.5326927	0.039078906
Vps52	0.7230967	0.74511886	2.9476469	0.025691297
Madd	0.19218214	0.8782817	3.9008439	0.011399596
Tmem87a	0.22999342	0.8496132	4.040552	0.006798464
Zfx	0.41627964	0.8609656	3.4525816	0.010654006
Brpf3	0.29247937	0.9484173	3.213643	0.01828293
Jrkl	0.5435012	0.9413882	2.6317518	0.033826392
Rbm39	0.48131838	0.9155187	2.9452748	0.02155107
Golga4	0.30404538	1.030618	2.6651375	0.037267577
Tfap2a	0.60686105	0.881113	2.7478771	0.028591381
Ccnd3	0.56583333	0.838158	3.0933197	0.017485354
Spata2	0.6961633	0.8437004	2.6320195	0.033813234
4931406P16Rik	0.68034136	0.9147077	2.3659296	0.04990409
Slc9a3r1	0.4199101	0.8802602	3.3251781	0.012674631
Fam160a2	0.44770044	0.80820495	3.667785	0.00798761
Lemd3	0.28939173	0.92756474	3.3578362	0.015270467
Traf2	0.58860505	0.88668454	2.7774503	0.027398612
Tnrc6a	0.511472	0.9447334	2.7020664	0.030547556
NR_029456	0.65506744	0.9291513	2.373567	0.04934667
Dlg4	0.5196946	0.8870266	2.9876306	0.020294316
Gmfg	0.42317215	0.7901299	3.867104	0.006154682

Gene Name	ΔNfl/fl; p53-/-	ΔNp63Δ/Δ;p53-/- ΔNp73Δ/Δ;p53-/-	t-value	p-value
Upf3a	0.6123128	0.8699901	2.7842424	0.02713211
Pnn	0.41805092	0.96476513	2.8300912	0.025402868
Smarca4	0.6719411	0.90782696	2.4226136	0.045915656
Awat2	0.5209645	0.9677513	2.5530062	0.03793679
Rnf40	0.3068969	1.0508443	2.5327797	0.044512395
Rbbp6	0.5850337	0.80909884	3.1716893	0.015670931
Brf1	0.4712073	1.0162349	2.4089258	0.046847846
Rltpr	0.34825724	1.0382304	2.5381734	0.044189647
Zfp944	0.6489769	0.89386845	2.5568717	0.037723396
Acbd3	0.40046698	1.0362217	2.447836	0.04993729
Ppt2	0.37942636	0.96377856	2.9272077	0.026382707
Otud5	0.49579063	1.0041763	2.4180584	0.046223752
Klraq1	0.533447	0.82808465	3.255893	0.013943267
Kctd18	0.5246526	0.93503547	2.7176883	0.02986521
Nosip	0.5893446	0.9329006	2.5456784	0.038344756
Zbtb6	0.47570738	1.0147368	2.4068995	0.04698749
Son	0.47068703	0.9096398	3.0082474	0.019710906
NR_033144	0.33773857	0.901285	3.4182365	0.014174408
NR_033533	0	0.8434303	4.37366	0.007197289
Rara	0.47495085	0.93557715	2.851272	0.024643514
Arfgap1	0.4605324	0.958281	2.7617369	0.028025743
Morf4l1	0.16247232	1.0578351	2.678828	0.043881696
NR_040364	0.33407247	1.0161631	2.7011828	0.03552007
Ctxn1	0.4020231	0.97524655	2.806226	0.026288034
Rpl7	0.1919353	1.0504241	2.6975646	0.04290877

Gene Name	ΔNfl/fl; p53-/-	ΔNp63Δ/Δ;p53-/- ΔNp73Δ/Δ;p53-/-	t-value	p-value
Hnrnpm	0.2584016	0.882235	3.7372499	0.009653731
Ip6k2	0.29890493	0.9385806	3.2647974	0.017145496
Csrnp2	0.38077858	1.01384	2.6223764	0.039460406
Taok2	0.1777848	1.0426848	2.7648022	0.039608512
Gm15308	0.4768259	0.99174565	2.5332248	0.039048538
Padi4	0.36532962	0.90153503	3.3457909	0.012321553
Mad2l1bp	0.12638676	1.020686	2.9631574	0.031404153
Tnip1	0.22696185	1.059517	2.59527	0.048526328
Fbxw5	0.15047543	1.0633327	2.65292	0.04526728
Hnrnpa2b1	0.17599827	0.96665406	3.2853882	0.021824293
Dnajc5b	0	1.0000035	3.1622527	0.02503172
Htr1a	0	1.0000107	3.1622012	0.025033167
Trpc5	0	1.0000254	3.1620963	0.025036117
NR_046179	0	1.0000457	3.161953	0.025040148
NR_040623	0	1.0000765	3.1617327	0.025046345
Hs3st2	0	1.0001408	3.1612759	0.025059203
Abcc6	0	1.0001798	3.160998	0.025067024
Hoxc13	0	1.0001892	3.1609318	0.025068892
4921517D21Rik	0	1.0001997	3.1608567	0.025071006
NR_045048	0	1.0002116	3.1607728	0.025073372
Serpinb9f	0	1.0002161	3.1607397	0.025074305
6030405A18Rik	0	1.0003294	3.1599348	0.025096994
Sstr5	0	1.0003574	3.1597345	0.025102643
NR_003959	0	1.0012333	3.1535068	0.025279019
Dnajc5b	0	1.0015857	3.1510015	0.025350364

Gene Name	ΔNfl/fl; p53-/-	ΔNp63Δ/Δ;p53-/- ΔNp73Δ/Δ;p53-/-	t-value	p-value
NR_033632	0	1.0018922	3.1488233	0.02541258
Tas2r129	0	1.0064082	3.1167903	0.02634765
NR_024257	0	1.0238483	2.9939997	0.03030757
Tecrl	0	1.0314263	2.941053	0.03221734
NR_024326	0	1.0000061	3.1622343	0.03411084
NR_045451	0	1.0006084	3.157949	0.03425143

Appendix 3: Pramlintide treatment as a preventive approach to suppress thymic lymphomagenesis in p53-deficient mice

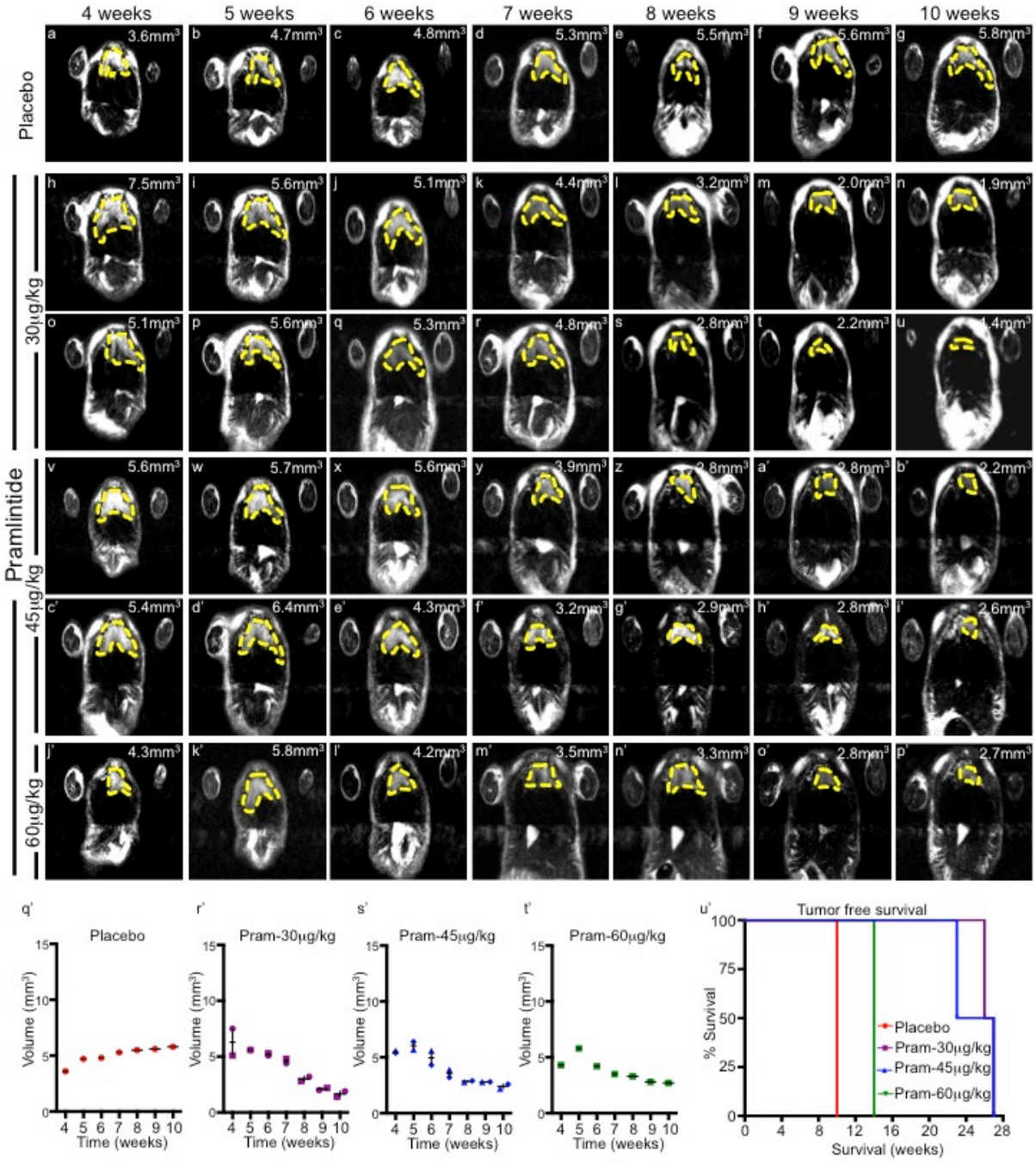

Bibliography

1. Lane DP. Cancer p53, guardian of the genome. Nature. 1992;358:15-6.

2. Villunger A. p53- and drug-induced apoptotic responses mediated by BH3-only proteins Puma and Noxa. Science. 2003;302:1036-8.

3. Brachmann RK, Yu K, Eby Y, Pavletich NP, Boeke JD. Genetic selection of intragenic suppressor mutations that reverse the effect of common p53 cancer mutations. EMBO J. 1998;17:1847-59.

4. Cho Y, Gorina S, Jeffrey PD, Pavletich NP. Crystal structure of a p53 tumor suppressor-DNA complex: understanding tumorigenic mutations. Science. 1994;265:346-55.

5. Lane DP, Brown CJ, Verma C, Cheok CF. New insights into p53 based therapy. Discov Med. 2011;12:107-17.

6. Iwakuma T, Lozano G, Flores ER. Li-Fraumeni syndrome: a p53 family affair. Cell Cycle. 2005;4:865-7.

7. Lang GA. Gain of function of a p53 hot spot mutation in a mouse model of Li-Fraumeni syndrome. Cell. 2004;119:861-72.

8. Olive KP. Mutant p53 gain of function in two mouse models of Li-Fraumeni syndrome. Cell. 2004;119:847-60.

9. Mendrysa SM. Mdm2 is critical for inhibition of p53 during lymphopoiesis and the response to ionizing irradiation. Mol Cell Biol. 2003;23:462-72.

10. Ringshausen I, O'Shea CC, Finch AJ, Swigart LB, Evan GI. Mdm2 is critically and continuously required to suppress lethal p53 activity in vivo. Cancer Cell. 2006;10:501-14.

11. Happo L. Maximal killing of lymphoma cells by DNA damage-inducing therapy requires not only the p53 targets Puma and Noxa, but also Bim. Blood. 2010;116:5256-67.

12. Michalak EM, Villunger A, Adams JM, Strasser A. In several cell types tumour suppressor p53 induces apoptosis largely via Puma but Noxa can contribute. Cell Death Differ. 2008;15:1019-29.

13. Chipuk JE. Direct activation of Bax by p53 mediates mitochondrial membrane permeabilization and apoptosis. Science. 2004;303:1010-4.

14. Henry RE, Andrysik Z, Paris R, Galbraith MD, Espinosa JMA. DR4:tBID axis drives the p53 apoptotic response by promoting oligomerization of poised BAX. EMBO J. 2012;31:1266-78.

15. Li T. Tumor suppression in the absence of p53-mediated cell-cycle arrest, apoptosis, and senescence. Cell. 2012;149:1269-83.

16. Schlereth K. DNA binding cooperativity of p53 modulates the decision between cell-cycle arrest and apoptosis. Mol Cell. 2010;38:356-68.

17. Jackson JG, Pant V, Li Q, Chang LL, Quintas-Cardama A, Garza D, et al. p53-mediated senescence impairs the apoptotic response to chemotherapy and clinical outcome in breast cancer. Cancer Cell. 2012;21(6):793-806.

18. Valente LJ. p53 efficiently suppresses tumor development in the complete absence of its cell-cycle inhibitory and proapoptotic effectors p21, Puma, and Noxa. Cell Rep. 2013;3:1339-45.

19. Jackson JG. p53-mediated senescence impairs the apoptotic response to chemotherapy and clinical outcome in breast cancer. Cancer Cell. 2012;21:793-806.

20. Lehmann BD. A dominant role for p53-dependent cellular senescence in radiosensitization of human prostate cancer cells. Cell Cycle. 2007;6:595-605.

21. Donehower LA. The p53-deficient mouse: a model for basic and applied cancer studies. Seminars in cancer biology. 1996;7(5):269-78.

22. Jacks T. Tumor spectrum analysis in p53-mutant mice. Curr Biol. 1994;4:1-7.

23. Petitjean A. Impact of mutant p53 functional properties on TP53 mutation patterns and tumor phenotype: lessons from recent developments in the IARC TP53 database. Hum Mutat. 2007;28:622-9.

24. Adorno M. A Mutant-p53/Smad complex opposes p63 to empower TGF[beta]-induced metastasis. Cell. 2009;137:87-98.

25. Muller PA. Mutant p53 drives invasion by promoting integrin recycling. Cell. 2009;139:1327-41.

26. Di Como CJ, Gaiddon C, Prives C. p73 function is inhibited by tumor-derived p53 mutants in mammalian cells. Mol Cell Biol. 1999;19:1438-49.

27. Gaiddon C, Lokshin M, Ahn J, Zhang T, Prives C. A subset of tumor-derived mutant forms of p53 down-regulate p63 and p73 through a direct interaction with the p53 core domain. Mol Cell Biol. 2001;21:1874-87.

28. Bykov VJ. Restoration of the tumor suppressor function to mutant p53 by a low-molecular-weight compound. Nature Med. 2002;8:282-8.

29. Liu X. Small molecule induced reactivation of mutant p53 in cancer cells. Nucleic Acids Res. 2013;41:6034-44.

30. Zache N, Lambert JM, Wiman KG, Bykov VJ. PRIMA-1MET inhibits growth of mouse tumors carrying mutant p53. Cell Oncol. 2008;30:411-8.

31. Martins CP, Brown-Swigart L, Evan GI. Modeling the therapeutic efficacy of p53 restoration in tumors. Cell. 2006;127:1323-34.

32. Ventura A. Restoration of p53 function leads to tumour regression in vivo. Nature. 2007;445:661-5.

33. Xue W. Senescence and tumour clearance is triggered by p53 restoration in murine liver carcinomas. Nature. 2007;445:656-60.

34. Lane DP, Verma C. Mdm2 in evolution. Genes Cancer. 2012;3:320-4.

35. Bottger A. Design of a synthetic Mdm2-binding mini protein that activates the p53 response in vivo. Curr Biol. 1997;7:860-9.

36. Carvajal D. Activation of p53 by MDM2 antagonists can protect proliferating cells from mitotic inhibitors. Cancer Res. 2005;65:1918-24.

37. Coll-Mulet L. MDM2 antagonists activate p53 and synergize with genotoxic drugs in B-cell chronic lymphocytic leukemia cells. Blood. 2006;107:4109-14.

38. Vassilev LT. Small-molecule antagonists of p53-MDM2 binding: research tools and potential therapeutics. Cell Cycle. 2004;3:419-21.

39. Ding Q. Discovery of RG7388, a potent and selective p53-MDM2 inhibitor in clinical development. J Med Chem. 2013;56:5979-83.

40. Verma R, Rigatti MJ, Belinsky GS, Godman CA, Giardina C. DNA damage response to the Mdm2 inhibitor nutlin-3. Biochem Pharmacol. 2010;79:565-74.

41. Vu B. Discovery of RG7112: a small-molecule MDM2 inhibitor in clinical development. ACS Med Chem Lett. 2013;4:466-9.

42. Azmi AS. MI-219-zinc combination: a new paradigm in MDM2 inhibitor-based therapy. Oncogene. 2011;30:117-26.

43. Joerger AC, Fersht AR. Structure-function-rescue: the diverse nature of common p53 cancer mutants. Oncogene. 2007;26:2226-42.

44. Kaar JL. Stabilization of mutant p53 via alkylation of cysteines and effects on DNA binding. Protein Sci. 2010;19:2267-78.

45. Su X, Chakravarti D, Flores ER. p63 steps into the limelight: crucial roles in the suppression of tumorigenesis and metastasis. Nature Rev Cancer. 2013;13:136-

46. Flores ER. Tumor predisposition in mice mutant for p63 and p73: evidence for broader tumor suppressor functions for the p53 family. Cancer Cell. 2005;7:363-73.

47. Yang A. p63, a p53 homolog at 3q27-29, encodes multiple products with transactivating, death-inducing, and dominant-negative activities. Mol Cell. 1998;2:305-16.

48. Yang A. Relationships between p63 binding, DNA sequence, transcription activity, and biological function in human cells. Mol Cell. 2006;24:593-602.

49. Sniezek JC, Matheny KE, Westfall MD, Pietenpol JA. Dominant negative p63 isoform expression in head and neck squamous cell carcinoma. Laryngoscope. 2004;114:2063-72.

50. Su X. TAp63 prevents premature aging by promoting adult stem cell maintenance. Cell Stem Cell. 2009;5:64-75.

51. Yang A. p63 is essential for regenerative proliferation in limb, craniofacial and epithelial development. Nature. 1999;398:714-8.

52. Chakravarti D, Su X, Cho MS, Bui NH, Coarfa C, Venkatanarayan A, et al. Induced multipotency in adult keratinocytes through down-regulation of DeltaNp63 or DGCR8. Proc Natl Acad Sci U S A. 2014;111(5):E572-81.

53. Romano RA. [Delta]Np63 knockout mice reveal its indispensable role as a master regulator of epithelial development and differentiation. Development. 2012;139:772-82.

54. Agostini M. p73 regulates maintenance of neural stem cell. Biochem Biophys Res Commun. 2010;403:13-7.

55. Flores ER. p73 is critical for the persistence of memory. Cell Death Differ. 2011;18:381-2.

56. Gonzalez-Cano L. p73 deficiency results in impaired self renewal and premature neuronal differentiation of mouse neural progenitors independently of p53. Cell Death Dis. 2010;1:e109.

57. Talos F. p73 is an essential regulator of neural stem cell maintenance in embryonal and adult CNS neurogenesis. Cell Death Differ. 2010;17:1816-29.

58. Yang A. p73-deficient mice have neurological, pheromonal and inflammatory defects but lack spontaneous tumours. Nature. 2000;404:99-103.

59. Vilgelm AE, Hong SM, Washington MK, Wei J, Chen H, El-Rifai W, et al. Characterization of DeltaNp73 expression and regulation in gastric and esophageal tumors. Oncogene. 2010;29(43):5861-8.

60. Zaika AI, Slade N, Erster SH, Sansome C, Joseph TW, Pearl M, et al. Np73, A Dominant-Negative Inhibitor of Wild-type p53 and TAp73, Is Up-regulated in Human Tumors. Journal of Experimental Medicine. 2002;196(6):765-80.

61. Buza N, Cohen PJ, Pei H, Parkash V. Inverse p16 and p63 expression in small cell carcinoma and high-grade urothelial cell carcinoma of the urinary bladder. Int J Surg Pathol. 2010;18:94-102.

62. Comperat E. p63 gene expression study and early bladder carcinogenesis. Urology. 2007;70:459-62.

63. Flores ER. p63 and p73 are required for p53-dependent apoptosis in response to DNA damage. Nature. 2002;416:560-4.

64. Guo X. TAp63 induces senescence and suppresses tumorigenesis in vivo. Nature Cell Biol. 2009;11:1451-7.

65. Su X. TAp63 suppresses metastasis through coordinate regulation of Dicer and miRNAs. Nature. 2010;467:986-90.

66. Su X, Chakravarti D, Cho MS, Liu L, Gi YJ, Lin YL, et al. TAp63 suppresses metastasis through coordinate regulation of Dicer and miRNAs. Nature. 2010;467(7318):986-90.

67. Su X, Gi YJ, Chakravarti D, Chan IL, Zhang A, Xia X, et al. TAp63 is a master transcriptional regulator of lipid and glucose metabolism. Cell Metab. 2012;16(4):511-25.

68. Su X, Paris M, Gi YJ, Tsai KY, Cho MS, Lin YL, et al. TAp63 prevents premature aging by promoting adult stem cell maintenance. Cell Stem Cell. 2009;5(1):64-75.

69. Lin YL, Sengupta S, Gurdziel K, Bell GW, Jacks T, Flores ER. p63 and p73 transcriptionally regulate genes involved in DNA repair. PLoS Genet. 2009;5(10):e1000680.

70. Belloni L. DNp73[alpha] protects myogenic cells from apoptosis. Oncogene. 2006;25:3606-12.

71. Liu G, Nozell S, Xiao H, Chen X. Np73 Is Active in Transactivation and Growth Suppression. Molecular and Cellular Biology. 2003;24(2):487-501.

72. Petrenko O, Zaika A, Moll UM. Np73 Facilitates Cell Immortalization and Cooperates with Oncogenic Ras in Cellular Transformation In Vivo. Molecular and Cellular Biology. 2003;23(16):5540-55.

73. Wilhelm MT, Rufini A, Wetzel MK, Tsuchihara K, Inoue S, Tomasini R, et al. Isoform-specific p73 knockout mice reveal a novel role for delta Np73 in the DNA damage response pathway. Genes & development. 2010;24(6):549-60.

74. Venkatanarayan A, Raulji P, Norton W, Chakravarti D, Coarfa C, Su X, et al. IAPP-driven metabolic reprogramming induces regression of p53-deficient tumours in vivo. Nature. 2015;517(7536):626-30.

75. Vander Heiden MG, Cantley LC, Thompson CB. Understanding the Warburg Effect: The Metabolic Requirements of Cell Proliferation. Science. 2009;324(5930):1029-33.

76. Lunt SY, Vander Heiden MG. Aerobic glycolysis: meeting the metabolic requirements of cell proliferation. Annual review of cell and developmental biology. 2011;27:441-64.

77. Berkers CR, Maddocks OD, Cheung EC, Mor I, Vousden KH. Metabolic regulation by p53 family members. Cell metabolism. 2013;18(5):617-33.

78. Cairns RA, Harris IS, Mak TW. Regulation of cancer cell metabolism. Nature Rev Cancer. 2011;11:85-95.

79. Vousden KH, Ryan KM. p53 and metabolism. Nat Rev Cancer. 2009;9(10):691-700.

80. Cheung EC, Athineos D, Lee P, Ridgway RA, Lambie W, Nixon C, et al. TIGAR is required for efficient intestinal regeneration and tumorigenesis. Developmental cell. 2013;25(5):463-77.

81. Li T, Kon N, Jiang L, Tan M, Ludwig T, Zhao Y, et al. Tumor suppression in the absence of p53-mediated cell-cycle arrest, apoptosis, and senescence. Cell. 2012;149(6):1269-83.

82. Suzuki S. Phosphate-activated glutaminase (GLS2), a p53-inducible regulator of glutamine metabolism and reactive oxygen species. Proc Natl Acad Sci USA. 2010;107:7461-6.

83. Pillay K, Govender P. Amylin uncovered: a review on the polypeptide responsible for type II diabetes. BioMed Res Int. 2013;2013:826706.

84. Castle AL, Kuo CH, Han DH, Ivy JL. Amylin-mediated inhibition of insulin-stimulated glucose transport in skeletal muscle. Am J Physiol. 1998;275:E531-E6.

85. Pillay K, Govender P. Amylin uncovered: a review on the polypeptide responsible for type II diabetes. BioMed research international. 2013;2013:826706.

86. <amylin p53 p21 RINf cells.pdf>.

87. Cao P, Abedini A, Wang H, Tu LH, Zhang X, Schmidt AM, et al. Islet amyloid polypeptide toxicity and membrane interactions. Proceedings of the National Academy of Sciences of the United States of America. 2013;110(48):19279-84.

88. Christopoulos G. Multiple amylin receptors arise from receptor activity-modifying protein interaction with the calcitonin receptor gene product. Mol Pharmacol. 1999;56:235-42.

89. Edelman S, Maier H, Wilhelm K. Pramlintide in the treatment of diabetes mellitus. BioDrugs. 2008;22:375-86.

90. Mates JM, Sanchez-Jimenez FM. Role of reactive oxygen species in apoptosis: implications for cancer therapy. The International Journal of Biochemistry & Cell Biology 32 (2000) 157-170 .

91. Ramsey MR, Sharpless NE. ROS as a tumour suppressor? Nature Cell Biology Vol. 8, Number 11 (2006).

92. Bell EL, Emerling BM, Chandel NS. Mitochondrial regulation of oxygen sensing. Mitochondrion. 2005;5(5):322-32.

93. Maddocks OD, Berkers CR, Mason SM, Zheng L, Blyth K, Gottlieb E, et al. Serine starvation induces stress and p53-dependent metabolic remodelling in cancer cells. Nature. 2013;493(7433):542-6.

94. Brown CJ, Lain S, Verma CS, Fersht AR, Lane DP. Awakening guardian angels: drugging the p53 pathway. Nature Rev Cancer. 2009;9:862-73.

95. Batista PJ, Chang HY. Long noncoding RNAs: cellular address codes in development and disease. Cell. 2013;152(6):1298-307.

96. Ponting CP, Oliver PL, Reik W. Evolution and functions of long noncoding RNAs. Cell. 2009;136(4):629-41.

97. Rinn JL, Chang HY. Genome regulation by long noncoding RNAs. Annual review of biochemistry. 2012;81:145-66.

98. Martens-Uzunova ES, Bottcher R, Croce CM, Jenster G, Visakorpi T, Calin GA. Long noncoding RNA in prostate, bladder, and kidney cancer. European urology. 2014;65(6):1140-51.

99. Zhang A, Xu M, Mo YY. Role of the lncRNA-p53 regualtory network in cancer. Journal of Molecular Cell Biology (2014).

100. Dimitrova N, Zamudio JR, Jong RM, Soukup D, Resnick R, Sarma K, et al. LincRNA-p21 activates p21 in cis to promote Polycomb target gene expression and to enforce the G1/S checkpoint. Molecular cell. 2014;54(5):777-90.

101. Huarte M, Guttman M, Feldser D, Garber M, Koziol MJ, Kenzelmann-Broz D, et al. A large intergenic noncoding RNA induced by p53 mediates global gene repression in the p53 response. Cell. 2010;142(3):409-19.

102. Marin-Bejar O, Marchese FP, Athie A, Sanchez Y, Gonzalez J, Segura V, et al. Pint lincRNA connects the p53 pathway with epigenetic silencing by the Polycomb repressive complex 2. Genome biology. 2013;14(9):R104.

103. Liu P, Jenkins NA, Copeland NG. A highly efficient recombineering-based method for generating conditional knockout mutations. Genome Res. 2003;13:476-8

104. Lewandoski M, Wassarman KM, Martin GR. Zp3-cre, a transgenic mouse line for the activation or inactivation of loxP-flanked target genes specifically in the female germ line. Curr Biol. 1997;7:148-51.

105. Abbas HA, Maccio DR, Coskun S, Jackson JG, Hazen AL, Sills TM, et al. Mdm2 is required for survival of hematopoietic stem cells/progenitors via dampening of ROS-induced p53 activity. Cell Stem Cell. 2010;7(5):606-17.

106. Vin H. BRAF inhibitors suppress apoptosis through off-target inhibition of JNK signaling. eLife. 2013;2:e00969.

107. Su X. TAp63 is a master transcriptional regulator of lipid and glucose metabolism. Cell Metab. 2012;16:511-25.

108. Trapnell C. Transcript assembly and quantification by RNA-Seq reveals unannotated transcripts and isoform switching during cell differentiation. Nature Biotechnol. 2010;28:511-5.

109. Huang DW, Sherman BT, Lempicki RA. Systematic and integrative analysis of large gene lists using DAVID bioinformatics resources. Nature Protocols. 2009;4:44-57.

110. Sandulache VC. Glycolytic inhibition alters anaplastic thyroid carcinoma tumor metabolism and improves response to conventional chemotherapy and radiation. Mol Cancer Ther. 2012;11:1373-80.

111. Ardenkjaer-Larsen JH. Increase in signal-to-noise ratio of > 10,000 times in liquid-state NMR. Proc Natl Acad Sci USA. 2003;100:10158-63.

112. Maddocks OD. Serine starvation induces stress and p53-dependent metabolic remodelling in cancer cells. Nature. 2013;493:542-6.

113. Comprehensive genomic characterization of squamous cell lung cancers. Nature. 2012;489:519-25.

114. Agrawal N. Exome sequencing of head and neck squamous cell carcinoma reveals inactivating mutations in NOTCH1. Science. 2011;333:1154-7.

115. Banerji S. Sequence analysis of mutations and translocations across breast cancer subtypes. Nature. 2012;486:405-9.

116. Comprehensive molecular characterization of human colon and rectal cancer. Nature. 2012;487:330-7.

117. Cerami E. The cBio Cancer Genomics Portal: an open platform for exploring multidimensional cancer genomics data. Cancer Discovery. 2012;2:401-4.

118. Muller PA, Vousden KH. p53 mutations in cancer. Nature cell biology. 2013;15(1):2-8.

119. Brown CJ, Lain S, Verma CS, Fersht AR, Lane DP. Awakening guardian angels: drugging the p53 pathway. Nat Rev Cancer. 2009;9(12):862-73.

120. Tomasini R. TAp73 knockout shows genomic instability with infertility and tumor suppressor functions. Genes Dev. 2008;22:2677-91.

121. Dhillon PK. Aberrant cytoplasmic expression of p63 and prostate cancer mortality. Cancer Epidemiol Biomarkers Prev. 2009;18:595-600.

122. Vogelstein B, Lane D, Levine AJ. Surfing the p53 network. Nature. 2000;408:307-10.

123. Bensaad K. TIGAR, a p53-inducible regulator of glycolysis and apoptosis. Cell. 2006;126:107-20.

124. Castle AL, Kuo CH, Han DH, Ivy JL. Amylin-mediated inhibiton of insulin-stimulated glucose transport in skeletel muscle. American Physiological Society (1998) E531-E536.

125. Cairns RA, Harris IS, Mak TW. Regulation of cancer cell metabolism. Nat Rev Cancer. 2011;11(2):85-95.

126. Emerling BM, Hurov JB, Poulogiannis G, Tsukazawa KS, Choo-Wing R, Wulf GM, et al. Depletion of a putatively druggable class of phosphatidylinositol kinases inhibits growth of p53-null tumors. Cell. 2013;155(4):844-57.

127. Christopoulos G, Perry KJ, Morfis M, Tilakaratne N, Gao Y, Fraser NJ, Main MJ, Foord SM, Sexton PM. Multiple amylin receptors arise from receptor activity

modifying protein interaction with the calcitonin receptor gene product. Molecular Pharmacology, 56:235-242 (1999).

128. Khoo KH, Verma CS, Lane DP. Drugging the p53 pathway: understanding the route to clinical efficacy. Nature reviews Drug discovery. 2014;13(3):217-36.

129. Olivier M, Hollstein M, Hainaut P. TP53 mutations in human cancers: origins, consequences, and clinical use. Cold Spring Harbor perspectives in biology. 2010;2(1):a001008.

130. Arlette JP, Trotter MJ. Squamous cell carcinoma in situ of the skin: history, presentation, biology and treatment. The Australasian journal of dermatology. 2004;45(1):1-9; quiz 10.

131. Ozpolat B, Sood AK, Lopez-Berestein G. Liposomal siRNA nanocarriers for cancer therapy. Advanced drug delivery reviews. 2014;66:110-6.

132. Pecot CV, Wu SY, Bellister S, Filant J, Rupaimoole R, Hisamatsu T, et al. Therapeutic silencing of KRAS using systemically delivered siRNAs. Molecular cancer therapeutics. 2014;13(12):2876-85.

133. Brady CA. Distinct p53 transcriptional programs dictate acute DNA-damage responses and tumor suppression. Cell. 2011;145:571-83.

134. Huang L. The p53 inhibitors MDM2/MDMX complex is required for control of p53 activity in vivo. Proc Natl Acad Sci USA. 2011;108:12001-6.

135. Deng C, Zhang P, Harper JW, Elledge SJ, Leder P. Mice lacking p21CIP1/WAF1 undergo normal development, but are defective in G1 checkpoint control. Cell. 1995;82:675-84.

136. Lee DF, Su J, Ang YS, Carvajal-Vergara X, Mulero-Navarro S, Pereira CF, et al. Regulation of embryonic and induced pluripotency by aurora kinase-p53 signaling. Cell Stem Cell. 2012;11(2):179-94.

137. Flores ER, Lozano G. The p53 family grows old. Genes Dev. 2012;26:1997-2000.

138. Lang GA, Iwakuma T, Suh YA, Liu G, Rao VA, Parant JM, et al. Gain of function of a p53 hot spot mutation in a mouse model of Li-Fraumeni syndrome. Cell. 2004;119(6):861-72.

139. Chene P. A small synthetic peptide, which inhibits the p53-hdm2 interaction, stimulates the p53 pathway in tumour cell lines. J Mol Biol. 2000;299:245-53.

140. Casciano I, Mazzocco K, Boni L, Pagnan G, Banelli B, Allemanni G, Ponzoni M, Tonini GP, Romani M. Expression of ΔNp73 is a molecular marker for adverse outcome in neuroblastoma patients. Cell Death and Differentiation (2002) 9, 246-251.

VITA

Avinashnarayan Venkatanarayan was born in Chennai, the capital of the southern state of Tamil Nadu, India. He was born on 4th August 1985 to Mr. A. Venkatanarayan and Mrs. V. Ashalatha. After completing his high school at Don Bosco MHSS and S.B.O.A MHSS, Avinash, continued his college education at St. Joseph's College of Engineering, Anna University, Chennai from 2003-2007. Avinash graduated from college with an Honor's distinction and obtained his Bachelor's in Technology (B.Tech) majoring in Industrial Biotechnology. Following his undergraduate training, Avinash moved to the United States of America to pursue his Master's of Science majoring in Biotechnology at The University of Texas at San Antonio (UTSA). At UTSA, Avinash completed his Master's dissertation project titled "Hunchback suppresses Notch-induced apoptosis in the serotonergic lineage of Drosophila" under the mentorship of Dr. Martha Lundell. After graduating from UTSA in 2009, Avinash, joined the PhD graduate program at the Graduate School of Biomedical Sciences, a joint venture of The University of Texas Health Science Center at Houston and The University of Texas MD Anderson Cancer Center, Houston. Avinash, joined the lab of Dr. Elsa R. Flores to pursue his PhD dissertation project. His project focuses on understanding the isoform specific regulation of the p53-family members, p63 and p73 to develop and therapeutically treat human cancers with alterations in the tumor suppressor gene, TP53.